Summer 2016

Low-complexity iterative receiver algorithms for multiple-input multiple-output underwater wireless communications

Weimin Duan

Department: Electrical and Computer Engineering

LOW-COMPLEXITY ITERATIVE RECEIVER ALGORITHMS FOR MULTIPLE-INPUT MULTIPLE-OUTPUT UNDERWATER WIRELESS COMMUNICATIONS

by

WEIMIN DUAN

A DISSERTATION

Presented to the Faculty of the Graduate School of the

MISSOURI UNIVERSITY OF SCIENCE AND TECHNOLOGY

In Partial Fulfillment of the Requirements for the Degree

DOCTOR OF PHILOSOPHY

in

ELECTRICAL ENGINEERING

2016

Approved by

Yahong Rosa Zheng, Advisor
Randy H. Moss
Egemen K. Çetinkaya
Maciej Zawodniok
Maggie Cheng

PUBLICATION DISSERTATION OPTION

This dissertation consists of the following four published or to be published papers, formatted in the style used by the Missouri University of Science and Technology, listed as follows:

Paper I, (pages 8–45) W. Duan, Y. R. Zheng,"Bidirectional Soft-Decision Feedback Turbo Equalization for MIMO Systems", has been accepted by IEEE Trans. Veh. Technol., Aug. 2015.

Paper II, (pages 46–80) W. Duan, J. Tao and Y. R. Zheng,"Efficient Adaptive Turbo Equalization for MIMO Underwater Acoustic Communications", has been submitted to IEEE J. Ocean. Eng, Apr. 2016.

Paper III, (pages 81–96) W. Duan, Y. R. Zheng, D. Sun and Y. Zhang,"Block Iterative FDE for MIMO Underwater Acoustic Communications", has been accepted by MTS/IEEE COA2016, Harbin, China, Jan. 9-11, 2016.

Paper IV, (pages 97–118) W. Duan, Y. R. Zheng,"Experimental Evaluation of Turbo Receivers in Single-Input Single Output (SISO) Underwater Acoustic Channels", has been accepted by MTS/IEEE OCEANS, Shanghai, China, Apr. 11-14, 2016.

ABSTRACT

This dissertation proposes three low-complexity iterative receiver algorithms for multiple-input multiple-output (MIMO) underwater acoustic (UWA) communications. First is a bidirectional soft-decision feedback Turbo equalizer (Bi-SDFE) which harvests the time-reverse diversity in severe multipath MIMO channels. The Bi-SDFE outperforms the original soft-decision feedback Turbo equalizer (SDFE) while keeping its total computational complexity similar to that of the SDFE. Second, this dissertation proposes an efficient direct adaptation Turbo equalizer for MIMO UWA communications. Benefiting from the usage of soft-decision reference symbols for parameter adaptation as well as the iterative processing inside the adaptive equalizer, the proposed algorithm is efficient in four aspects: robust performance in tough channels, high spectral efficiency with short training overhead, time efficient with fast convergence and low complexity in hardware implementation. Third, a frequency-domain soft-decision block iterative equalizer combined with iterative channel estimation is proposed for the uncoded single carrier MIMO systems with high data efficiency. All the three new algorithms are evaluated by data recorded in real world ocean experiment or pool experiment. Finally, this dissertation also compares several Turbo equalizers in single-input single-output (SISO) UWA channels. Experimental results show that the channel estimation based Turbo equalizers are robust in SISO underwater transmission under harsh channel conditions.

ACKNOWLEDGMENTS

First and foremost, I would like to acknowledge my advisor Dr. Yahong Rosa Zheng. I sincerely appreciate her continuous support and devoted guidance throughout my Ph.D study. Without her numerous constructive suggestions, insightful comments and generous financial support, this dissertation would have been impossible. She has also provided me the opportunity to teach the wireless communication course, which improves my communication skills. Her enthusiasm, dedication and down-to-earth attitude towards research have set a role of academic perfection, from which I will benefit in my future research career.

My deep appreciation also goes to Dr. Chengshan Xiao for his guidance on my research work. He often share his experience in both research and career to teach me working smartly and efficiently, not only diligently. I also would like to thank Dr. Jun Tao for his generous assistance in research and technical writing. I enjoyed our collaborations and publications.

I would like to thank the members of my advisory committee, Drs. Randy H. Moss, Maciej Zawodniok, Egemen K. Çetinkaya and Maggie Cheng for generously offering their time and invaluable advice for my research.

I thank all the current and past members in the research lab for their kindly support and friendship. I cherish the time we spent together in Rolla.

I indebted my family for their unselfish love, everlasting support and sacrifice. Particularly, this dissertation is dedicated to my beloved wife, Qin Long and our smart, lovely baby girl, Sophie Siyong Duan. Last, but certainly not the least, I would like to express my eternal gratitude to my parents and parents-in-law for their unconditional love and support throughout the years.

TABLE OF CONTENTS

LIST OF ILLUSTRATIONS

LIST OF TABLES

SECTION

1 INTRODUCTION

1.1 BACKGROUND

Underwater wireless communications have played an important role in the wide range of oceanic engineering applications, such as environmental monitoring, offshore exploration, and disaster prevention. Particularly, acoustic communications are considered as the most effective means for medium and long range underwater communications, although optical and magneto-inductive systems may also be suited for short range underwater communications [1]. However, current underwater acoustic (UWA) communication systems can only achieve very low data rates such as 1 kbps to 10 kbps at medium range (1 km to 10 km) due to the limited channel bandwidth.

Recently, the multiple-input multiple-output (MIMO) technology has been considered in UWA communication systems to increase the data rate without additional bandwidth or transmit power [2, 3]. The MIMO systems employ multiple elements at both the transmitter and receiver sides. Theoretically, the MIMO channel capacity grows linearly with the minimum number of transmit and receive antennas. However, the practical application of MIMO technology to achieve reliable underwater high-data-rate transmission still exhibits unique technical challenges. Typically, UWA MIMO channels are severe triply-selective, which simultaneously experience frequency selectivity, temporal selectivity, and spatial selectivity. The severe frequency selectivity is caused by the extremely long multipath delay spread, which results in severe inter-symbol interference (ISI). The time selectivity is due to the large doppler spread, which causes high carrier frequency offest (CFO) and waveform compression or depression. The spatial selectivity means the strong spatial correlation among multiple transmit

and receive elements, and the resulting co-channel interference further challenges the robust symbol detection.

Turbo equalization is a promising detection scheme to achieve near optimal performance in MIMO UWA communications. Typical turbo equalizers consist of two components: a soft-input soft-output (SISO) equalizer and a SISO decoder, which iteratively exchanges extrinsic information with each other. The optimal Turbo equalizer was designed with a maximum a posteriori probability (MAP) equalizer and a MAP decoder [4]. However, the complexity of the MAP based Turbo equalizer grows exponentially with the product of the MIMO size and channel length, which is prohibitively high in extremely long delayed UWA channels. To greatly lower the computational complexity, the Minimum Mean Square Error (MMSE) based Turbo Equalizers have been proposed [5, 6, 7]. Currently, two classes of MMSE turbo equalizers are commonly used in UWA communications: channel estimation based MMSE turbo equalizer (CE MMSE-TEQ) [3] and direct adaptation turbo equalizer (DA-TEQ) [12]. In CE MMSE-TEQ, the UWA channel is explicitly estimated and incorporated into the calculation of MMSE equalizer coefficients. Alternatively, the DA-TEQ uses adaptive algorithms to directly equalize the received symbols without the knowledge of the UWA channel.

1.2 PROBLEM STATEMENT

The existing CE MMSE-TEQs can be roughly classified into two categories. First, Turbo MMSE Linear Equalizers (LE) have been proposed in [5, 6, 7]. The exact implementation of the Turbo MMSE LE is capable of approaching the performance of MAP equalizer, but requires equalizer coefficients computation at each symbol, resulting in a time-varying equalizer whose complexity is quadratic with the MIMO size and the equalizer length, which is prohibitively high for UWA communications. The approximate implementation of Turbo MMSE LE (approximate Turbo LE) with no a priori information only updates the equalizer coefficients once at each block. Hence the approximate Turbo LE achieves complexity that is a linear function of the product of

the MIMO size and equalizer length. However, the approximate Turbo LE requires a large number of iterations to converge in tough channels, which leads to long latency and may be impractical in real-time applications.

Second, Turbo decision feedback equalizers (DFE) have been proposed for severe ISI channels, which exhibit the advantages of low complexity and fast convergence [8,11,9,10]. Especially, for harsh channels with deep spectral nulls, Turbo DFEs exhibit less noise enhancement and better Bit-Error-Rate (BER) performance than Turbo LEs. For example, the soft-decision feedback Turbo equalizer (SDFE) [9, 10] achieves good performance in severe ISI channels while its complexity is a linear function of the product of the MIMO size and channel length. In single-input single-output (SISO) systems with multilevel modulations, the SDFE even achieves better performance with lower complexity, lower Signal-to-Noise-Ratio (SNR) threshold and faster convergence than the exact Turbo LE [9]. However, the SDFE suffers from a higher error floor than the exact Turbo LE at high SNR region. Besides, the SDFE only considers the causal feedback and ignores the residual anti-causal ISI, which limits its performance in severe triply selective MIMO UWA channels [10].

In CE MMSE-TEQ, the UWA channel is explicitly estimated for the calculation of MMSE equalizer coefficients. The performance of the CE MMSE-TEQs have been verified by many oceans experiments [2, 3]. However, due to the typically long channel impulse response, the large-dimension matrix inversion involved in the equalizer coefficients computation contributes greatly to the overall receiver complexity. Alternatively, the DA-TEQ greatly lowers the complexity of the receiver by using the adaptive algorithms to directly estimate the coefficients of the equalizer without matrix inversion operation [12]. In most existing DA-TEQs, equalizer coefficient adaptation is performed with the decision-directed (DD) method after the training phase. At the DD mode, the current tentative hard decision at the output of the equalizer is used to drive the adaptation of the equalizer coefficients. Such an empirical processing method is widely used in existing UWA communication systems employing adaptive turbo equalizers.

The main drawback of the hard decision directed adaptation is the error propagation, which may results into a catastrophic failure of the convergence. Especially in fast time varying MIMO UWA channels, due to the higher probability of incorrect symbol decision and extremely long equalizer length, the error propagation effect is further amplified.

Motivated by the respective advantages and limitations of the methods in the literature, we proposed several low-complexity receiver algorithms to enable robust MIMO UWA communications.

1.3 SUMMARY OF CONTRIBUTIONS

This dissertation consists of a couple of journal publications and conference papers listed in the publication list. My contributions that are published or under review are:

1. This dissertation proposes a bidirectional soft-decision feedback turbo equalization (Bi-SDFE) for MIMO Systems. The proposed Bi-SDFE incorporates the bidirectional structure with two parallel SDFEs: a time-reversed SDFE and a normal SDFE. To harvest the time-reverse diversity in MIMO systems with multilevel modulations, a simple and effective linear combining scheme is derived to combine the extrinsic information at the outputs of the two SDFEs. Both BER simulation results and Extrinsic Information Transfer (EXIT) chart analysis show that the Bi-SDFE achieves significant performance improvement over the original SDFE without increasing computation complexity. Moreover, the Bi-SDFE even outperforms the well-known exactly implemented Turbo LE at medium-to-high SNR region. The obvious performance gain of the proposed Bi-SDFE has been verified through a real world underwater acoustic communication experiment with tough channel conditions.

2. A efficient DA-TEQ scheme is proposed for MIMO UWA communications. Compared with existing DA-TEQs, the proposed DA-TEQ scheme is enhanced through using the *a posterior* soft decisions as the reference symbols for filter adaptation as well

as the iterative processing inside the adaptive equalizer itself. The proposed DA-TEQ is efficient in four aspects: first, it achieves robust performance in tough MIMO UWA channels with extremely long delay spread, fast time variation and strong spatial correlation; second, it exhibits high spectral efficiency by requiring relatively short training overhead; third, the proposed adaptive turbo receiver converges rapidly in the highly dispersive MIMO UWA channels, thus is time efficient; fourth, it is computationally efficient by adopting the low complexity adaptive algorithm without matrix inversion operation. The aforementioned efficiencies of the proposed DA-TEQ have been verified by the experimental data collected in the 2008 Surface Processes and Acoustic Communications Experiment (SPACE08). Both the normalized least mean square (NLMS) and the sparsity enhanced improved proportionate normalized least mean squares (IPNLMS) algorithm are tested in the proposed turbo receiver. Moreover, the proposed scheme achieves satisfactory performance even in MIMO transmission with multilevel modulations and more than two concurrent data streams, which has not been reported for any existing DA-TEQs.

3. A low complexity frequency domain iterative detection scheme is proposed for the uncoded zero padding (ZP) single carrier (SC) transmission in MIMO UWA channels. A soft-decision block iterative frequency-domain equalization (BI-FDE) combined with iterative channel estimation is designed to enhance the performance of the ZP SC systems with high data efficiency. Benefiting from the iteratively increased quality of symbol detection and channel estimation, the proposed BI-FDE achieves obvious performance gain over the non-iterative FDE. The performance enhancement of the proposed iterative receiver has been verified through a pool test. Moreover, since both the feedfoward and feedback filters are designed in frequency domain without channel coding, the proposed iterative receive scheme is promising for hardware implementation.

4. This dissertation also evaluates the CE MMSE-TEQs and the DA-TEQ in single-input single-output (SISO) UWA channels. For CE MMSE-TEQ, the recently proposed Bi-SDFE is compared with the SDFE and the approximate Turbo LE in terms

of the BER performance. For DA-TEQ, the recently proposed soft-decision DA-TEQ is evaluated with the same set of experimental data. The field trial data collected in SPACE08 experiment are used in the performance evaluation. Experimental results show that the CE-TEQs are robust in SISO underwater acoustic transmission under tough channel conditions. With low pilot overheads, the recently proposed Bi-SDFE achieved lowest BER performance in all cases with slightly higher computational complexity. For QPSK modulation, all CE-TEQs and DA-TEQ are capable to achieve extraordinary low BER performance for in all packets.

1.4 REFERENCES

[1] M. Stojanovic and J. Preisig, "Underwater acoustic communication channels: Propagation models and statistical characterization," *IEEE Commun. Mag.*, vol. 47, no. 1, pp. 84–89, Jan. 2009.

[2] J. Tao, Y. R. Zheng, C. Xiao, and T. Yang, "Robust MIMO underwater acoustic communications using turbo block decision-feedback equalization," *IEEE J. Oceanic Eng.*, vol. 35, no. 1, pp. 90–99, Jan. 2010.

[3] Z. Yang and Y. R. Zheng, "Iterative channel estimation and turbo equalization for multiple-input multiple-output underwater acoustic communications," *IEEE J. Ocean. Eng.*, vol. 41, no. 41, pp. 232–242, Jan. 2016.

[4] C. Douillard, M. Jézéquel, C. Berrou, D. Electronique, A. Picart, P. Didier, and A. Glavieux, "Iterative correction of intersymbol interference: Turbo-equalization," *European Trans. Telecommun.*, vol. 6, no. 5, pp. 507–511, May 1995.

[5] M. Tuchler, R. Koetter, and A. C. Singer, "Turbo equalization: principles and new results," *IEEE Trans. Commun.*, vol. 50, no. 5, pp. 754–767, May 2002.

[6] M. Tuchler, A. C. Singer, and R. Koetter, "Minimum mean squared error equalization using a priori information," *IEEE Trans. Signal Process.*, vol. 50, no. 3, pp. 673–683, Mar. 2002.

[7] T. Abe, S. Tomisato, and T. Matsumoto, "A MIMO turbo equalizer for frequency-selective channels with unknown interference," *IEEE Trans. Veh. Technology*, vol. 52, no. 3, pp. 476–482, Mar. 2003.

[8] R. R. Lopes and J. R. Barry, "The soft-feedback equalizer for turbo equalization of highly dispersive channels," *IEEE Trans. Commun.*, vol. 54, no. 5, pp. 783–788, May 2006.

[9] H. Lou and C. Xiao, "Soft-decision feedback turbo equalization for multilevel modulations," *IEEE Trans. Signal Process.*, vol. 59, no. 1, pp. 186–195, Jan. 2011.

[10] A. Rafati, H. Lou, and C. Xiao, "Low-complexity soft-decision feedback turbo equalization for MIMO systems with multilevel modulations," *IEEE Trans. Veh. Technology*, vol. 60, no. 7, pp. 3218–3227, Jul. 2011.

[11] J. Wu and Y. R. Zheng, "Low complexity soft-input soft-output block decision feedback equalization," *IEEE J. Sel. Areas Commun.*, vol. 26, no. 2, pp. 281–289, Feb. 2008.

[12] J. W. Choi, T. J. Riedl, K. Kim, A. C. Singer, and J. C. Preisig, "Adaptive linear turbo equalization over doubly selective channels," *IEEE J. Ocean. Eng.*, vol. 36, no. 4, pp. 473–489, Oct. 2011.

PAPER

I. BIDIRECTIONAL SOFT-DECISION FEEDBACK TURBO EQUALIZATION FOR MIMO SYSTEMS

Weimin Duan and Yahong Rosa Zheng, *Fellow, IEEE*

ABSTRACT—This paper proposes a bidirectional soft-decision feedback Turbo equalizer (Bi-SDFE) for severe triply-selective fading channels. The proposed Bi-SDFE uses a time-reversed soft-decision feedback equalizer (SDFE) in conjunction with a normal SDFE to harvest time-reverse diversity and mitigate error propagation. A simple and effective linear combining scheme is derived for combining the extrinsic information of the two SDFEs for multiple-input multiple-output (MIMO) systems with both Binary Phase Shift Keying (BPSK) and multilevel modulation. The Bit-Error-Rate (BER) simulation results show that the proposed Bi-SDFE exhibits a lower Signal-to-Noise-Ratio (SNR) threshold than the original SDFE and outperforms the well-known Exact Turbo Minimum Mean Square Error (MMSE) Linear Equalizers at medium-to-high SNRs. Moreover, both Extrinsic Information Transfer (EXIT) chart analysis and BER simulation results show that the Bi-SDFE achieves better performance than the original SDFE while the Bi-SDFE uses only half the number of iterations of the SDFE. Therefore, the total computational complexity of the Bi-SDFE is similar to that of the original SDFE, which is a linear function of the channel length, MIMO size, and modulation constellation size. The performance gain of the proposed Bi-SDFE is also verified through an underwater acoustic communication experiment with tough channel conditions.

1 INTRODUCTION

Multiple-input-multiple-output (MIMO) communication technology has long been recognized as an essential part of high performance wireless communication systems [1]. However, robust MIMO receiver design still exhibits unique technical challenges, especially in severe triply-selective MIMO channels [2]. By severe triply-selective channel, we mean those MIMO channels that simultaneously experience frequency selectivity, temporal selectivity, and spatial selectivity. Severe frequency selectivity means extremely long delay spread. Temporal selectivity is caused by large Doppler spread and spatial selectivity is due to angular spreads among multiple transmit elements or among multiple receive elements. Examples of such channels include applications of mobile television receivers [3], underwater acoustic (UWA) MIMO communications [4, 5], and high data-rate communications involving multiple MIMO relays [6].

Turbo equalization is an effective means to achieve near optimal detection for MIMO triply-selective channels with affordable computational complexity. The maximum *a posteriori* probability (MAP) equalizer and MAP decoder were adopted in the initially proposed Turbo equalizer [7]. However, the complexity of the MAP equalizer grows exponentially with the product of the MIMO size and channel length, which is prohibitively high in severe triply-selective channels. To reduce the computational complexity, Turbo Minimum Mean Square Error (MMSE) Linear Equalizers (LE) have been designed [8, 9, 10]. Especially, the low-complexity Turbo LE can achieve a complexity that is a linear function of the product of the MIMO size and channel length. However, the low-complexity Turbo LE requires a large number of iterations to converge, which leads to long processing time and may be impractical in real-time applications.

Recently, Turbo decision feedback equalizers (DFE) have been proposed for severe ISI channels, which exhibit the advantages of low complexity and fast convergence [11,12,13,14]. Especially, for harsh channels with deep spectral nulls, Turbo DFEs

exhibit less noise enhancement and better Bit-Error-Rate (BER) performance than Turbo LEs [1]. For example, the soft-decision feedback Turbo equalizer (SDFE) [13,14] achieves good performance in severe ISI channels while maintaining linear computational complexity. In single-input single-output (SISO) systems with multilevel modulations, the SDFE [13] achieves better performance with lower complexity, lower Signal-to-Noise-Ratio (SNR) threshold and faster convergence than the exact Turbo LE [9]. However, the SDFE suffers from a higher error floor than the exact MMSE-LE at high SNRs. In addition, the SDFE only includes causal feedback and ignores the residual interference from anti-causal symbols, which limits its performance in MIMO channels with severe ISI and co-channel interference [14].

Interestingly, a bidirectional structure has been developed for decision feedback equalizer to improve its performance by utilizing a time-reversed DFE in combination with a normal DFE [15, 16, 17, 18, 19, 20, 21, 22]. Bidirectional equalizers were first introduced for hard-decision DFEs [15, 16, 17] to reduce error propagation inherent to DFEs. It was shown [18] that the bidirectional structure can also harvest the diversity provided by the two DFEs because the past symbols are known to the normal DFE and the future symbols are known to the time-reversed DFE. The diversity not only reduces error propagation, but also lowers noise enhancement because the noise of the two DFEs have low correlation. This hard-decision bidirectional DFE is used in a time reversal UWA communication system as a post processor [19] while the time-reversal filters are used for pre-processing. The work in [23] introduces an arbitration mechanism with filtering to exploit the error distributions at the outputs of the normal and time-reversed DFEs. Later, the bidirectional structure is applied in trellis-based delayed decision feedback soft-output turbo equalizers [20, 21] which combines the soft symbols of the two DFEs in each iteration and feeds the combined symbols to the decoder. More recently, a low-complexity soft-input soft-output bidirectional DFE (Bi-DFE) [22] combines extrinsic information instead of soft symbols of the two DFEs. The performance of the soft Bi-DFE [22] is said to approach that of MAP equalizers for

Binary Phase Shift Keying (BPSK) after a large number of iterations. However, most of the existing Bi-DFE schemes [15,16,17,18,19,20,21,22] are investigated for single-input single-output systems and use hard-decision symbols as the input to the feedback filter. In addition, the Bi-DFE in [22] is based on a modified hard-decision turbo DFE which has to estimate the probability of error sequences, thus exhibiting high computational load when the number of feedback filter taps or the size of the signal constellation is large.

In this paper, we propose a bidirectional SDFE (Bi-SDFE) that incorporates the bidirectional structure with the SDFE for MIMO systems. The proposed Bi-SDFE scheme utilizes the soft symbols in both feed-forward and feedback filtering and extends the extrinsic information combining scheme to MIMO systems with multilevel modulation. We derive a simple and effective linear combining scheme to explore the time-reverse diversity in the two sets of SDFE outputs for severe triply-selective channels. The computational complexity of the Bi-SDFE is slightly higher than the original SDFE because the Bi-SDFE uses only half the number of iterations required by the original SDFE. The overall complexity of the proposed Bi-SDFE and the original SDFE remains a linear function of the channel length, constellation size, and MIMO size. The BER performance and convergence property of the proposed Bi-SDFE are demonstrated by computer simulations and Extrinsic Information Transfer (EXIT) chart analysis. In addition, we verify the performance of the Bi-SDFE using field test data collected in an undersea acoustic communication experiment, where the MIMO channels exhibit not only severe ISI and Doppler spread, but also impulsive interference. Results of the real-world experiment show that the proposed Bi-SDFE achieves consistent improvement of BER performance over the original MIMO SDFE [14].

Throughout this paper, we use the following notational conventions: superscripts $(\cdot)^T$ and $(\cdot)^H$ represent matrix transpose and conjugate transpose, $E\{\cdot\}$ denotes statistical expectation and $\mathrm{diag}(a_1, \cdots, a_k)$ denotes a diagonal matrix with $a_1, \cdots, a_k$ being the diagonal entries.

2 SYSTEM DESCRIPTION

We consider an $N \times M$ MIMO communication system depicted in Fig. 2.1, where N and M are the numbers of transmit and receive elements, respectively. At the transmitter, the information bit sequence is converted into N parallel streams $\{\mathbf{b}^{(n)}\}_{n=1}^{N}$. Each bit stream is then independently encoded, interleaved, and modulated. The output of the nth interleaver is grouped as a length-K_c block $\mathbf{c}^{(n)} = \left[\mathbf{c}_1^{(n)} \;\; \mathbf{c}_2^{(n)} \cdots \mathbf{c}_{K_c}^{(n)}\right]$ where $\mathbf{c}_k^{(n)}$ represents the kth bit vector $\left[c_{k,1}^{(n)} \;\; c_{k,2}^{(n)} \cdots c_{k,q}^{(n)}\right]$ with the jth bit $c_{k,j}^{(n)} \in \{0, 1\}$. The mapper then maps each bit vector $\mathbf{c}_k^{(n)}$ to a symbol $x_k^{(n)}$ from the 2^q-ary constellation set $S = \{\alpha_1, \alpha_2, \cdots, \alpha_{2^q}\}$, where α_i corresponds to the deterministic bit pattern $\mathbf{s}_i = [s_{i,1} \;\; s_{i,2} \cdots s_{i,q}]$ with $s_{i,j} \in \{0, 1\}$, which specifies the mapping between the interleaved encoded bits and the elements of the constellation. After symbol mapping, the baseband signal is partitioned into blocks and modulated with a single carrier, then transmitted to the MIMO multipath channel.

On the receiver side, the received signals are demodulated and sampled to yield symbol rate baseband signals. The baseband signal at the mth receive element at time instant k can be written as

$$y_k^{(m)} = \sum_{n=1}^{N} \sum_{l=0}^{L-1} h_l^{(m,n)} x_{k-l}^{(n)} + w_k^{(m)} \tag{1}$$

where $x_{k-l}^{(n)}$ is the symbol transmitted by the nth transmit element at time instant $k-l$ and $h_l^{(m,n)}$ is the lth coefficient of the baseband equivalent channel between the nth transmitter and the mth receiver. In addition, L is the length of the baseband equivalent channel, and $w_k^{(m)}$ represents the noise sample at the mth receiver, which is assumed to be zero mean additive white Gaussian noise (AWGN) with variance σ_w^2. Stacking up

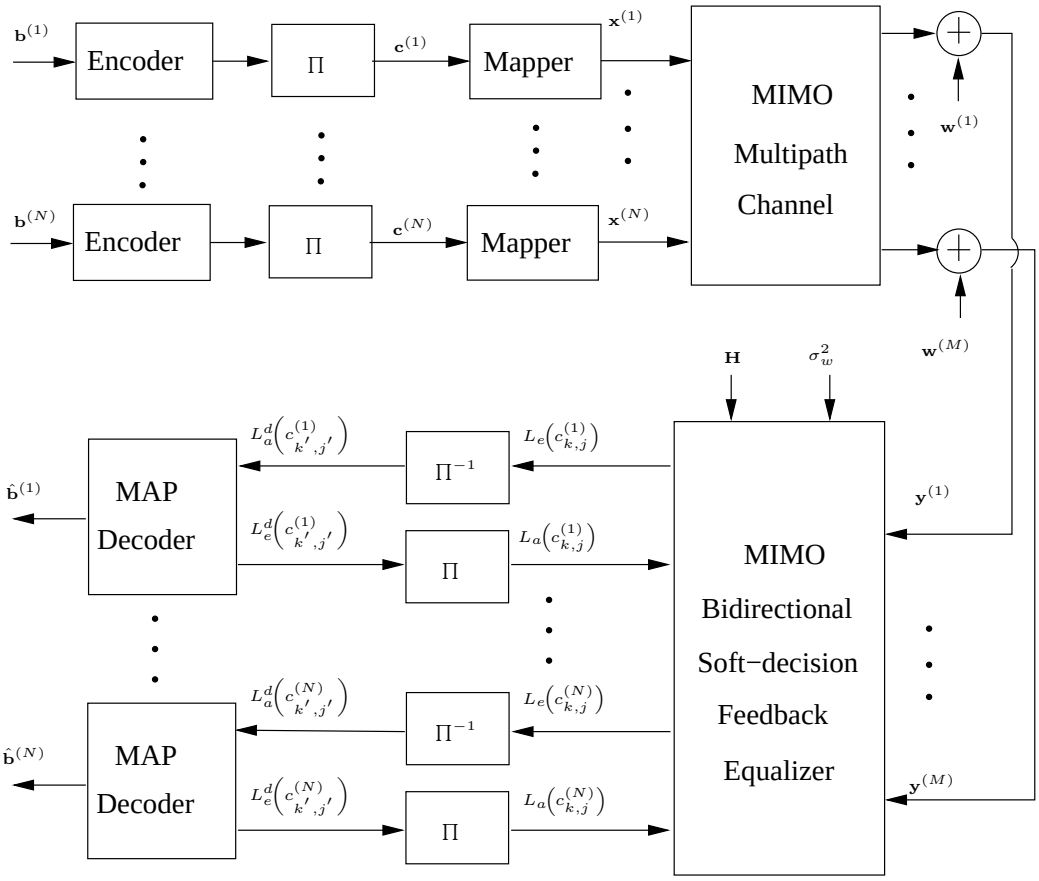

Figure 2.1. Structure of a MIMO communication system with turbo equalizer.

the received symbols at all M receiver antennas as $\mathbf{y}_k = [y_k^{(1)}, y_k^{(2)}, \ldots, y_k^{(M)}]^T$, we have

$$\mathbf{y}_k = \sum_{l=0}^{L-1} \mathbf{h}_l \mathbf{x}_{k-l} + \mathbf{w}_k \tag{2}$$

where

$$\mathbf{x}_k = [x_k^{(1)}, x_k^{(2)}, \ldots, x_k^{(N)}]^T \tag{2a}$$

$$\mathbf{w}_k = [w_k^{(1)}, w_k^{(2)}, \ldots, w_k^{(M)}]^T \tag{2b}$$

$$\underbrace{\begin{bmatrix} \mathbf{y}_{k-N_2} \\ \vdots \\ \mathbf{y}_k \\ \vdots \\ \mathbf{y}_{k+N_1} \end{bmatrix}}_{\mathbf{Y}_k} = \underbrace{\begin{bmatrix} \mathbf{h}_{L-1} & \cdots & \mathbf{h}_0 & \cdots & \cdots & 0 \\ \vdots & \ddots & \ddots & \ddots & & \vdots \\ & & \ddots & \ddots & \ddots & \vdots \\ 0 & \cdots & & \mathbf{h}_{L-1} & \cdots & \mathbf{h}_0 \end{bmatrix}}_{\mathbf{H}} \times \underbrace{\begin{bmatrix} \mathbf{x}_{k-N_2-L+1} \\ \vdots \\ \mathbf{x}_k \\ \vdots \\ \mathbf{x}_{k+N_1} \end{bmatrix}}_{\mathbf{X}_k} + \underbrace{\begin{bmatrix} \mathbf{w}_{k-N_2} \\ \vdots \\ \mathbf{w}_k \\ \vdots \\ \mathbf{w}_{k+N_1} \end{bmatrix}}_{\mathbf{W}_k} \tag{4}$$

and

$$\mathbf{h}_l = \begin{bmatrix} h_l^{(1,1)} & h_l^{(1,2)} & \cdots & h_l^{(1,N)} \\ h_l^{(2,1)} & h_l^{(2,2)} & \cdots & h_l^{(2,N)} \\ \vdots & \vdots & \ddots & \vdots \\ h_l^{(M,1)} & h_l^{(M,2)} & \cdots & h_l^{(M,N)} \end{bmatrix}. \tag{2c}$$

Therefore, the space-time representation of the MIMO system is given by

$$\mathbf{Y}_k = \mathbf{H}\mathbf{X}_k + \mathbf{W}_k \tag{3}$$

where $\mathbf{Y}_k$, $\mathbf{H}$, $\mathbf{X}_k$ and $\mathbf{W}_k$ are defined in (4). Note that $\mathbf{Y}_k$, $\mathbf{X}_k$ and $\mathbf{W}_k$ are the concatenated column vectors with elements defined in (2), (3) and (4), respectively. The observation window lengths N_1 and N_2 denote the causal and noncausal parts, respectively, of the received symbols at time instant k which are determined by the location of the strongest tap of the channel impulse response with respect to the other taps.

The iterative equalization and decoding process is also depicted in Fig. 2.1, where the MIMO Bi-SDFE estimates the symbols $\hat{x}_k^{(n)}$ block by block, and outputs the corresponding extrinsic information of the transmitted bits $L_e\left(c_{k,j}^{(n)}\right)$. The extrinsic

information is then passed to the de-interleaver, and the de-interleaved extrinsic information $L_e\left(c_{k',j'}^{(n)}\right)$ is treated as the *a priori* information $L_a^d\left(c_{k',j'}^{(n)}\right)$ for MAP decoding. After decoding, the decoder outputs its extrinsic information $L_e^d\left(c_{k',j'}^{(n)}\right)$, which is further fed back to the equalizer (after interleaving) as the *a priori* information $L_a\left(c_{k,j}^{(n)}\right)$ of the transmitted bit sequence. Based on the turbo principle, the extrinsic information and the *a priori* information are exchanged between the equalizer and decoder iteratively with the reliability of the soft information increasing with the number of iterations. The final hard decision $\hat{b}_k^{(n)}$ is made after multiple iterations or after the decoder output converges.

3 PROPOSED BIDIRECTIONAL SDFE

In this section, a MIMO Bi-SDFE scheme with multilevel modulation is developed.

3.1 BIDIRECTIONAL SOFT-DECISION FEEDBACK EQUALIZER STRUCTURE

The structure of the proposed Bi-SDFE is depicted in Fig. 3.1, where two SDFEs run in parallel: one is a normal SDFE with details illustrated in the dashed box, the other is a time-reversed SDFE whose internal structure is the same as the normal SDFE. Note, time reverse here refers to the operation of blockwise sequence flipping in time without filtering, which is slightly different from the concept of time reversal in underwater acoustic communications [24]. The log likelihood ratio (LLR) outputs of the two SDFEs, denoted as $L_{e,f}\left(c_{k,j}^{(n)}\right)$ and $L_{e,b}\left(c_{k,j}^{(n)}\right)$ for $n = 1, \cdots, N$, are combined via the weighting factors $\lambda_{j,f}^{(n)}$ and $\lambda_{j,b}^{(n)}$, respectively.

At the front end of the time-reversed SDFE, the received sequence $\mathbf{y}_k$ and the

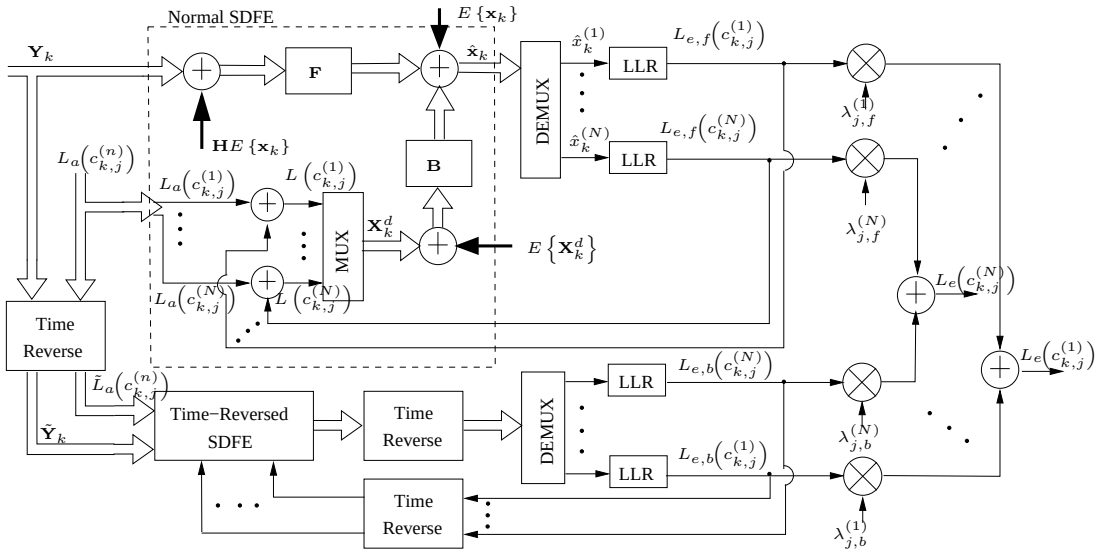

Figure 3.1. Block Diagram of the Proposed MIMO Bi-SDFE

channel impulse response matrix $\mathbf{h}$ are both flipped, resulting in an equivalent time-reversed baseband discrete model

$$\tilde{\mathbf{y}}_k = \sum_{l=0}^{L-1} \tilde{\mathbf{h}}_l \tilde{\mathbf{x}}_{k-l} + \tilde{\mathbf{w}}_k \tag{5}$$

where

$$\tilde{\mathbf{y}}_k = [y^{(M)}_{K_c-k+1}, y^{(M-1)}_{K_c-k+1}, \ldots, y^{(1)}_{K_c-k+1}]^T \tag{5a}$$

$$\tilde{\mathbf{x}}_k = [x^{(1)}_{K_c-k+1}, x^{(2)}_{K_c-k+1}, \ldots, x^{(N)}_{K_c-k+1}]^T \tag{5b}$$

$$\tilde{\mathbf{w}}_k = [w^{(M)}_{K_c-k+1}, w^{(M-1)}_{K_c-k+1}, \ldots, w^{(1)}_{K_c-k+1}]^T \tag{5c}$$

and

$$\tilde{\mathbf{h}}_l = \begin{bmatrix} h^{(M,1)}_{L-l+1} & h^{(M,2)}_{L-l+1} & \cdots & h^{(M,N)}_{L-l+1} \\ h^{(M-1,1)}_{L-l+1} & h^{(M-1,2)}_{L-l+1} & \cdots & h^{(M-1,N)}_{L-l+1} \\ \vdots & \vdots & \ddots & \vdots \\ h^{(1,1)}_{L-l+1} & h^{(1,2)}_{L-l+1} & \cdots & h^{(1,N)}_{L-l+1} \end{bmatrix}. \tag{5d}$$

Rewriting the time-reversed system model (5) into matrix form, we have

$$\tilde{\mathbf{Y}}_k = \tilde{\mathbf{H}}\tilde{\mathbf{X}}_k + \tilde{\mathbf{W}}_k \tag{6}$$

where $\tilde{\mathbf{Y}}_k$, $\tilde{\mathbf{H}}$ and $\tilde{\mathbf{X}}_k$ are defined in a similar manner as in (4), but with the time-reversed signals $\tilde{\mathbf{y}}_k$, $\tilde{\mathbf{x}}_k$, $\tilde{\mathbf{w}}_k$, and the time-reversed channel impulse response $\tilde{\mathbf{h}}_l$.

The equivalent channel impulse response in the time-reversed system model (5d) is the time reverse of the original channel impulse response, which results in reversed root locations, *i.e.,* the minimum phase roots of the original channel response become the maximal phase roots of the time-reversed channel and vice-versa. This property partially explains the performance improvement of the Bi-SDFE over the original SDFE in two aspects. First, if the channel is asymmetric, then the equivalent time-reversed channel is different from the original channel, which results in different error patterns

at the outputs of the normal SDFE and the time-reversed SDFE. The low correlation of the error locations at the output of the two SDFEs provides diversity which can be exploited to improve system performance. Second, without an anti-causal feedback filter, the original SDFE is inefficient at removing the precursor ISI. However, with the bidirectional structure, past symbols are detected by the normal SDFE, and future symbols are available from the time-reversed SDFE, thus Bi-SDFE can effectively cancel both precursor ISI and postcursor ISI.

3.2 SOFT-DECISION FEEDBACK EQUALIZERS FOR BI-SDFE

The SDFEs in the proposed Bi-SDFE are modified from the original SDFE [13], [14]. The original SDFE is a mixed soft-decision DFE which adopts a linear equalizer in the first iteration and utilizes soft DFE in the subsequent iterations. However, the proposed Bi-SDFE uses soft DFE in all iterations because the bidirectional structure can effectively reduce error propagation, resulting in better performance than a linear equalizer, especially in severe ISI channels with deep spectrum nulls.

The SDFE consists of a feedforward filter $\mathbf{F}_k \in \mathcal{C}^{N\times M(N_1+N_2+1)}$ and a feedback filter $\mathbf{B}_k \in \mathcal{C}^{N\times(NN_3)}$, where $N_3 = N_2 + L - 1$. The feedback filter is designed to cancel the residual causal ISI after feedforward filtering, and the time-varying offset $\mathbf{d}_k$ compensates for a possibly nonzero mean of the data symbols. Based on this SDFE structure, the estimated symbol $\hat{\mathbf{x}}_k$ is expressed as

$$\hat{\mathbf{x}}_k = \mathbf{F}_k\mathbf{Y}_k + \mathbf{B}_k\mathbf{X}_k^d + \mathbf{d}_k \tag{7}$$

where $\mathbf{Y}_k$ is defined in (4) and

$$\mathbf{X}_k^d = \left[\mathbf{x}_{k-N_3}^d, \mathbf{x}_{k-N_3+1}^d, \cdots, \mathbf{x}_{k-1}^d\right]^T \tag{7a}$$

$$\mathbf{x}_k^d = \left[(x_k^{(1)})^d, (x_k^{(2)})^d, \cdots, (x_k^{(N)})^d\right]^T. \tag{7b}$$

Here the superscript $(\cdot)^d$ denotes the operation of soft decision based on the *a posteriori* information $L\left(c_{k,j}^{(n)}\right)$. That is

$$\left(x_k^{(n)}\right)^d = \sum_{\alpha_i \in S} \alpha_i P\left(\left(\tilde{x}_k^{(n)}\right)^d = \alpha_i\right) \tag{8}$$

$$P\left(\left(\tilde{x}_k^{(n)}\right)^d = \alpha_i\right) = \prod_{j=1}^{q} \frac{1}{2}\left[1 + \tilde{s}_{i,j} \tanh\left(\frac{L\left(c_{k,j}^{(n)}\right)}{2}\right)\right] \tag{9}$$

where

$$\tilde{s}_{i,j} = \begin{cases} +1, & \text{if } s_{i,j} = 0 \\ -1, & \text{if } s_{i,j} = 1 \end{cases}$$

and

$$L\left(c_{k,j}^{(n)}\right) = L_a\left(c_{k,j}^{(n)}\right) + L_e\left(c_{k,j}^{(n)}\right). \tag{10}$$

In this paper, we use the low-complexity SDFE for the Bi-SDFE, which is implemented by forcing the related covariance matrices to be time invariant. The coefficients of the feedforward and feedback filter in the low-complexity SDFE are only updated at every iteration rather than for each time instance k. Therefore we drop the subscript k and design the filters of the SDFE [14] as

$$\mathbf{F}^H = \left[\sigma_w^2 \mathbf{I}_{N_o} + \mathbf{H}\left(\mathbf{C}^{ff} - \mathbf{C}^{fb}(\mathbf{C}^{bb})^{-1}(\mathbf{C}^{fb})^H\right)\mathbf{H}^H\right]^{-1}\mathbf{s} \tag{11}$$

$$\mathbf{B}^H = -\left(\mathbf{C}^{bb}\right)^{-1}\left(\mathbf{H}\mathbf{C}^{fb}\right)^H \mathbf{F}^H \tag{12}$$

$$\mathbf{d}_k = E\left\{\mathbf{x}_k\right\} - \mathbf{F}\mathbf{H}E\left\{\mathbf{X}_k\right\} - \mathbf{B}E\left\{\mathbf{X}_k^d\right\} \tag{13}$$

where $\mathbf{C}^{ff}$, $\mathbf{C}^{fb}$ and $\mathbf{C}^{bb}$ are the covariance matrices defined as

$$\mathbf{C}^{ff} = E\left\{\mathbf{X}_k\mathbf{X}_k^H\right\} - E\left\{\mathbf{X}_k\right\}E\left\{\mathbf{X}_k^H\right\} \tag{14a}$$

$$\mathbf{C}^{fb} = E\left\{\mathbf{X}_k\mathbf{X}_k^{dH}\right\} - E\left\{\mathbf{X}_k\right\}E\left\{\mathbf{X}_k^{dH}\right\} \tag{14b}$$

$$\mathbf{C}^{bb} = E\left\{\mathbf{X}_k^d\mathbf{X}_k^{dH}\right\} - E\left\{\mathbf{X}_k^d\right\}E\left\{\mathbf{X}_k^{dH}\right\} \tag{14c}$$

which are computed by the *a priori* information and the *a posteriori* information, as detailed in [14], and $\mathbf{s} = \mathbf{H}[\mathbf{0}_{N\times(N(N_2+L-1))}\ \mathbf{I}_N\ \mathbf{0}_{N\times(NN_1)}]^T$ is the selection vector. Note that $N_o = M(N_1 + N_2 + 1)$ is the overall length of the feedforward filter.

The design of the feedforward and feedback filters for the time-reversed SDFE follows the same principle as the normal SDFE. The details are omitted here for brevity.

3.3 EXTRINSIC INFORMATION COMBINING FOR BI-SDFE

In this subsection, we derive the weighting factors for extrinsic information combining of the MIMO Bi-SDFE with general modulation schemes. This is an extension to the LLR combining scheme derived for single-input single-output BPSK modulation in [22].

First, we form a vector of the two extrinsic LLRs from the normal SDFE and the time-reversed SDFE with respect to the same bit position j as

$$\mathbf{L}_{k,j}^{(n)} = \left[L_{e,f}\left(c_{k,j}^{(n)}\right)\ L_{e,b}\left(c_{k,j}^{(n)}\right)\right]^T. \tag{15}$$

We assume the random vector is jointly Gaussian and with a mean vector $\boldsymbol{\mu}_{k,j}^{(n)}$ and a covariance matrix $\boldsymbol{\Phi}_{j,n}$, such that the joint probability density function (PDF) of the two LLRs given a coded bit is

$$P\left(L_{e,f}\left(c_{k,j}^{(n)}\right), L_{e,b}\left(c_{k,j}^{(n)}\right)|c_{k,j}^{(n)}\right) = \frac{1}{2\pi\sqrt{\det(\boldsymbol{\Phi}_{j,n})}}\times \exp\left\{-\frac{1}{2}(\mathbf{L}_{k,j}^{(n)} - \boldsymbol{\mu}_{k,j}^{(n)})^T\boldsymbol{\Phi}_{j,n}^{-1}(\mathbf{L}_{k,j}^{(n)} - \boldsymbol{\mu}_{k,j}^{(n)})\right\} \tag{16}$$

where the mean vector $\boldsymbol{\mu}_{k,j}^{(n)} = \tilde{c}_{k,j}^{(n)}[\gamma_{j,f}^{(n)} \quad \gamma_{j,b}^{(n)}]^T$ with

$$\tilde{c}_{k,j}^{(n)} = \begin{cases} +1, & \text{if } c_{k,j}^{(n)} = 0 \\ -1, & \text{if } c_{k,j}^{(n)} = 1 \end{cases}$$

and the covariance matrix is

$$\mathbf{\Phi}_{j,n} = \begin{bmatrix} (\sigma_{j,f}^{(n)})^2 & \varrho_{j,n}\sigma_{j,f}^{(n)}\sigma_{j,b}^{(n)} \\ \varrho_{j,n}\sigma_{j,f}^{(n)}\sigma_{j,b}^{(n)} & (\sigma_{j,b}^{(n)})^2 \end{bmatrix}$$

with $\varrho_{j,n}$ being the correlation coefficients. Note that we use subscript n instead of superscript $^{(n)}$ in $\mathbf{\Phi}_{j,n}$ and $\varrho_{j,n}$ for notation convenience. Here we assume that the correlation coefficients remain the same for all k, because we use the low-complexity SDFEs in the Bi-SDFE scheme, which only designs one set of coefficients for all time instants k and the LLR outputs at all time instants approximately follow the same second-order statistics. We also assume that $\gamma_{j,f}^{(n)}$ (and $\gamma_{j,b}^{(n)}$) and $\sigma_{j,f}^{(n)}$ (and $\sigma_{j,b}^{(n)}$) are the same for all k. Note that $\gamma_{j,f}^{(n)}$ and $\sigma_{j,f}^{(n)}$ are the mean and variance of the extrinsic information $L_{e,f}\left(c_{k,j}^{(n)}\right)$ given $c_{k,j}^{(n)} = 0$, which are defined as

$$\gamma_{j,f}^{(n)} = E\left\{ L_{e,f}\left(c_{k,j}^{(n)}\right) \mid c_{k,j}^{(n)} = 0 \right\} \tag{17}$$

$$\sigma_{j,f}^{(n)} = E\left\{ \left(L_{e,f}\left(c_{k,j}^{(n)}\right)\right)^2 \mid c_{k,j}^{(n)} = 0 \right\} - \left(\gamma_{j,f}^{(n)}\right)^2. \tag{18}$$

Similarly, $\gamma_{j,b}^{(n)}$ and $\sigma_{j,b}^{(n)}$ are the mean and variance of the extrinsic information $L_{e,b}\left(c_{k,j}^{(n)}\right)$ given $c_{k,j}^{(n)} = 0$. A semi-analytical method for estimating the mean and variance of the extrinsic LLRs is given in [25].

The assumption of a joint Gaussian distribution for (16) is justified from the effectiveness of a Gaussian approximation of the individual SDFE output. It is commonly assumed that the extrinsic LLR output of soft equalizers is Gaussian distributed for linear and decision feedback equalizers [8, 26, 27, 25]. However, the LLR outputs of the two SDFEs in the proposed Bi-SDFE scheme are correlated because both SDFEs process the same received signal of the same channel, only with time reversed order. Therefore, we treat the two extrinsic LLRs as correlated Gaussian. Our simulation results, which will be presented in Sec. 4, also verifies that the joint Gaussian assumption is mostly accurate.

Next, we derive the weighting factors for LLR combining. The likelihood function of the extrinsic information of the Bi-SDFE is defined as

$$L_e\Big(c_{k,j}^{(n)}\Big) \triangleq \log \frac{P(L_{e,f}\Big(c_{k,j}^{(n)}\Big), L_{e,b}\Big(c_{k,j}^{(n)}\Big) | c_{k,j}^{(n)} = 0)}{P(L_{e,f}\Big(c_{k,j}^{(n)}\Big), L_{e,b}\Big(c_{k,j}^{(n)}\Big) | c_{k,j}^{(n)} = 1)}. \tag{19}$$

Note that the extrinsic LLRs are computed from the joint conditional probabilities of the LLR outputs of the two SDFEs.

To compute the LLR in (19), we note that the PDF in (16) can be re-written as [1]

$$\begin{aligned} &P\Big(L_{e,f}\Big(c_{k,j}^{(n)}\Big), L_{e,b}\Big(c_{k,j}^{(n)}\Big) | \tilde{c}_{k,j}^{(n)} = \pm 1\Big) \\ &\qquad = C \exp\left\{-\frac{A_f^2(\pm 1) - 2\varrho_{j,n} A_f(\pm 1) A_b(\pm 1) + A_b^2(\pm 1)}{2(1-\varrho_{j,n}^2)}\right\} \end{aligned} \tag{20}$$

where

$$\begin{aligned} A_f(\pm 1) &= \Big(L_{e,f}\Big(c_{k,j}^{(n)}\Big) \mp \gamma_{j,f}^{(n)}\Big) / \sigma_{j,f}^{(n)} \\ A_b(\pm 1) &= \Big(L_{e,b}\Big(c_{k,j}^{(n)}\Big) \mp \gamma_{j,b}^{(n)}\Big) / \sigma_{j,b}^{(n)} \\ C &= \frac{1}{2\pi \sigma_{j,f}^{(n)} \sigma_{j,b}^{(n)} \sqrt{1-\varrho_{j,n}^2}}. \end{aligned}$$

Then, substituting (20) into (19), and noting that

$$\begin{aligned} &A_f^2(-1) - A_f^2(+1) = 4 L_{e,f}\Big(c_{k,j}^{(n)}\Big) \gamma_{j,f}^{(n)} / (\sigma_{j,f}^{(n)})^2 \\ &A_b^2(-1) - A_b^2(+1) = 4 L_{e,b}\Big(c_{k,j}^{(n)}\Big) \gamma_{j,b}^{(n)} / (\sigma_{j,b}^{(n)})^2 \\ &A_f(+1) A_b(+1) - A_f(-1) A_b(-1) \\ &= -2 \Big[L_{e,f}\Big(c_{k,j}^{(n)}\Big) \gamma_{j,b}^{(n)} + L_{e,b}\Big(c_{k,j}^{(n)}\Big) \gamma_{j,f}^{(n)}\Big] / \Big(\sigma_{j,f}^{(n)} \sigma_{j,b}^{(n)}\Big) \end{aligned}$$

we find

$$L_{\mathrm{e}}\Big(c_{k,j}^{(n)}\Big) = \lambda_{j,f}^{(n)} L_{e,f}\Big(c_{k,j}^{(n)}\Big) + \lambda_{j,b}^{(n)} L_{e,b}\Big(c_{k,j}^{(n)}\Big) \tag{21}$$

where

$$\lambda_{j,f}^{(n)} = \frac{2/\sigma_{j,f}^{(n)}}{1-\varrho_{j,n}^2}\left(\frac{\gamma_{j,f}^{(n)}}{\sigma_{j,f}^{(n)}} - \frac{\varrho_{j,n}\gamma_{j,b}^{(n)}}{\sigma_{j,b}^{(n)}}\right) \tag{20a}$$

$$\lambda_{j,b}^{(n)} = \frac{2/\sigma_{j,b}^{(n)}}{1-\varrho_{j,n}^2}\left(\frac{\gamma_{j,b}^{(n)}}{\sigma_{j,b}^{(n)}} - \frac{\varrho_{j,n}\gamma_{j,f}^{(n)}}{\sigma_{j,f}^{(n)}}\right) \tag{20b}$$

which is a linear combining of the extrinsic information from the normal and time-reversed SDFEs.

Since the same parameters for the feedforward and feedback filters are used in both the normal and the time-reversed SDFEs, it is reasonable to assume that $\gamma_{j,f}^{(n)} \approx \gamma_{j,b}^{(n)}$ and $\sigma_{j,f}^{(n)} \approx \sigma_{j,b}^{(n)}$, which simplifies the combining weights into

$$\lambda_{j,f}^{(n)} = \lambda_{j,b}^{(n)} = \frac{2\gamma_{j,f}^{(n)}}{(1+\varrho_{j,n})(\sigma_{j,f}^{(n)})^2}. \tag{21}$$

Moreover, for both BPSK and multilevel modulation, it was observed from simulations that $\sigma_{j,f}^{(n)} \cong \sqrt{2\gamma_{j,f}^{(n)}}$, which was also found in [25]. This may be justified using the consistency condition [28] for the LLR-value distribution. The combining weights are further simplified to

$$\lambda_{j,f}^{(n)} = \lambda_{j,b}^{(n)} = \frac{1}{1+\varrho_{j,n}}. \tag{22}$$

As a special case of (22), if the system is single-input single-output with BPSK modulation, then $j = 1$, $n = 1$, and the linear combining scheme (21) coincides with the extrinsic information combining scheme in [22]. Note that if $\varrho_{j,n} = 1$, (20) becomes the PDF of a single Gaussian random variable and $\lambda_{j,f}^{(n)} = \lambda_{j,b}^{(n)} = 0.5$, then the proposed

combiner can be considered as a mean combining scheme.

To find the combining factors in (20a) and (20b), the variances are estimated via numerical estimation

$$(\hat{\sigma}_{j,f}^{(n)})^2 = \frac{1}{K_c - 1} \sum_{k=1}^{K_c} \left[L_{e,f}\Big(c_{k,j}^{(n)}\Big) - \hat{\mu}_{j,f}^{(n)} \right]^2 \tag{23a}$$

$$(\hat{\sigma}_{j,b}^{(n)})^2 = \frac{1}{K_c - 1} \sum_{k=1}^{K_c} \left[L_{e,b}\Big(c_{k,j}^{(n)}\Big) - \hat{\mu}_{j,b}^{(n)} \right]^2 \tag{23b}$$

where the mean $\hat{\mu}_{j,f}^{(n)}$ and $\hat{\mu}_{j,b}^{(n)}$ are estimated by time-averaging.

Similarly the correlation coefficient is estimated by averaging over k as

$$\hat{\varrho}_{j,n} = \frac{\sum_{k=1}^{K_c} \left[L_{e,f}\Big(c_{k,j}^{(n)}\Big) - \hat{\mu}_{j,f}^{(n)} \right] \left[L_{e,b}\Big(c_{k,j}^{(n)}\Big) - \hat{\mu}_{j,b}^{(n)} \right]}{(K_c - 1)\hat{\sigma}_{j,f}^{(n)} \hat{\sigma}_{j,b}^{(n)}}. \tag{24}$$

4 SIMULATION RESULTS

In this section, the performance of the proposed Bi-SDFE is evaluated by BER simulation in comparison to the Exact MMSE LE and the original SDFE. For all cases, the transmitted bits are encoded by a rate $R = 1/2$ convolutional code with generator polynomial $G = [7, 5]$ in octal notation, followed by a size-10560 random interleaver. We adopt a five tap 2×2 MIMO channel, which is also used in [14]. After normalization, the tap coefficients for each sub-channel are chosen as

$$\mathbf{h}_0 = \begin{bmatrix} 0.1965 & 0.4233 \\ 0.1818 & 0.8656 \end{bmatrix}, \quad \mathbf{h}_1 = \begin{bmatrix} 0.2031 & 0.3603 \\ 0.2208 & 0.8833 \end{bmatrix},$$

$$\mathbf{h}_2 = \begin{bmatrix} 0.2159 & 0.1283 \\ 0.2259 & 0.9412 \end{bmatrix}, \quad \mathbf{h}_3 = \begin{bmatrix} 0.2208 & 0 \\ 0.1728 & 0.9599 \end{bmatrix},$$

$$\mathbf{h}_4 = \begin{bmatrix} 0.2169 & 0 \\ 0.2006 & 0.9554 \end{bmatrix},$$

where $\mathbf{h}_k$ is defined in (5). These channels are considered severe ISI channels, as their frequency responses exhibit spectrum nulls.

For the normal SDFE and the time-reversed SDFE in the Bi-SDFE, we use the same filter parameters as the original SDFE: $N_1 = 9$, $N_2 = 5$, $N_3 = N_2 + L - 1$. For the Exact MMSE LE, the filter parameters are set as: $N_1 = 9$, $N_2 = 5$. The MAP decoder is implemented using the log-MAP algorithm.

The Gaussianity of the extrinsic information at the SDFE output is verified by numerical simulation, as illustrated in Fig. 4.1. The normalized histograms of the extrinsic LLRs at the equalizer output are plotted in dashed lines for the three bits of an 8PSK modulated signal stream of 10^4 symbols, while the solid lines are the theoretical Gaussian PDFs with the same means and variances as the measured ones in

the simulation. Comparing the simulated histograms with the theoretical PDF curves, we can see that they match with each other very well.

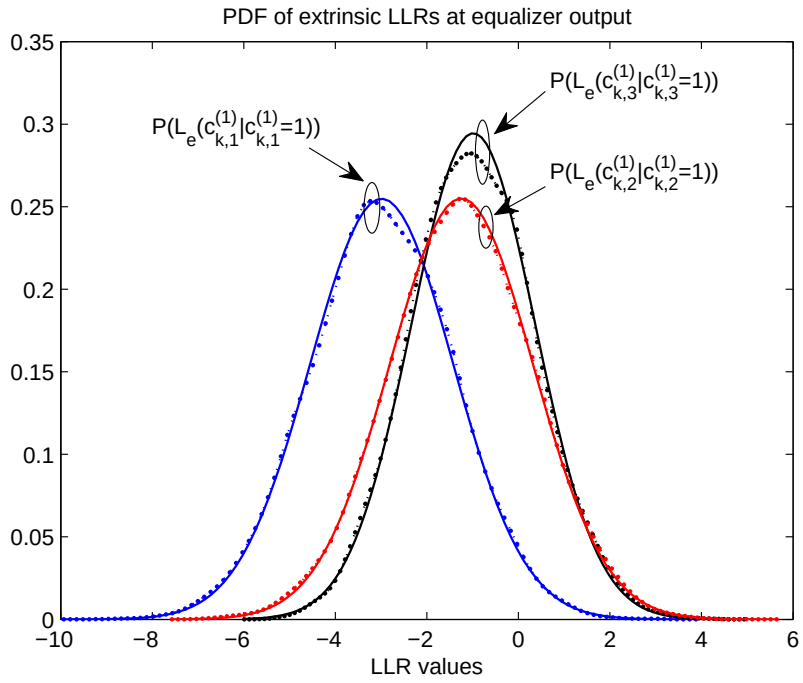

Figure 4.1. Extrinsic LLR distribution of the equalizer output at the second iteration, 8PSK modulation, SNR=26 dB. Note only the curves for the first transmitted signal stream ($n = 1$) with bits $c_{k,j}^{(1)} = 1$, $j = 1, 2, 3$ are plotted. The zero-bit LLR PDFs $P(L_e(c_{k,j}^{(1)}|c_{k,j}^{(1)} = 0))$ are symmetrical to those of $P(L_e(c_{k,j}^{(1)}|c_{k,j}^{(1)} = 1))$.

The BER performance of the proposed Bi-SDFE is shown in Fig. 4.2 with BPSK, QPSK, 8PSK and 16QAM modulation schemes with Gray mapping. In each sub-figure, the solid, dotted, and dashed lines denote the performance of the Bi-SDFE, the original SDFE, and the Exact MMSE LE, respectively. Note that the BER curves of the original SDFE of the first iteration are the same as the ones of the Exact MMSE LE because the original SDFE uses the MMSE LE in its first iteration.

Comparing the BER curves of the proposed Bi-SDFE with those of the original SDFE, we can see obvious improvement in all modulation schemes. At the BER level of 10^{-4}, the Bi-SDFE with two iterations gains about 3 dB over the original SDFE with

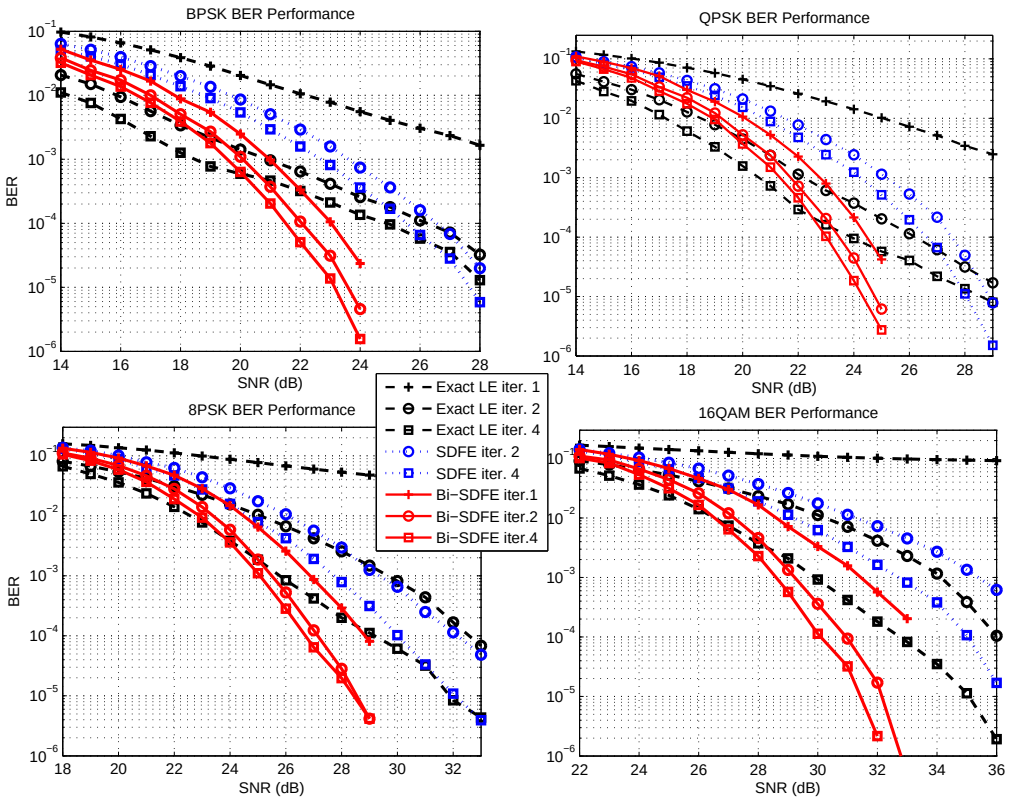

Figure 4.2. BER performance of different Turbo equalizers for a 2×2 MIMO system over a five-tap ISI channel.

four iterations for BSPK, QPSK, and 8PSK, while with 16QAM modulation, the performance gain is 4 dB. Since two SDFEs are used in parallel, the Bi-SDFE requires roughly twice as many computational operations per iteration as the original SDFE. Hence the computational load of the Bi-SDFE with two iterations is approximately the same as that of the original SDFE with four iterations. Considering the saved computation in decoding of the Bi-SDFE scheme, it is safe to say that the Bi-SDFE achieves significant performance improvement over the original SDFE without increasing complexity.

We also observe that, in the medium-to-high SNR region, the first iteration Bi-SDFE outperforms the original SDFE with multiple iterations. This performance enhancement is brought by the bidirectional decision feedback structure and the extrinsic information combining, which effectively lower the error propagation compared

with the original SDFE.

Comparing the performance of the proposed Bi-SDFE with the Exact MMSE LE, we see that the Bi-SDFE exhibits a lower SNR threshold than the Exact MMSE LE for all modulation schemes. For 8PSK and 16QAM modulation, the Bi-SDFEs also approaches the performance of the Exact MMSE LEs in the low SNR region. At the BER level of 10^{-4}, after four iterations, the Bi-SDFE outperforms the Exact MMSE LE by 3.5 dB, 1 dB, 2.5 dB and 3 dB with BPSK, QPSK, 8PSK and 16QAM modulation, respectively. The complexity of the Exact MMSE LE is a quadratic function of the filter length, while the complexity of the Bi-SDFE is a linear function of the number of filter coefficients. We conclude that the Bi-SDFE achieves a good trade-off between performance and complexity. Moreover, the Bi-SDFE converges faster than both the original SDFE and the Exact MMSE LE.

It is also interesting to note the performance difference between the original SDFE and the Exact MMSE LE in Fig. 4.2, where the Exact MMSE LE outperforms the original SDFE in all modulation schemes in the low-to-medium SNR region, although the original SDFE performs better than the Low complexity MMSE LE in the medium-to-high SNR regions for MIMO systems [14]. It is this performance gap that motivated the development of the proposed Bi-SDFE.

5 CONVERGENCE ANALYSIS

Turbo equalization is a highly nonlinear dynamic process which makes mathematical analysis difficult. However, the numerical tool of the EXIT chart [26] provides good insight of the convergence properties of the turbo process. EXIT charts visualize the exchange of mutual information between the equalizer and the decoder by describing the evolution of the average mutual information (MI) between the extrinsic information and the corresponding information (or coded) bits.

Assume the coded bits are equally likely and are denoted by $\tilde{c} \in \{\pm 1\}$. Denoting $\mathcal{L}$ as the LLR output of either the equalizer or decoder corresponding to the coded bit $\tilde{c}$, the mutual information between a coded bit and its LLR is given by [26]

$$\begin{aligned} \mathcal{I}_{\mathcal{L}}(\tilde{c}) &= \frac{1}{2}\sum_{\tilde{c}\in\pm 1}\int_{-\infty}^{\infty} P_{\mathcal{L}}(\xi|\tilde{c})\log_2\left(\frac{2P_{\mathcal{L}}(\xi|\tilde{c})}{P_{\mathcal{L}}(\xi|\tilde{c}=-1)+P_{\mathcal{L}}(\xi|\tilde{c}=+1)}\right)d\xi \qquad (25)\\ &= 1-\int_{-\infty}^{\infty} P_{\mathcal{L}}(\xi|\tilde{c}=+1)\log_2(1+e^{-\xi})d\xi \end{aligned}$$

where $P_{\mathcal{L}}(\mathcal{L}|\tilde{c})$ is the conditional PDF of the extrinsic information. The mutual information computed for the output of the turbo equalizer is denoted as IE_{on} for the nth transmit bit stream, and that computed for the output of the soft decoder is denoted as ID_{on}. The *a priori* MIs at the input of the equalizer (decoder) are the interleaved (de-interleaved) ID_{on} (IE_{on}) as

$$IE_{in} = \Pi(ID_{on}) \qquad (26)$$

$$ID_{in} = \Pi^{-1}(IE_{on}) \qquad (27)$$

for $n = 1, \cdots, N$.

For MIMO systems with $N = 2$ transmit elements, the EXIT curve is a two dimensional surface. In our analysis, we consider the five-tap 2×2 MIMO channel

that is used in the BER simulations in Section 4. We use the same filter parameters: $N_1 = 9, N_2 = 5, N_3 = N_2 + L - 1$ and the rate $R = 1/2$ convolutional code with generator polynomial $G = [7, 5]$. Figure 5.1 shows the EXIT charts for four modulation schemes at different SNRs, where only the MI transfer curves between the decoder of the first transmit bit stream ($n = 1$) and the equalizers of the first and second bit streams ($n = 1, 2$) are presented. In all sub-figures, the two dimensional surfaces of the proposed Bi-SDFE are above those of the original SDFE, which indicate faster convergence.

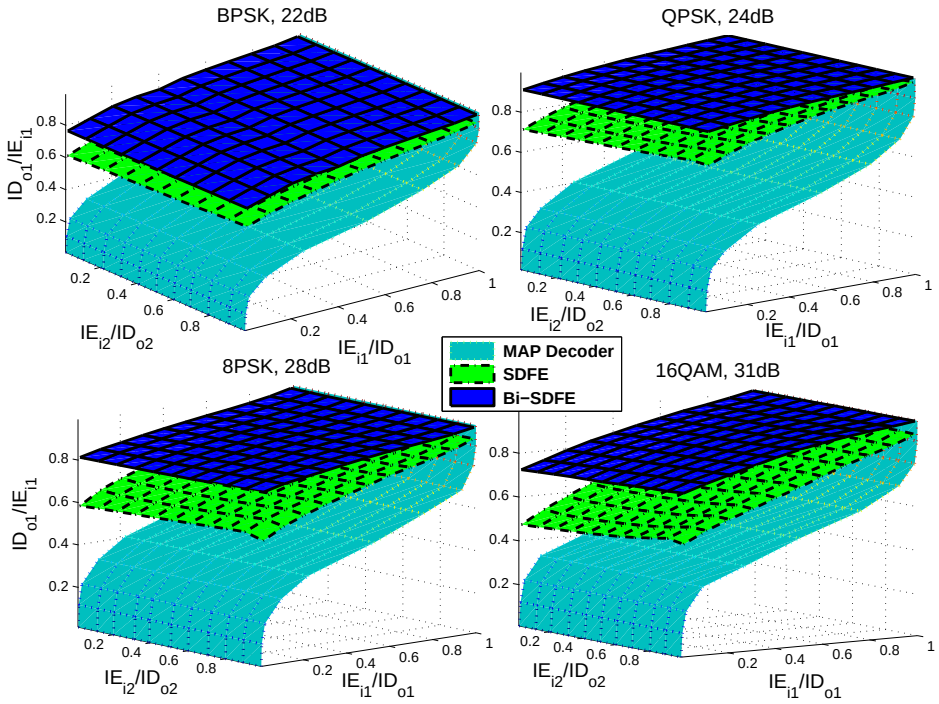

Figure 5.1. Three dimensional EXIT charts for the proposed Bi-SDFE and the original SDFE.

To better visualize the behaviors of the iterative equalizers, we further project the three dimensional EXIT chart for 16QAM modulation into a plane, as shown in Fig 5.2. Note that the lower and upper bounds are calculated by setting the decoder MI of the second transmitter as 0 and 1 respectively. Obviously, the MI gap between the

Bi-SDFE and the MAP decoder is larger than those between the original SDFE and the MAP decoder. As a benchmark, we also plot the MI transfer curves for the Exact MMSE LE in Fig 5.2. The tunnel widths between the transfer curves of the equalizers and the MAP decoder indicate that the Exact MMSE LE converges slightly faster than SDFE, but still slower than the Bi-SDFE, although it achieves almost the same highest mutual information as Bi-SDFE.

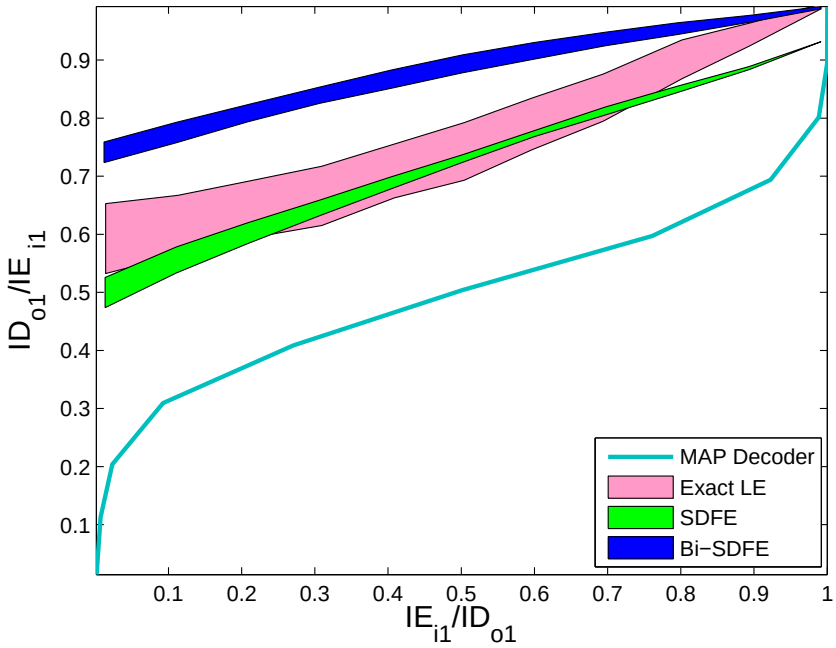

Figure 5.2. Two dimensional EXIT chart for 16QAM at SNR = 31 dB.

6 UNDERSEA EXPERIMENTAL RESULTS

The proposed MIMO Bi-SDFE was also verified by UWA communication data collected in the SPACE08 experiment which was conducted at the coast of Martha's Vineyard, Edgartown, MA, in October 2008. In this experiment, a MIMO single carrier acoustic communication system with QPSK, 8PSK, and 16QAM modulation was tested. A $rate = 1/2$ convolutional code with generator polynomial in octal notation $G = [17, 13]$ was chosen as the channel code. The center carrier frequency was $f_c = 13$ kHz. The symbol interval was 0.1024 ms, and the roll-off factor for the square-root raised cosine pulse shaping filter was chosen as $\beta = 0.2$. Thus the occupied bandwidth was 11.71875 kHz. Four transducers numbered 0 to 3 were used at the transmitter with Transducer 0 located on a fixed tripod at about 4 m above the ocean bottom. The other 3 transducers were fixed on a vertical array with 50 cm spacing. The top transducer on the vertical array was about 3 m above the ocean bottom. The depth of the experimental water area was about 15 m. Six sets of receive hydrophone arrays were used with a sampling rate of 39.0625 kilo-samples/s. The hydrophone arrays were also fixed with tripods. The top hydrophone of each array was about 3.3 m above the ocean bottom. Experiments were conducted for three transmission ranges: 60 m, 200 m and 1000 m. In this paper, we present the 2×6 MIMO results for 200 m and 1000 m transmissions which recorded 45 packets and 19 packets for the two-transducer systems, respectively.

The format of the transmission packet in the SPACE08 experiment is illustrated in Fig. 6.1, where each packet starts with an m-sequence (maximal-length sequence) [29] of length 511, followed by the data payload of 30 000 symbols with QPSK, 8PSK and 16QAM modulation, respectively.

Considering the harsh UWA channels in the experiment, we partitioned the received signals in the data payload into pilot blocks and overlapped subblocks, as

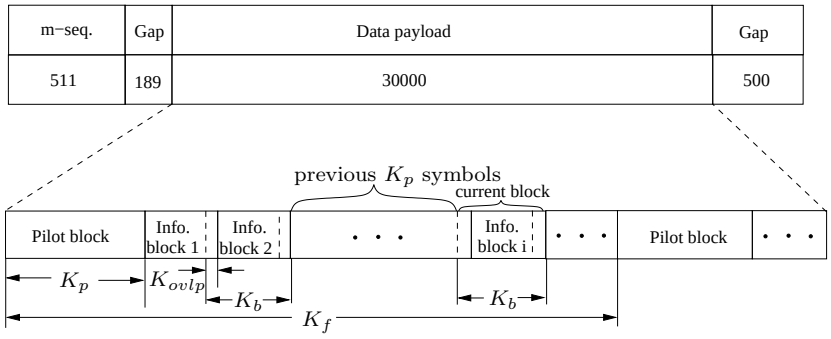

Figure 6.1. The format of transmission packet in the SPACE08 experiment

depicted in Fig. 6.1. First, K_p pilot symbols were inserted for every K_f symbols, which provided pilot-aided channel estimation. Second, the blocks were partitioned to have K_{ovlp} overlapped symbols where the size of each block was K_b. The overlapped symbols at the tail of the previous block were re-equalized in the current block to compensate for SNR degradation. Third, the symbols detected by the current block was utilized for channel re-estimation as a means for decision-directed channel tracking. The size of each block K_b was chosen to guarantee that the time duration of the $K_p + K_b$ symbols was smaller than the channel coherence time. According to the channel scattering function analyzed by the 511-bit m sequence, the channel coherence time was approximately 100 ms. Hence, we set the size of each subblock as $K_b = 200$, and the number of pilot symbols as $K_p = 600$. The parameter K_f was adjusted to adapt to the MIMO channels and the modulation levels. The noise variance in each packet was estimated using the received samples during the gap intervals. Typically, the estimated SNR is in the dynamic range from 20 dB to 32 dB.

For channel estimation, we adopted the low-complexity normalized least mean squares (NLMS) algorithm to estimate the UWA channels [30]. In Fig. 6.2, we present several typical channels experienced by one data payload transmission, where "T#" and "H#" denote the indexes of the transducer and hydrophone, respectively. The channel impulse responses (CIR) were clearly time-varying, which changed its multipath structure during a transmission block. The channels were also non-minimum phase

systems because the strongest multipath components were not located at the very beginning of the CIR. Interestingly, the 200 m channels experienced more severe ISI than the 1000 m channels, hence channel equalization in the 200 m transmission was more challenging.

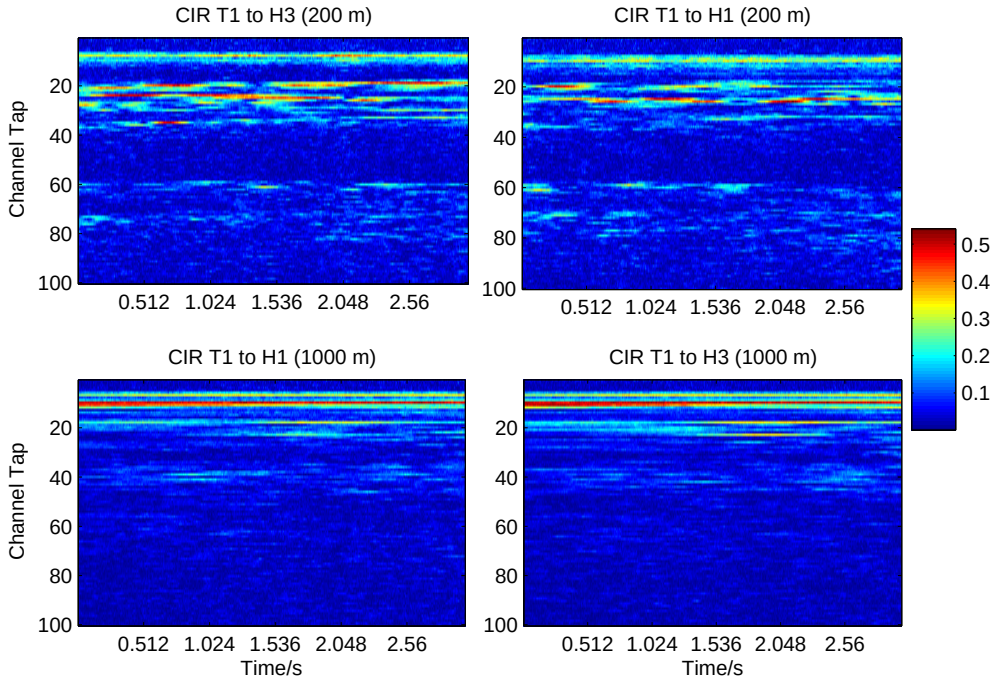

Figure 6.2. Examples of channel impulse response over long term observation. Note that the 200 m channels experience more severe multipath ISI than the 1000 m channels.

On the other hand, many of the 1000 m packets experienced low signal strength and strong impulsive interference. We plotted two examples of the received signals of the 200 m and 1000 m transmissions, as shown in Fig. 6.3. The received signal in the 200 m channel had clean signals with 0.38 peak-to-peak amplitude, while the 1000 m channel had only 0.038 peak-to-peak amplitude and was corrupted by impulsive interference with large amplitude and duration. Only 19 packets contained usable signals and we processed these 19 packets.

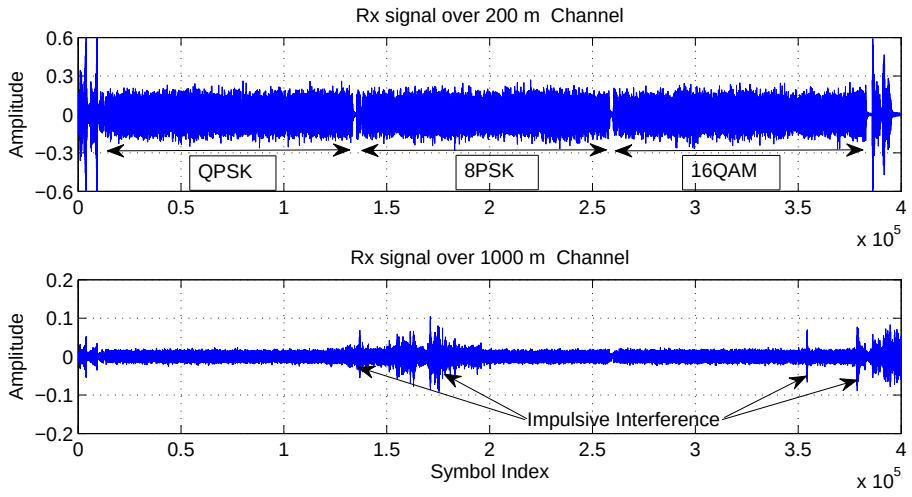

Figure 6.3. Examples of received signals in 200 m and 1000 m transmissions.

The recorded packets were processed by the proposed Bi-SDFE in comparison to the original SDFE. For the Bi-SDFE, the extrinsic LLRs at the output of normal SDFE and time-reversed SDFE are stored into a buffer in each subblock processing. After block-wise processing, we use the collected extrinsic LLRs to estimate the correlation coefficient $\hat{\varrho}_{j,n}$ for LLR combining.

6.1 RESULTS OF 200 M UWA CHANNELS WITH SEVERE ISI

For the 200 m transmission, the UWA channels exhibits fast time-variations and long multipath delays. Therefore, we set the pilot overhead as 12% and 16% for the QPSK and 8PSK data payload, respectively. For the 16QAM data, the overhead was increased to 23% because the transmission source level for all modulation schemes were the same, which made the channel estimation and symbol detection of higher-level modulation systems more difficult.

The detection results for each modulation scheme in the 200 m transmission are summarized in Table 6.1. The proposed Bi-SDFE achieved zero BER for all 45 QPSK packets using only three iterations. In contrast, the original SDFE had 42 packets achieving zero BER. With the 3 QPSK packets that experienced tough channels, the

SDFE could not improve the performance with more iterations. For 8PSK packets, the proposed Bi-SDFE achieved BER $< 10^{-4}$ for 37 packets with 5 iterations, while the original SDFE only had 17 packets achieving BER $< 10^{-4}$. For the 16QAM packets, the Bi-SDFE achieved BER $< 10^{-3}$ for 24 packets in three iterations, and for 35 packets in six iterations. The original SDFE only had 11 packets achieving BER $< 10^{-3}$. Again, increasing the number of iterations failed to improve the performance of the original SDFE for higher-level modulation schemes.

Table 6.1. Number of packets that achieves the specified BER performance (2×6 MIMO over 200 m channels)

iter.	QPSK(BER=0)		8PSK(BER<10^{-4})		16QAM(BER<10^{-3})	
	SDFE	Bi-SDFE	SDFE	Bi-SDFE	SDFE	Bi-SDFE
1	28	36	0	0	0	0
2	13	7	11	17	3	4
3	1	2	5	11	5	20
4	0	0	1	6	3	7
5	0	0	0	3	0	3
6	0	0	0	0	0	1
total	42	45	17	37	11	35

The performance comparison between Bi-SDFE and the original SDFE with higher-level modulation is further demonstrated in Fig. 6.4, where the percentages of all the 45 packets in different BER ranges are depicted after two and six iterations. We find that after multiple iterations, the performance gaps between Bi-SDFE and the original SDFE become much larger than the gaps after one iteration. This is the case for both 8PSK and 16QAM packets, which indicates that the bidirectional structure indeed helped to reduce the error floor through multiple iterations. The BER performance improvement was one to two orders of magnitude better than the original SDFE. After 6 iterations, Bi-SDFE successfully detected 95.6% of the 8PSK packets with BER less than 10^{-3}. However, with the original SDFE, there are still 13.3% 8PSK

packets that failed with BER larger than 10^{-1}. For 16QAM modulation, 77.8% packets are detected with BER lower than 10^{-3} after using the proposed Bi-SDFE, while only 24.4% packets are detected with the original SDFE at the same BER level.

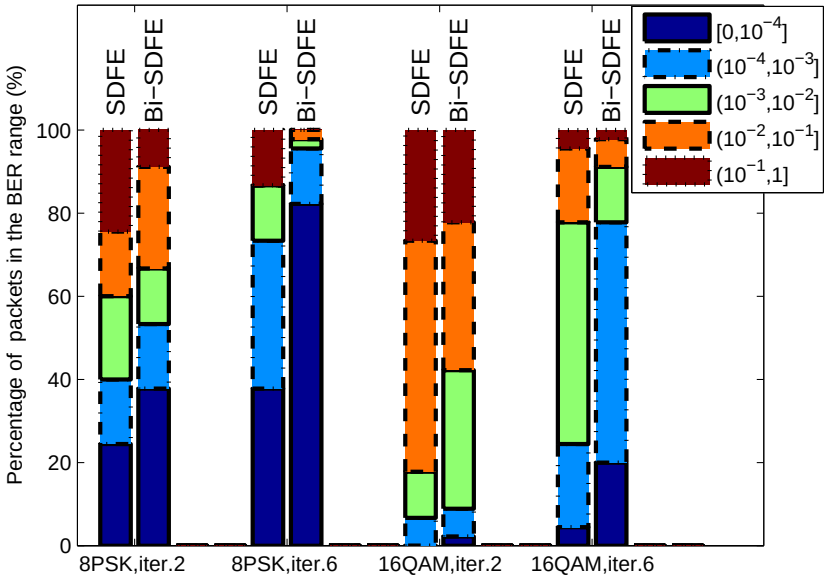

Figure 6.4. Performance comparison between the Bi-SDFE and the SDFE for 2×6 MIMO over 200 m UWA channels.

6.2 RESULTS OF 1000 M UWA CHANNELS WITH IMPULSIVE INTERFERENCE

As the multipath in the 1000 m channel was shorter and more stable than the 200 m channels, the overhead for channel estimation was set lower, at 9%, 12% and 20% for QPSK, 8PSK and 16QAM modulation, respectively. Since the impulsive interference was random and occupied the same frequency band as the signals, filtering did little help to the signal processing. The MIMO detection relied solely on the capability of joint equalization and forward error correction decoding. The BER performance of the 2×6 MIMO systems is summarized in Table 6.2. For QPSK, 16 out of the 19 packets

achieved zero BER within 3 iterations using both Bi-SDFE and SDFE. For 8PSK, the Bi-SDFE had 15 packets achieving BER $< 10^{-4}$ using six iterations, while the original SDFE had 6 packets achieving the same BER with six iterations. For 16QAM, the proposed Bi-SDFE had nine packets achieving BER $< 10^{-3}$ using six iterations, while the original SDFE had six packets achieving the same BER with six iterations.

Table 6.2. Number of packets that achieves the specified BER performance (2×6 MIMO over 1000 m channels)

	QPSK(BER=0)		8PSK(BER<10^{-4})		16QAM(BER<10^{-3})	
	SDFE	Bi-SDFE	SDFE	Bi-SDFE	SDFE	Bi-SDFE
packets	16	16	6	13	6	9
iter. #	3	3	6	6	6	6

The performance of the higher-level modulation schemes is further shown in Fig. 6.5, in terms of the percentage of the packets that fall in the specified BER ranges. In the 8PSK transmission, 78.9% packets achieved BER $< 10^{-3}$ with Bi-SDFE. However, with the original SDFE, there were still 26.3% packets failed with BER $> 10^{-2}$ and 15.8% packets that failed with BER $> 10^{-1}$. For the 16QAM transmission, even though the percentages of packets achieving excellent BER performance were low, the percentages of failed packets with BER $> 10^{-2}$ were zero after using Bi-SDFE. In comparison, the original SDFE still had 36.8% packets failed with BER $> 10^{-2}$. In the tough packets with strong impulsive interference, Bi-SDFE was able to lower the BER to the level of 10^{-3}, but the original SDFE failed to do that. This indicates that the performance improved by the bidirectional decision feedback scheme is in fact from the time-reverse diversity which reduces the probability of catastrophic error propagation.

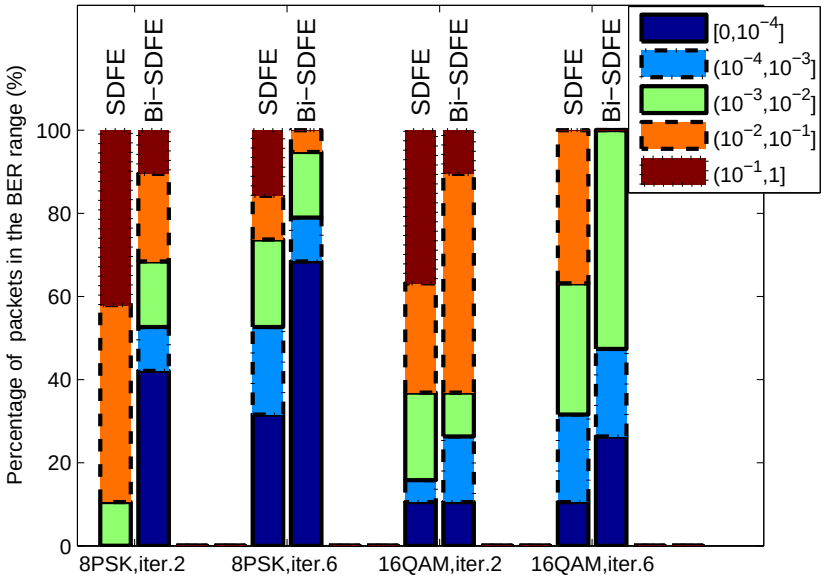

Figure 6.5. Performance comparison between the Bi-SDFE and the SDFE for 2×6 MIMO over 1000 m UWA channels.

7 CONCLUSION

In this paper, an iterative Bi-SDFE is proposed for triply selective fading channels. Based on a Gaussian approximation, a simple and effective linear combining scheme is derived to investigate the time-reverse diversity of the extrinsic LLRs at the output of the two SDFEs for MIMO systems with multilevel modulation. Simulation results show that the proposed Bi-SDFE has obvious performance gains over the original SDFE and even outperforms the near optimal but high-complexity Exact MMSE LE in the medium-to-high SNR region. The complexity of Bi-SDFE is roughly twice that of SDFE, but still remains a linear function of the channel length, MIMO size and modulation constellation size. In addition, the EXIT chart analysis shows that the proposed Bi-SDFE has a faster convergence rate than the original SDFE, which accomplishes a good trade-off between performance and complexity. The performance gain of the proposed MIMO SDFE was also verified by real-world undersea communication experimental data.

8 ACKNOWLEDGEMENT

The authors are grateful to Dr. C. Xiao for helpful discussion during the course of our research. This work was supported by the National Science Foundation under grants ECCS#0846486 and ECCS#1408316.

9 REFERENCES

[1] J. G. Proakis, *Digital Communications*. New York: McGraw-Hill, 2001.

[2] C. Xiao, J. Wu, S.-Y. Leong, Y. R. Zheng, and K. B. Letaief, "A discrete-time model for triply selective MIMO rayleigh fading channels," *IEEE Trans. Wireless Commun.*, vol. 3, no. 5, pp. 1678–1688, Sep. 2004.

[3] L. Dai, Z. Wang, and Z. Yang, "Next-generation digital television terrestrial broadcasting systems: Key technologies and research trends," *IEEE Communications Magazine*, vol. 50, no. 6, pp. 150–158, Jun. 2012.

[4] M. Chitre, S. Shahabudeen, L. Freitag, and M. Stojanovic, "Recent advances in underwater acoustic communications & networking," in *OCEANS 2008*, vol. 2008, 2008, pp. 1–10.

[5] A. Baggeroer, "An overview of acoustic communications from 2000-2012," *Underwater Commun.: Channel Modelling & Validation*, 2012.

[6] E. Biglieri, R. Calderbank, A. Constantinides, A. Goldsmith, A. Paulraj, and H. V. Poor, *MIMO wireless communications*. Cambridge University Press, 2007.

[7] C. Douillard, M. Jézéquel, C. Berrou, D. Electronique, A. Picart, P. Didier, and A. Glavieux, "Iterative correction of intersymbol interference: Turbo-equalization," *European Trans. Telecommun.*, vol. 6, no. 5, pp. 507–511, May 1995.

[8] M. Tuchler, R. Koetter, and A. C. Singer, "Turbo equalization: principles and new results," *IEEE Trans. Commun.*, vol. 50, no. 5, pp. 754–767, May 2002.

[9] M. Tuchler, A. C. Singer, and R. Koetter, "Minimum mean squared error equalization using a priori information," *IEEE Trans. Signal Process.*, vol. 50, no. 3, pp. 673–683, Mar. 2002.

[10] T. Abe, S. Tomisato, and T. Matsumoto, "A MIMO turbo equalizer for frequency-selective channels with unknown interference," *IEEE Trans. Veh. Technology*, vol. 52, no. 3, pp. 476–482, Mar. 2003.

[11] R. R. Lopes and J. R. Barry, "The soft-feedback equalizer for turbo equalization of highly dispersive channels," *IEEE Trans. Commun.*, vol. 54, no. 5, pp. 783–788, May 2006.

[12] J. Tao, Y. R. Zheng, C. Xiao, and T. Yang, "Robust MIMO underwater acoustic communications using turbo block decision-feedback equalization," *IEEE J. Oceanic Eng.*, vol. 35, no. 1, pp. 90–99, Jan. 2010.

[13] H. Lou and C. Xiao, "Soft-decision feedback turbo equalization for multilevel modulations," *IEEE Trans. Signal Process.*, vol. 59, no. 1, pp. 186–195, Jan. 2011.

[14] A. Rafati, H. Lou, and C. Xiao, "Low-complexity soft-decision feedback turbo equalization for MIMO systems with multilevel modulations," *IEEE Trans. Veh. Technology*, vol. 60, no. 7, pp. 3218–3227, Jul. 2011.

[15] S. Ariyavisitakul, "A decision-feedback equalizer with selective time-reversal operation for high-rate indoor radio communication," in *Proc. IEEE Global Telecommun. Conf.*, 1990, pp. 2035–2039.

[16] ——, "A decision feedback equalizer with time-reversal structure," *IEEE J. Sel. Areas Commun.*, vol. 10, no. 3, pp. 599–613, Mar. 1992.

[17] H. Suzuki, "Performance of a new adaptive diversity-equalisation for digital mobile radio," *Electronics Lett.*, vol. 26, no. 10, pp. 626–627, Oct 1990.

[18] J. Balakrishnan and C. Johnson, "Bidirectional decision feedback equalizer: infinite length results," in *Proc. Asilomar Conf. on Signals, Systems, and Computers, Pacific Grove, CA*, Nov. 2001.

[19] H. Song, "Bidirectional equalization for underwater acoustic communication," *J. Acoust. Soc. Am.*, vol. 131, no. 4, pp. EL342–EL347, 2012.

[20] X.-G. Tang and Z. Ding, "Low-complexity iterative equalization for EDGE with bidirectional processing," *IEEE Trans. Wireless Commun.*, vol. 4, no. 5, pp. 1963–1968, May 2005.

[21] C. W. Wong, J. M. Shea, and Y. Lee, "Hard- and soft-output trellis-based conflict resolution for bidirectional decision feedback equalization," *IEEE Trans. Wireless Commun.*, vol. 8, no. 7, pp. 3780–3788, Jul. 2009.

[22] S. Jeong and J. Moon, "Soft-in soft-out DFE and bi-directional DFE," *IEEE Trans. Commun.*, vol. 59, no. 10, pp. 2729–2741, Oct. 2011.

[23] J. Nelson, A. C. Singer, U. Madhow, and C. McGahey, "BAD: bidirectional arbitrated decision-feedback equalization," *IEEE Trans. Commun.*, vol. 53, no. 2, pp. 214–218, Feb. 2005.

[24] G. F. Edelmann, H. Song, S. Kim, W. Hodgkiss, W. Kuperman, and T. Akal, "Underwater acoustic communications using time reversal," *IEEE J. Oceanic Eng.*, vol. 30, no. 4, pp. 852–864, Apr. 2005.

[25] V. Ramon, C. Herzet, and L. Vandendorpe, "A semi-analytical method for predicting the performance and convergence behavior of a multiuser turbo-equalizer/demapper," *IEEE Trans. Signal Process.*, vol. 55, no. 3, pp. 1104–1117, Mar. 2007.

[26] S. ten Brink, "Convergence behavior of iteratively decoded parallel concatenated codes," *IEEE Trans. Commun.*, vol. 49, no. 10, pp. 1727–1737, Oct. 2001.

[27] M. Fu, "Stochastic analysis of turbo decoding," *IEEE Trans. Inf. Theor.*, vol. 51, no. 1, pp. 81–100, Jan 2005.

[28] T. J. Richardson and R. L. Urbanke, "The capacity of low-density parity-check codes under message-passing decoding," *IEEE Trans. Inf. Theor.*, vol. 47, no. 2, pp. 599–618, Feb. 2001.

[29] D. Chu, "Polyphase codes with good periodic correlation properties (corresp.)," *IEEE Trans. Inf. Theor.*, vol. 18, no. 4, pp. 531–532, Jul 1972.

[30] Z. Yang and Y. R. Zheng, "Robust adaptive channel estimation in MIMO underwater acoustic communications," in *Proc. MTS/IEEE Conf. Taipei, Taiwan*, 2014.

II. EFFICIENT ADAPTIVE TURBO EQUALIZATION FOR MIMO UNDERWATER ACOUSTIC COMMUNICATIONS

Weimin Duan, Jun Tao, *Member, IEEE*, and Yahong Rosa Zheng, *Fellow, IEEE*

ABSTRACT—An efficient direct adaptation turbo equalization scheme is proposed for multiple-input multiple-output (MIMO) underwater acoustic (UWA) communications. Compared with existing schemes, the proposed scheme benefits from the usage of soft-decision reference symbols for parameter adaptation as well as the iterative processing inside the adaptive equalizer itself (in addition to the turbo operation between the equalizer and the decoder). The proposed scheme is efficient in four aspects: first, it achieves robust performance especially in harsh MIMO UWA channels; second, it has high spectral efficiency by requiring relatively short training period; third, it converges fast thus is time efficient; fourth, it incurs low complexity by adopting the economic adaptive algorithms including the normalized least mean square (NLMS) and the improved proportionate normalized least mean squares (IPNLMS). The aforementioned efficiencies of the proposed scheme have been verified by the field trial data collected in the 2008 Surface Processes and Acoustic Communications Experiment (SPACE08). Especially, with the proposed scheme, satisfactory detection can be achieved even for MIMO transmission with more than two concurrent data streams, which to the best of our knowledge, has not been reported for any existing adaptive turbo equalization.

1 INTRODUCTION

Multiple-input multiple-output (MIMO) underwater acoustic (UWA) communication exhibits unique technical challenges due to the triply selective property of the underlying MIMO UWA channel, for which the transmit signal simultaneously experiences the frequency selectivity, the time selectivity, and the spatial selectivity [1]. The frequency selectivity and the time selectivity are generally very severe, for the extremely long delay spread and the rapid dynamics of the UWA channel. For example, a medium-range horizontal UWA channel can have a delay spread of several tens of milliseconds spanning several tens or even hundreds of symbol periods, and the channel coherence time is typically several tens of milliseconds. Further, the spatial selectivity leads to different gains among different transmit and receive elements [2], adding to the difficulty of signal detection.

The harsh MIMO UWA channel demands for powerful signal detection techniques, and turbo equalization has been recognized as one promising detection scheme. Turbo equalization typically consists of two components: a soft-decision (SD) equalizer and an SD decoder, which iteratively exchange extrinsic information to improve the detection performance. Turbo equalization applied to the UWA communications falls into two classes: the channel estimation based turbo equalization (CE-TEQ) [3,4,5,6,7] with explicit channel impulse response estimation, and the direct adaptation turbo equalization (DA-TEQ) with implicit channel knowledge [8, 9, 10, 11, 12, 13]. The equalizer for a CE-TEQ can be an SD minimum mean square error (MMSE) linear equalizer [3, 4] or an SD MMSE decision-feedback equalizer (DFE) [5, 6, 7], where the calculation of the SD MMSE equalizer coefficients requires the knowledge of the UWA channel. Since the length of the UWA channel is usually long, the computation of the equalizer coefficients involves a large-dimension matrix inversion, leading to high complexity. The complexity can be further amplified when a MIMO system with multiple transducers

and hydrophones is deployed, leading to increased size of the covariance matrix to be inverted. The high complexity means a long signal processing delay, making the CE-TEQ high cost for real-time implementation.

On the other hand, a DA-TEQ has the advantage of low complexity achieved by directly adjusting the equalizer coefficients without any matrix inversion. However, a DA-TEQ suffers from several drawbacks. First, a DA-TEQ generally achieves sub-optimal performance approaching that of the Wiener filtering. Second, a DA-TEQ requires fine parameter tuning, which is nontrivial for MIMO UWA communication due to the abundant equalizer taps to be adapted. Third, a DA-TEQ usually requires longer training sequence to converge than a CE-TEQ.

An SD equalizer adopted in the adaptive turbo equalization typically consists of two filters: a feedforward filter with the received samples as its input, and a soft interference cancelation (SIC) filter whose input is the estimated symbols [11, 12, 13]. The adaption of the feedforward and SIC filters, as well as the quality of the SIC filter input are the keys for the success of the adaptive turbo equalization. In the training mode, the filter adaptation and the SIC formulation are routine procedures since the reference symbols are perfectly known *a priori*. It is during the decision directed (DD) mode, diverse filter adaptation and SIC formulation methods are proposed, leading to different DA-TEQ schemes of different performance [11, 12, 13, 14, 15]. In [12, 13, 14], the hard decision on the equalizer output is used to drive the filter adaptation, and the SIC input is the *a priori* soft symbol estimation from the channel decoder. In [11], a similar filter adaptation and SIC formulation scheme as in [12, 13, 14] is adopted. The difference is that it also takes advantage of the data reuse technique originated in [16]. By data reuse, the filter adaptation and symbol detection are repeated several times over the same set of data. The repetition helps to improve the detection performance as well as to speed up the filter convergence. Therefore, it shortens the training sequence and improves the transmission efficiency. In [15], hard decisions of the *a priori* soft symbol estimates from the decoder are delivered as the SIC filter input. Different

from [11, 12, 13, 14], the decoder *a priori* soft estimations are also incorporated into the filter adaptation, aiming to mitigate the error propagation effect of hard decisions. The scheme however still requires a very long training sequence for the initialization of the equalizer. Furthermore, it is noted that most existing work on DA-TEQ for UWA communication deal with single-input multiple-output (SIMO) transmissions [12, 13, 14, 15], and the only MIMO result reported is for the two-transducer scenairo with a low-order modulation [11].

In this paper, an efficient DA-TEQ is proposed for MIMO UWA communication, with multiple transmit elements and multilevel modulation like 8PSK and 16QAM. The proposed scheme adopts the low-complexity normalized least mean squares (NLMS) algorithm as well as the improved proportionate normalized least mean squares (IPNLMS) algorithm, and also benefits from the data reuse technique [11]. Compared with the existing DA-TEQ schemes, the proposed scheme utilizes the *a posteriori* soft decisions at the equalizer output at each data reuse iteration. The *a posteriori* soft decisions have better fidelity than the *a priori* soft decisions, thanks to the extra information gleaned in the equalization process. Moreover, the *a posteriori* soft decisions are utilized block by block, leading to low complexity and high performance [17]. The proposed DA-TEQ scheme is tested by extensive experimental data collected in the 2008 Surface Processes and Acoustic Communications Experiment (SPACE08). Off-line processing results show the proposed DA-TEQ not only achieves error-free detection for most QPSK packets in the MIMO transmission with up to three transmit elements, but also works decently in the MIMO transmission with multilevel 8PSK and 16QAM modulations and up to three concurrent transmit streams. Furthermore, a relatively short training sequence is sufficient for the proposed DA-TEQ to converge, so that the transmission efficiency is improved over the existing works. Last, it is observed the performance gain of the IPNLMS algorithm over the NLMS algorithm depends heavily on the modulation and the MIMO size. For low-order MIMO transmission with QPSK or 8PSK modulations, the low-complexity NLMS algorithm is already sufficient for the

proposed DA-TEQ to achieve high performance. However, when 16QAM modulation or higher-order MIMO transmission is employed, the IPNLMS considerably outperforms the NLMS, by making use of the sparse property of the equalizer.

Notations: the superscripts $(\cdot)^*$, $(\cdot)^T$ and $(\cdot)^H$ represent, respectively, the conjugate, the matrix transpose, and the matrix Hermitian, and $\mathbb{E}\{\cdot\}$ denotes the statistical expectation. The function $\tanh(x)$ denotes the hyperbolic tangent, and the matrix $\text{diag}\{d_1, d_2, \cdots, d_j\}$ is a $j \times j$ diagonal matrix with diagonal elements $d_1, d_2, \cdots, d_j$.

2 SYSTEM DESCRIPTION AND ADAPTIVE TURBO EQUALIZATION PRELIMINARY

2.1 SYSTEM DESCRIPTION

An $N \times M$ single-carrier MIMO underwater acoustic communication system with spatial multiplexing is considered, where N and M are the number of transducers and the number of hydrophones, respectively. The system diagram is depicted in Fig. 2.1 where on the transmitter side, the incoming information bit stream is converted into N parallel streams $\{\mathbf{b}_n\}_{n=1}^{N}$, transmitted by the N transducers. On the n-th transmit branch, the information bit is encoded and interleaved. Every q interleaved bits, $\mathbf{c}_{n,k} \triangleq [c_{n,k}^1 \;\; c_{n,k}^2 \cdots c_{n,k}^q]$, are mapped to one modulation symbol $x_{n,k}$ taken from a 2^q-ary constellation set $S = \{\alpha_1, \alpha_2, \cdots, \alpha_{2^q}\}$. A given constellation point α_i is mapped to a pre-determined bit pattern $\mathbf{s}_i = [s_{i,1} \; s_{i,2} \cdots s_{i,q}]$ with $s_{i,j} \in \{0, 1\}$.

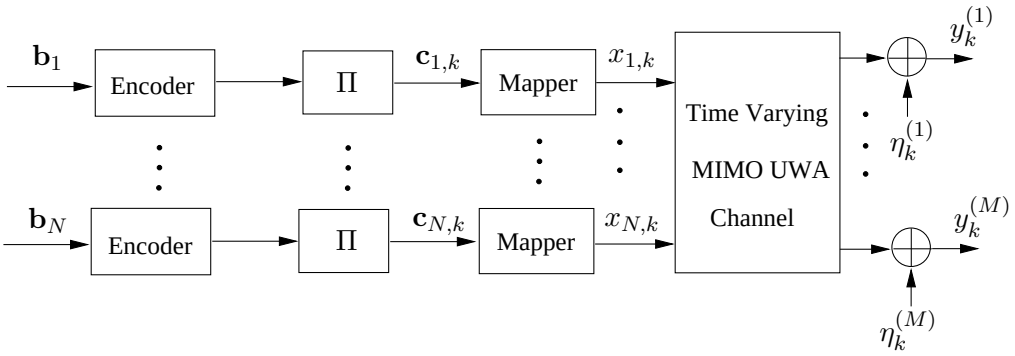

Figure 2.1. The block diagram of a MIMO underwater acoustic communication system (Π denotes an interleaver).

The received baseband signal on the m-th hydrophone element at the time k is given by

$$y_k^{(m)} = \sum_{n=1}^{N} \sum_{l=0}^{L-1} h_l^{(m,n)} x_{n,k-l} + \eta_k^{(m)} \tag{1}$$

where $h_l^{(m,n)}$ denotes the l-th tap of the length-L equivalent channel between the n-th transducer element and the m-th hydrophone element, and $\eta_k^{(m)}$ is the additive noise. Stacking up the receive samples of the M hydrophone as $\mathbf{y}_k = [y_k^{(1)}, y_k^{(2)}, \ldots, y_k^{(M)}]^T$, one has the space-time representation as

$$\mathbf{y}_k = \sum_{l=0}^{L-1} \mathbf{h}_l \mathbf{x}_{k-l} + \boldsymbol{\eta}_k \tag{2}$$

where

$$\mathbf{x}_k = [x_{1,k}, x_{2,k}, \ldots, x_{N,k}]^T \tag{3}$$

$$\boldsymbol{\eta}_k = [\eta_k^{(1)}, \eta_k^{(2)}, \ldots, \eta_k^{(M)}]^T \tag{4}$$

$$\mathbf{h}_l = \begin{bmatrix} h_l^{(1,1)} & h_l^{(1,2)} & \cdots & h_l^{(1,N)} \\ h_l^{(2,1)} & h_l^{(2,2)} & \cdots & h_l^{(2,N)} \\ \vdots & \vdots & \ddots & \vdots \\ h_l^{(M,1)} & h_l^{(M,2)} & \cdots & h_l^{(M,N)} \end{bmatrix}. \tag{5}$$

2.2 ADAPTIVE TURBO EQUALIZATION FOR MIMO SYSTEMS

The structure of the adaptive turbo equalization for MIMO systems is depicted in Fig. 2.2, where the adaptive equalizer consists of two units: the feedforward filtering unit and the soft interference cancelation unit. In most existing adaptive equalizers, the SIC is performed with the *a priori* soft decision $\bar{x}_{n,k}$, calculated with the bit *a priori* log likelihood ratio (LLR) $L_a(c_{n,k}^j)$ from the decoder as

$$\bar{x}_{n,k} = \mathbb{E}\left[x_{n,k} | \left\{L_a\left(c_{n,k}^j\right)\right\}_{j=1}^q\right] = \sum_{\alpha_i \in S} \alpha_i P\left(x_{n,k} = \alpha_i\right) \tag{6}$$

where

$$P\left(x_{n,k} = \alpha_i\right) = \prod_{j=1}^{q} \frac{1}{2}\left(1 + \tilde{s}_{i,j} \tanh\left(L_a\left(c_{n,k}^j\right)/2\right)\right) \tag{7}$$

with

$$\tilde{s}_{i,j} = \begin{cases} +1 & \text{if } s_{i,j} = 0 \\ -1 & \text{if } s_{i,j} = 1. \end{cases}$$

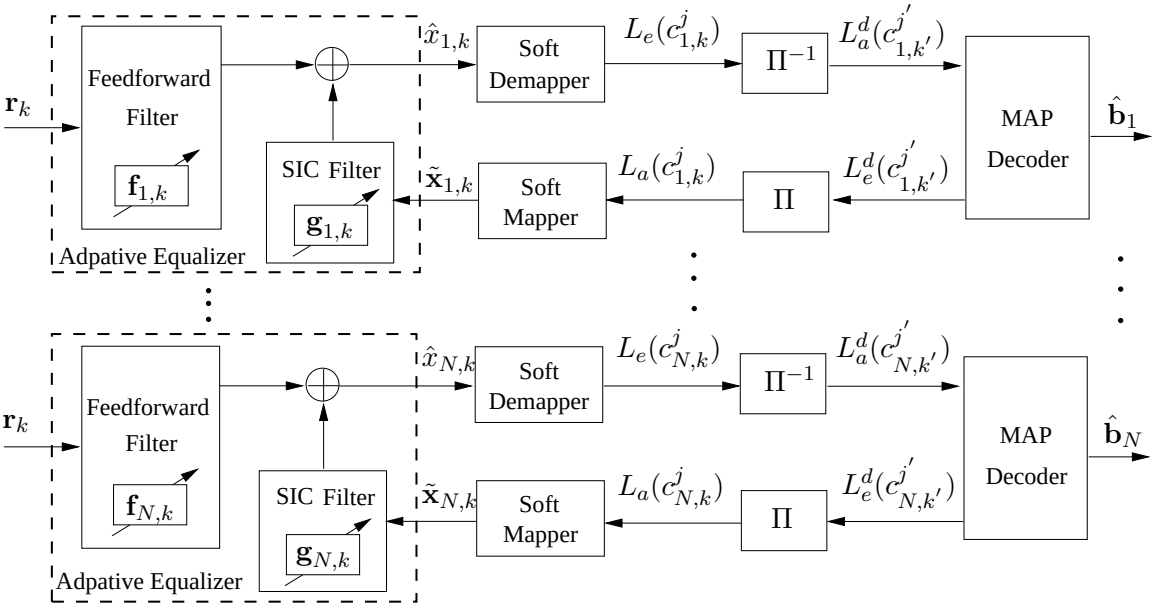

Figure 2.2. The structure of the adaptive turbo equalization for MIMO systems.

The equalizer output is given as

$$\hat{x}_{n,k} = \mathbf{f}^H_{n,k}\mathbf{r}_k + \mathbf{g}^H_{n,k}\tilde{\mathbf{x}}_{n,k} \tag{8}$$

where $\mathbf{r}_k = [\mathbf{y}^T_{k+K_1}, \ldots, \mathbf{y}^T_{k-K_2}]^T$, and $\tilde{\mathbf{x}}_{n,k} = [(\bar{\mathbf{x}}_{n,k-K_3})^T, \ldots, (\bar{\mathbf{x}}_{n,k})^T \ldots, (\bar{\mathbf{x}}_{n,k+K_4})^T]^T$ with $\bar{\mathbf{x}}_{n,k'} = [\bar{x}_{1,k'}, \bar{x}_{2,k'}, \ldots, \bar{x}_{N,k'}]^T$ when $k' \neq k$, and $\bar{\mathbf{x}}_{n,k'} = [\bar{x}_{1,k'}, \ldots, \bar{x}_{n-1,k'}, 0, \bar{x}_{n+1,k'}, \ldots, \bar{x}_{N,k'}]^T$ when $k' = k$. The parameters K_1, K_2, K_3, K_4 are non-negative integers. Obviously, the length of the feedforward filter and the length of the SIC filter are $M(K_1 + K_2 + 1)$ and $N(K_3 + K_4)$, respectively, leading to a combined filter length of $K_{eq} = M(K_1 + K_2 + 1) + N(K_3 + K_4)$. It is noted K_{eq} is the number of taps for a particular transmit stream, and the total number of taps for the adaptive equalizer

shall be scaled by a factor of N. For notation convenience, one expresses (8) as

$$\hat{x}_{n,k} = \mathbf{w}_{n,k}^H \mathbf{u}_k \tag{9}$$

where

$$\mathbf{w}_{n,k} = [\mathbf{f}_{n,k}^T \, \mathbf{g}_{n,k}^T]^T \tag{10}$$

$$\mathbf{u}_k = [\mathbf{r}_k^T \, \tilde{\mathbf{x}}_{n,k}^T]^T \tag{11}$$

The adaptive turbo equalization usually works in both training mode and DD mode, and the NLMS algorithm is used as an example without loss of generality. In the training mode, the adaptation of the equalizer vector is as follows

$$\mathbf{w}_{n,k+1} = \mathbf{w}_{n,k} + \frac{\mu(x_{n,k} - \hat{x}_{n,k})^* \mathbf{u}_k}{\delta_{\text{NLMS}} + \mathbf{u}_k^H \mathbf{u}_k}, \quad 1 \le k \le K_p \tag{12}$$

where μ is the step size, δ_{NLMS} is a small number for regularizing the adaptation at the initial stage, $x_{n,k}$ is the training symbol known *a priori*, and K_p is the length of the training sequence.

In the DD mode, the updating of the equalizer vector is as follows

$$\mathbf{w}_{n,k+1} = \mathbf{w}_{n,k} + \frac{\mu(Q(\hat{x}_{n,k}) - \hat{x}_{n,k})^* \mathbf{u}_k}{\delta_{\text{NLMS}} + \mathbf{u}_k^H \mathbf{u}_k}, \quad K_p < k \le K_b \tag{13}$$

where $Q(\hat{x}_{n,k})$ denotes the tentative hard decision on the equalizer output, and K_b is the length of each processed block.

As mentioned above, the length of the concatenated feedforward filter and the SIC filter is $K_{eq} = M(K_1 + K_2 + 1) + N(K_3 + K_4)$. Due to the long delay spread of the underwater channel as well as the multiple transmit and receive elements, the number of equalizer taps to be adapted is large. To make the adaptive equalizer converge, a long training sequence is required, which sacrifices the transmission efficiency. To avoid

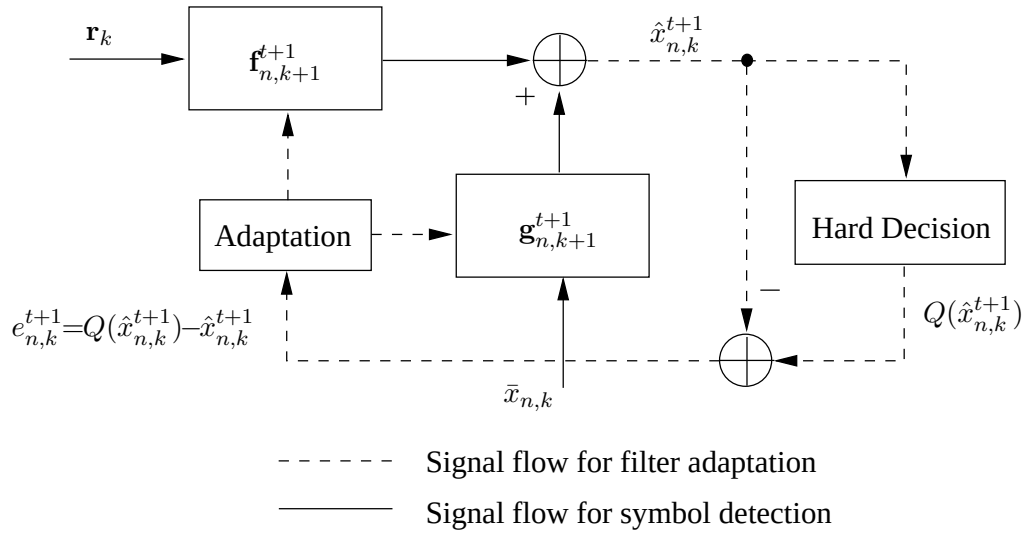

Figure 2.3. The block diagram of the hard-decision adaptive equalizer with data reuse.

long training sequence, the data reuse technique has been applied in the hard-decision directed adaptive turbo equalization (HD-DA-TEQ) [11] and the iterative channel estimation based turbo equalization [4]. The hard-decision directed equalizer adaptation with data reuse is demonstrated in Fig. 2.3, where the tap updating is repeated over the same block of received signals for a couple of times as follows

$$\mathbf{w}_{n,k+1}^{t+1} = \mathbf{w}_{n,k}^{t+1} + \frac{\mu(Q(\hat{x}_{n,k}^{t+1}) - \hat{x}_{n,k}^{t+1})^* \mathbf{u}_k}{\delta_{\text{NLMS}} + \mathbf{u}_k^H \mathbf{u}_k}, \quad K_p < k \leq K_b, t \geq 0. \tag{14}$$

where the superscript $t+1$ denotes the $(t+1)$-th round of data reuse, and $\hat{x}_{n,k}^{t+1} = {\mathbf{w}_{n,k}^{t+1}}^H \mathbf{u}_k$. The purpose of using $t+1$ as the index of the data reuse round is for the convenience of comparison with the proposed equalizer adaptation, as shown shortly. The adaptation of the equalizer vector $\mathbf{w}_{n,k+1}^0$ at the zero-th round of data reuse is actually the same as that of (14). It is noted that $\mathbf{w}_{n,1}^{t+1} = \mathbf{w}_{n,K_b+1}^t$. The HD-DA-TEQ [11] may suffer the error propagation (EP), which is highly possible in practical underwater acoustic communication [4]. When the EP happens, its effect can be catastrophic for turbo equalization. Moreover, the input of the SIC filter remains unchanged over the multiple rounds of data reuse [11].

As demonstrated in Fig. 2.2, the equalized symbol $\hat{x}_{n,k}$ is translated into the extrinsic bit LLRs $L_e(c^j_{n,k})$, which are de-interleaved and input as the *a priori* LLRs $L^d_a(c^{j'}_{n,k'})$ of the maximum *a posteriori* probability (MAP) decoder. After decoding, the decoder outputs its extrinsic LLRs $L^d_e(c^{j'}_{n,k'})$, which (after interleaving) are fed back to the equalizer as its *a priori* LLR input $L_a(c^j_{n,k})$. The extrinsic information are exchanged between the equalizer and the decoder iteratively, with its reliability increasing with the number of iterations. Once the iterative procedure is finished, the hard decisions on the information bits $\hat{\mathbf{b}}_n$ are made.

3 PROPOSED ADAPTIVE TURBO EQUALIZATION

In this work, an efficient adaptive turbo equalization scheme is proposed, by performing the equalizer adaptation and the SIC with the *a posteriori* soft decisions available due to the data reuse, as demonstrated in Fig. 3.1. For notation convenience, the proposed soft-decision driven adaptive turbo equalization is called the SD-DA-TEQ. There are two layers of iterative processing in the proposed SD-DA-TEQ: the outer-layer iteration between the equalizer and decoder, and the inner-layer iteration (data reuse) inside the adaptive equalizer itself. For convenience, the outer-layer iteration is called "turbo iteration", and the inner-layer iteration is named as "equalizer iteration". It is pointed out that the *a posteriori* soft decisions are fed back in a block-wise way inside the adaptive equalizer, which improves the robustness and performance of the adaptive turbo equalization as well as reduces the complexity [17].

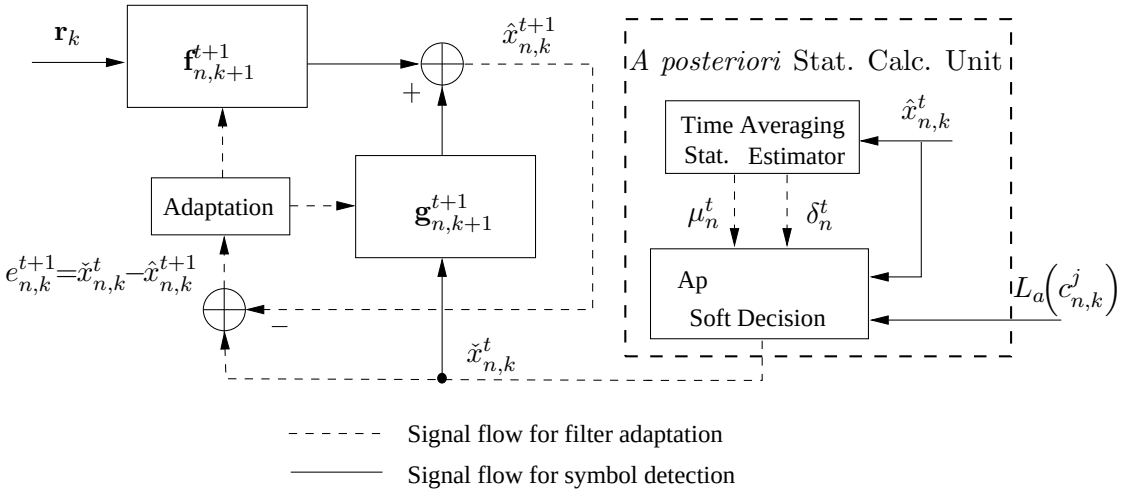

Figure 3.1. The block diagram of the proposed adaptive equalizer with data reuse.

In the following, the computation of the *a posteriori* soft decision is first presented, then the *a posteriori* soft decision based equalizer adaptation and SIC are detailed.

3.1 A POSTERIOR SOFT DECISION COMPUTATION IN THE EQUALIZER ITERATIONS

At the t-th ($t \geq 0$) round of equalizer iteration, the *a posteriori* soft decision $\check{x}_{n,k}^t$ of the equalized symbol $\hat{x}_{n,k}^t$ is calculated as

$$\check{x}_{n,k}^t = \sum_{\alpha_i \in S} \alpha_i P\left(x_{n,k} = \alpha_i | \hat{x}_{n,k}^t\right) \tag{15}$$

where the *a posteriori* probability $P\left(x_{n,k} = \alpha_i | \hat{x}_{n,k}^t\right)$ is given as

$$P\left(x_{n,k} = \alpha_i | \hat{x}_{n,k}^t\right) = \frac{p\left(\hat{x}_{n,k}^t | x_{n,k} = \alpha_i\right) P\left(x_{n,k} = \alpha_i\right)}{p\left(\hat{x}_{n,k}^t\right)}. \tag{16}$$

The *a priori* probability $P\left(x_{n,k} = \alpha_i\right)$ is computed with the *a priori* LLRs as in (7), and $p\left(\hat{x}_{n,k}^t\right)$ is obtained via the normalization $\sum_{i=1}^{2^q} P\left(x_{n,k} = \alpha_i | \hat{x}_{n,k}^t\right) = 1$. The equalizer output $\hat{x}_{n,k}^t$ conditioned on $x_{n,k} = \alpha_i$ is assumed to follow a Gaussian distribution [18, 19, 20], as

$$p\left(\hat{x}_{n,k}^t | x_{n,k} = \alpha_i\right) = \frac{1}{\pi \delta_n^t} \exp\left\{-\frac{|\hat{x}_{n,k}^t - \mu_n^t \alpha_i|^2}{\delta_n^t}\right\} \tag{17}$$

where

$$\mu_n^t = \frac{1}{K_d} \sum_{k=K_p+1}^{K_b} \frac{\hat{x}_{n,k}^t}{Q(\hat{x}_{n,k}^t)} \tag{18}$$

$$\delta_n^t = \frac{1}{K_d} \sum_{k=K_p+1}^{K_b} |\hat{x}_{n,k}^t - \mu_n^t Q(\hat{x}_{n,k}^t)|^2 \tag{19}$$

with $K_d = K_b - K_p$ being the length of information block. Obviously, the evaluation of μ_n^t and δ_n^t relies on the entire block of estimated symbols. As a result, the *a posteriori* soft decisions are available until all symbols in the block are equalized. This fact naturally leads to the block-wise soft-decision feedback operation, where the *a posteriori* soft decision $\check{x}_{n,k}^t$ of the t-th equalizer iteration is used in the $(t+1)$-th equalizer iteration, as shown in Fig. 3.1. Over equalizer iterations, the reliability of the *a posteriori* soft decision $\check{x}_{n,k}^t$ keeps increasing thus speeds up the convergence of the equalizer. The

block-wise soft-decision feedback mechanism has shown the advantage of low complexity and high performance [17].

3.2 A POSTERIOR SOFT DECISION BASED EQUALIZER ADAPTATION AND SIC

3.2.1 A Posterior Soft Decision Based Equalizer Adaptation. At the $(t+1)$-th equalizer iteration, the block of *a posteriori* soft decisions from the t-th equalizer iteration $\{\breve{x}_{n,k}^{t}\}_{k=K_p+1}^{K_b}$ are fed into the filter adaptation unit, and the equalizer vector is updated as

$$\mathbf{w}_{n,k+1}^{t+1} = \mathbf{w}_{n,k}^{t+1} + \frac{\mu(\breve{x}_{n,k}^{t} - \hat{x}_{n,k}^{t+1})^{*}\mathbf{u}_k}{\delta_{\text{NLMS}} + \mathbf{u}_k^H \mathbf{u}_k} \quad (t \geq 0) \tag{20}$$

The equalizer adaption at the zero-th equalizer iteration is different from (20), since there are no *a posteriori* soft decisions available. When the number of turbo iteration $N_{iter} > 0$, the *a priori* soft decisions $\{\bar{x}_{n,k}\}_{k=K_p+1}^{K_b}$ are instead used for the equalizer adaptation. When $N_{iter} = 0$, even the *a priori* soft decision $\bar{x}_{n,k}$ is unavailable, so the hard-decision directed equalizer adaptation as (14) is adopted. In summary, one has the following equalizer adaptation at the zero-th equalizer iteration

$$\mathbf{w}_{n,k+1}^{0} = \begin{cases} \mathbf{w}_{n,k}^{0} + \frac{\mu(\bar{x}_{n,k} - \hat{x}_{n,k}^{0})^{*}\mathbf{u}_k}{\delta_{\text{NLMS}} + \mathbf{u}_k^H \mathbf{u}_k}, & (N_{iter} > 0) \\ \mathbf{w}_{n,k}^{0} + \frac{\mu(Q(\hat{x}_{n,k}^{0}) - \hat{x}_{n,k}^{0})^{*}\mathbf{u}_k}{\delta_{\text{NLMS}} + \mathbf{u}_k^H \mathbf{u}_k}, & (N_{iter} = 0) \end{cases} \tag{21}$$

Last, the training-mode equalizer adaptation as given by (12) is performed at each equalizer iteration of the data reuse procedure.

The sparsity enhanced IPNLMS algorithm has also been adopted to process the experimental data. The IPNLMS proportionately adapts the equalizer vector as

$$\mathbf{w}_{n,k+1}^{t+1} = \mathbf{w}_{n,k}^{t+1} + \frac{\mu(\breve{x}_{n,k}^{t} - \hat{x}_{n,k}^{t+1})^{*}\mathbf{G}_{n,k}\mathbf{u}_k}{\mathbf{u}_k^H \mathbf{G}_{n,k}\mathbf{u}_k + \delta_{\text{IPNLMS}}} \quad (t \geq 0) \tag{22}$$

and

$$\mathbf{w}_{n,k+1}^{0} = \begin{cases} \mathbf{w}_{n,k}^{0} + \frac{\mu(\bar{x}_{n,k} - \hat{x}_{n,k}^{0})^{*}\mathbf{G}_{n,k}\mathbf{u}_k}{\mathbf{u}_k^H \mathbf{G}_{n,k}\mathbf{u}_k + \delta_{\text{IPNLMS}}}, & (N_{iter} > 0) \\ \mathbf{w}_{n,k}^{0} + \frac{\mu(Q(\hat{x}_{n,k}^{0}) - \hat{x}_{n,k}^{0})^{*}\mathbf{G}_{n,k}\mathbf{u}_k}{\mathbf{u}_k^H \mathbf{G}_{n,k}\mathbf{u}_k + \delta_{\text{IPNLMS}}}, & (N_{iter} = 0) \end{cases} \tag{23}$$

where δ_{IPNLMS} is a small positive number for regularization, and $\mathbf{G}_{n,k} = \text{diag}\{g_{n,k}(0), g_{n,k}(1), \ldots, g_{n,k}(K_{eq} - 1)\}$ is a diagonal proportionate matrix with the $l^{'}$-th diagonal element given by

$$g_{n,k}(l^{'}) = \frac{1-\alpha}{2K_{eq}} + (1+\alpha)\frac{|\mathbf{w}_{n,k}^{t+1}(l^{'})|}{2\|\mathbf{w}_{n,k}^{t+1}\|_1 + \epsilon}, \quad 0 \le l^{'} \le K_{eq} - 1 \tag{24}$$

where ϵ is also a regularization parameter introduced to avoid numerical instability, $\mathbf{w}_{n,k}^{t+1}(l^{'})$ is the l'-th element of $\mathbf{w}_{n,k}^{t+1}$, and $|\cdot|$ and $\|\cdot\|_1$ are the absolute operator and the l_1-norm operator, respectively. The selection of α depends on the sparsity of the equalizer. When $\alpha = -1$, the IPNLMS reduces to the NLMS [21] and the equalizer sparsity is not exploited. When $\alpha = 1$, the IPNLMS behaves like the proportionate normalized least mean squares (PNLMS) [22]. It is noted that the IPNLMS is still of linear complexity without involving any matrix inversion operation.

3.2.2 A Posterior Soft Decision Based SIC Scheme. The performance of the SIC depends heavily on the quality of the soft decision. Most adaptive turbo equalization schemes employ the *a priori* soft decisions for SIC [12, 13, 14, 11]. By utilizing the *a posteriori* soft decisions, which possess higher fidelity than the *a priori* soft decisions due to the extra information gleaned in the equalization process, one is able to improve the SIC. Specifically, with the improved SIC, the equalizer output $\hat{x}_{n,k}^{t+1}$ is given by

$$\hat{x}_{n,k}^{t+1} = \mathbf{f}_{n,k}^{t+1^H}\mathbf{r}_k + \mathbf{g}_{n,k}^{t+1^H}\breve{\mathbf{x}}_{n,k}^{t} \tag{25}$$

Obviously, the *a priori* soft decisions $\tilde{\mathbf{x}}_{n,k}$ in (8) have been replaced with the *a posteriori* soft decisions $\breve{\mathbf{x}}_{n,k}^{t} = [(\breve{\mathbf{x}}_{n,k-K_3}^{t})^T, \ldots, (\breve{\mathbf{x}}_{n,k}^{t})^T, \ldots, (\breve{\mathbf{x}}_{n,k+K_4}^{t})^T]^T$, where $\breve{\mathbf{x}}_{n,k'}^{t} = [\breve{x}_{1,k'}^{t}, \breve{x}_{2,k'}^{t}, \ldots, \breve{x}_{N,k'}^{t}]^T$ when $k^{'} \neq k$, and $\breve{\mathbf{x}}_{n,k'}^{t} = [\breve{x}_{1,k'}^{t}, \ldots, \breve{x}_{n-1,k'}^{t}, 0, \breve{x}_{n+1,k'}^{t}, \ldots, \breve{x}_{N,k'}^{t}]^T$ when $k^{'} = k$.

4 UNDERSEA EXPERIMENTAL RESULTS

The proposed adaptive turbo detection scheme has been tested by field trial data collected in the SPACE08 undersea experiment, conducted off the coast of Martha's Vineyard, Edgartown, MA, in October 2008. The water depth of this sea trial was about 15 m. On the transmitter side, four transducers numbered 0 through 3 were deployed. Transducer 0 was fixed on a stationary tripod about 4 m above the ocean bottom. Transducers 1-3 were evenly mounted on a vertical array with 50 centimeters (cm) spacing, and the top transducer in the array was about 3 m above the ocean bottom. Six hydrophone arrays placed at different locations were deployed for signal reception, with detailed information given in Table 4.1. Obviously, the communication distances were 60 m, 200 m, and 1000 m. The top hydrophone of each array was approximately 3.3 m above the sea bottom.

Table 4.1. Description of the Hydrophone Arrays

Rx Array name/type	Range (m)	Orientation	Number of hydrophones	Hydrophone spacing (cm)
S1/Cross	60	Southeast	16	3.75
S2/Cross	60	Southwest	16	3.75
S3/Vertical	200	Southeast	24	5
S4/Vertical	200	Southwest	24	5
S5/Vertical	1000	Southeast	12	12
S6/Vertical	1000	Southwest	12	12

For MIMO transmission, the horizontal encoding (HE) scheme [23] with BICM in time domain was adopted at the transmitter, as shown in Fig. 2.1. The channel coding was a rate $R_c = 1/2$ convolutional code with generator polynomial [17, 13] in octal notation. The modulations include QPSK, 8PSK, and 16QAM. The transmission

power for all modulation schemes were the same, so detection becomes more difficult when the modulation level increases. The carrier frequency was $f_c = 13$ kHz and the symbol rate was 9.77 kilo symbol per second (ksps). A square-root raised cosine filter with a roll-off factor of 0.2 was used for pulse shaping, leading to the occupied channel bandwidth of about 11.72 kHz. At the receiver side, the passband sampling rate was 39.0625 kHz.

The signal format at the n-th transducer is illustrated in Fig. 4.1, where the transmit burst starts with a header linear frequency modulation (LFM) signal named LFMB and ends with a trailing LFM signal named LFME. The LFM signals are used for coarse synchronization, Doppler shift estimation, and channel structure measurement. Following the header LFM signal are three data packets with QPSK, 8PSK, and 16QAM modulations, each starts with a m-sequence of length 511, followed by a data payload consisting of $30,000$ symbols. The use of long data payload improves the transmission efficiency. Gaps are inserted in the transmission burst, and they can be used for estimating the noise power. For the SPACE08 experiment, the typical SNR estimation is in the range of 20 dB to 32 dB.

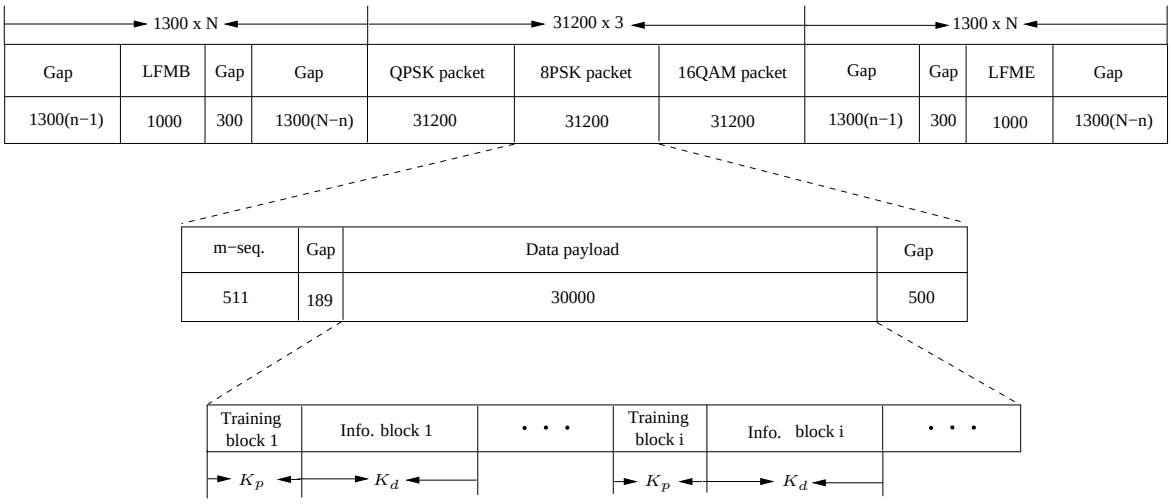

Figure 4.1. Format of the transmit signal on the n-th transducer in the SPACE08 experiment.

The received bursts of the 200-m channel and the 1000-m channel are shown in Fig. 4.2. Obviously, the strength of the 200-m signal (peak-to-peak amplitude of 0.38) is much stronger than the 1000-m signal (peak-to-peak amplitude of 0.038), which is reasonable since the acoustic signal attenuates with distance. Besides, impulsive interference is observed in the 1000-m signal.

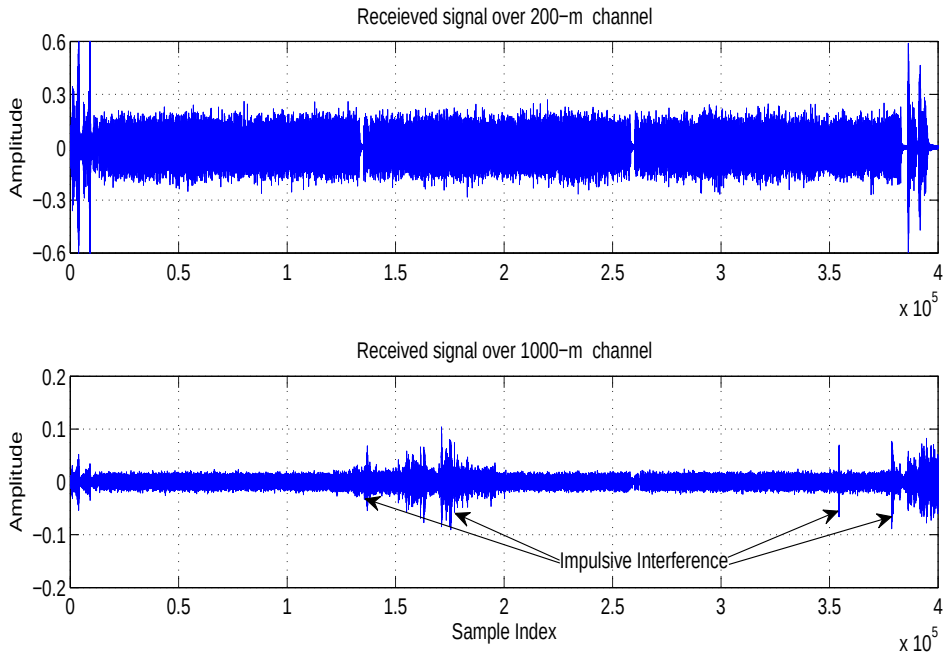

Figure 4.2. An example of the received signals in 200-m and 1000-m transmissions.

In Fig. 4.3, the channel impulse response (CIR) measured in the experiment is shown for both the 200-m transmission and the 1000-m transmission, where "T#" and "H#" denote the indices of the transducer and the hydrophone, respectively. The following observations are made: first, the multipath energy spread over a time window of 10 ms, corresponding to a channel length of 100 taps in terms of the symbol period $T_s = 0.1024$ ms; second, the channels are non-minimum phase as the strongest multipath component is not at the very beginning of the CIR, which add to the difficulty for

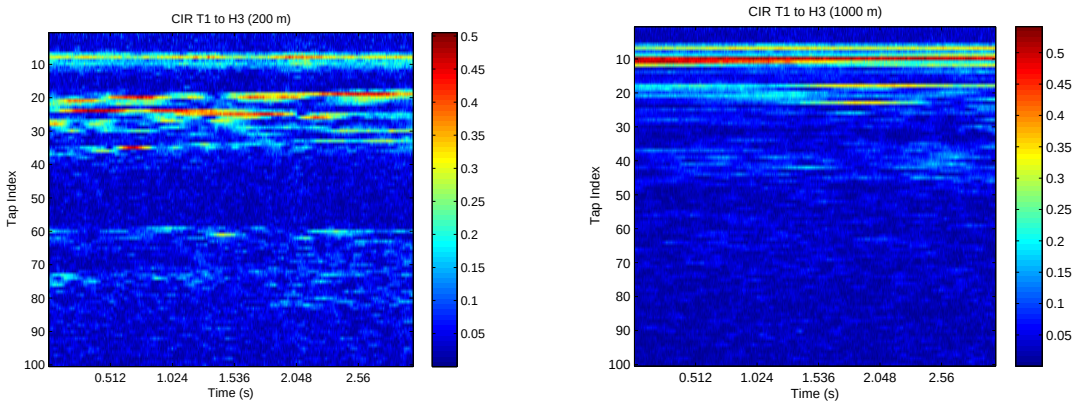

(a) (b)

Figure 4.3. An example of the channel impulse responses over a period of time.

equalization; third, the channel is fast time-varying, especially for the 200-m channel, making the adaptive symbol detection quite challenging.

4.1 PARAMETER SETUP

Due to the fast time variations of the UWA channels, the adaptive turbo detector partitions each long data payload into multiple blocks of size K_b for processing, as shown in Fig. 4.1. For each partition block, the first K_p symbols are used as the training symbols to initialize the adaptive receiver, and the remaining K_d symbols carries information bits. The resulting training overhead is $\xi = K_p/(K_p + K_d)$ and the corresponding data rate is $9.77 \times \xi q N R_c$ kilo bits per second (kbps). In the data processing, K_p is fixed as 500 and the choice of K_d is flexible depending on the modulation and the MIMO size. In Table 4.2, the choice of the training overheads (equivalent to the choice of K_b since K_p is fixed) and the corresponding information rates are summarized, for different combinations of modulation and MIMO size.

The step size μ of the adaptive algorithms was set to be exponentially decaying with each data reuse iteration as in [11, 4], and the decaying factor was set as $\beta = 0.9$. The initial step size was chosen as $\mu = 1$ during the training period, and decreased to

Table 4.2. List of training overheads (block sizes) and the corresponding data rates for different combinations of modulation and MIMO size

Modulation	MIMO size	Block size	Training overhead	Data rate (kbps)
QPSK	2×6	3600	13.89%	16.82
	3×12	2200	22.73%	22.64
	4×12	1800	27.78%	28.22
8PSK	2×6	2200	22.73%	22.64
	3×12	1800	27.78%	31.74
	4×12	1200	41.76%	34.18
16QAM	2×6	1800	27.78%	28.22
	3×12	1500	33.33%	39.06
	4×12	1050	47.62%	**40.92**

$\mu = 0.1$ at the DD mode. The choices of $K_1 = 100$, $K_2 = 50$ and $K_3 = K_4 = 50$ are used for the feedforward filter and the SIC filter, respectively, in this particular experiment. The maximum number of equalizer iteration (or data reuse) was set as 4. Other relevant parameters in the adaptive algorithm were set as $\delta_{\text{NLMS}} = 0.01, \delta_{\text{IPNLMS}} = 5 \times 10^{-5}, \epsilon = 0.01$, and $\alpha = 0$.

4.2 EXPERIMENTAL RESULTS

The results for the 200-m and 1000-m transmissions are presented. For the 200-m transmission, 30 S3 files and 15 S4 files were recorded in two days during the experiment. Each file contains one burst as shown above, and all 45 files were processed. For the 1000-m transmission, 34 data files were recorded during the trial but only 19 of them are valid. The 19 valid files including eight S5 files and eleven S6 files, were all processed.

4.2.1 Results On The Two-transducer MIMO Transmission. In this subsection, the processing of the two-transducer MIMO data is discussed. Table 4.3 provides a summary of the results, and the figure of merit is the number of packets achieving a specific BER level. From the table, the following observations are made: first, the effectiveness of the turbo equalization is clearly shown, as the detection perfor-

mance increases with the number of turbo iterations; second, the proposed SD-DA-TEQ with either NLMS or IPNLMS manifests fast convergence, since most packets achieve the specified BER performance within $3 \sim 4$ turbo iterations; third, the IPNLMS-based SD-DA-TEQ exhibits better performance than the NLMS-based SD-DA-TEQ, and the performance gain tends to increase with the modulation level. With QPSK or 8PSK modulations, the NLMS achieves comparable performance to the IPNLMS while at lower complexity, thus is a desired choice for practical use. With 16QAM modulation, however, the IPNLMS achieves considerable performance gain over the NLMS so is more preferred.

Table 4.3. Number of packets achieving the specified BER level (2×6 MIMO)

Range	Turbo iter.	QPSK (BER = 0)		8PSK (BER $< 10^{-4}$)		16QAM (BER $< 10^{-3}$)	
		NLMS	IPNLMS	NLMS	IPNLMS	NLMS	IPNLMS
200 m	0	0	0	0	0	0	0
	1	14	26	7	8	3	12
	2	20	14	9	16	5	13
	3	8	3	4	2	6	7
	4	0	0	4	5	5	3
	5	1	1	2	0	1	0
	Total	43	44	26	31	20	35
1000 m	0	0	3	0	0	0	0
	1	10	13	7	7	4	7
	2	5	0	1	1	4	6
	3	1	0	0	0	2	0
	4	0	1	0	0	1	0
	5	0	0	0	0	0	0
	Total	16	17	8	8	11	13

Fig. 4.4 provides a more intuitive demonstration of the final detection results (after five turbo iterations) in Table 4.3. It is easy to see that for the QPSK modulation, the NLMS and the IPNLMS achieve similar performance for both the 200-m and the 1000-m transmissions. For the 8PSK modulation, the IPNLMS is slightly better than

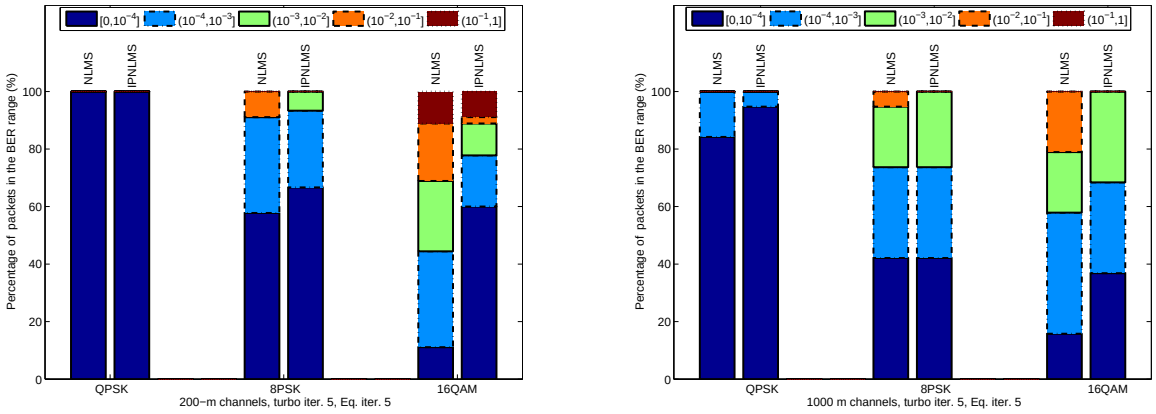

(a) (b)

Figure 4.4. Detection results of the two-transducer MIMO transmission after 5 turbo iterations. (a) Results of the 200-m channels. (b) Results of the 1000-m channels.

the NLMS. With the 16QAM modulation, however, the performance gap between the NLMS and IPNLMS is substantial. For example, the 200-m result shows the percentage of the packets with BER $< 10^{-4}$ increases from 11.1% for the NLMS to 60% for the IPNLMS after five turbo iterations.

Finally, performance analysis is provided for the proposed adaptive equalization via the mean square error (MSE) curve. For a given turbo iteration, the MSE of the n-th transmit stream at the $(t+1)$-th equalization iteration is estimated via a leaky integrator as [12, 13]

$$MSE_{n,k+1}^{t+1} = \lambda MSE_{n,k}^{t+1} + (1-\lambda)|e_{n,k}^{t+1}|^2 \tag{26}$$

where $k = 1, \cdots, K_b$, $e_{n,k}^{t+1}$=$\breve{x}_{n,k}^{t}$–$\hat{x}_{n,k}^{t+1}$ and λ is set as 0.99. It is noted that $MSE_{n,1}^{t+1} = MSE_{n,K_b+1}^{t}$, $e_{n,k}^{0}$=$Q(\hat{x}_{n,k}^{0})$–$\hat{x}_{n,k}^{0}$ when $N_{iter} = 0$,and $e_{n,k}^{0}$=$\bar{x}_{n,k}$–$\hat{x}_{n,k}^{0}$ when $N_{iter} > 0$. In Fig. 4.5, the MSE curves obtained in the detection of 200-m 2×6 MIMO packet with 8PSK and 16QAM modulations are presented, for the first and the third turbo iteration. Obviously, the MSE gaps between the NLMS and the IPNLMS tend to decrease with the number of equalization iterations. Even though, for the 16QAM modulation, there

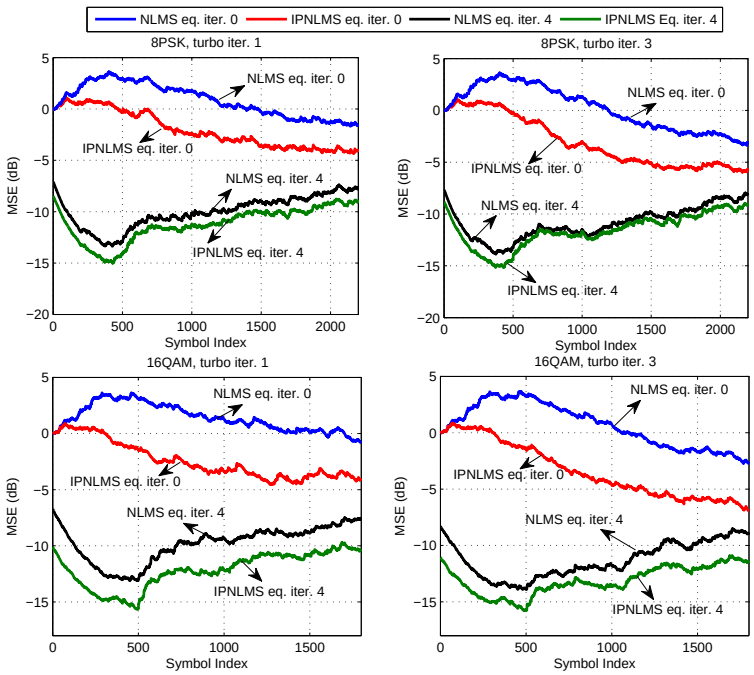

Figure 4.5. The MSE curves of the 2×6 MIMO detection with 8PSK and 16QAM modulations (200-m channel).

is still nonnegligible 2 dB difference between the IPNLMS and the NLMS, after multiple equalizer iterations. This observation matches the BER results in Table 4.3.

4.2.2 Results On The MIMO Transmission With More Than Two Transducers. This subsection presents the processing results for 3×12 and 4×12 MIMO transmission. Compared with the two-transducer transmission, the detection gets more difficult with more concurrent transmission streams, due to the increased co-channel interference (CCI). Figure 4.6 presents the results of the 1000-m 3×12 transmission. Though the 3×12 UWA channels experienced severe spatial selectivity due to the comparable channel gain between the third transducer and the receive hydrophones. The SD-DA-TEQ still enabled robust detection in the QPSK and 8PSK packets with reasonable training overhead. With a 22.73% training overhead, both the NLMS and the IPNLMS based SD-DA-TEQs detected successfully most QPSK packets with BER $< 10^{-4}$. Specifically, with the IPNLMS algorithm, 84.2% of the packets achieve BER $< 10^{-4}$ and the remaining packets have the BER $< 10^{-3}$. As to the

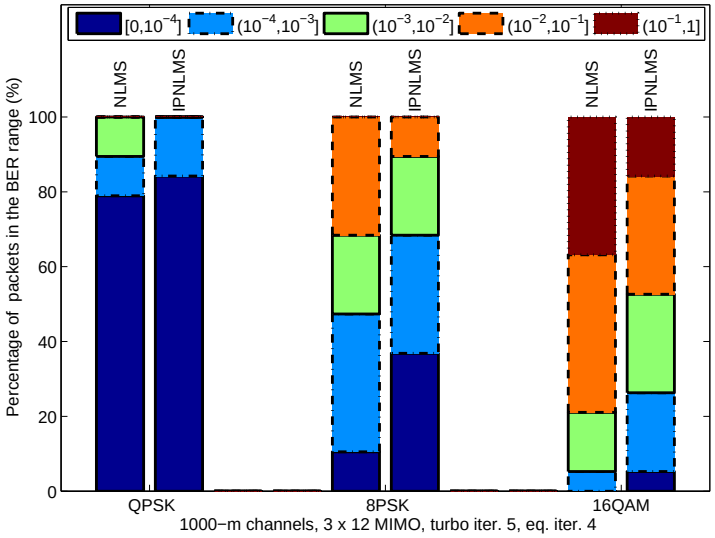

Figure 4.6. Detection results of the 3×12 MIMO transmission after 5 turbo iterations (1000-m channel).

8PSK packets, 89.5% of them achieve satisfactory performance with BER $< 10^{-2}$ with the IPNLMS algorithm, at a 27.78% training overhead. The training overhead for the 16QAM modulation was increased to 33.3%. With the IPNLMS-based SD-DA-TEQ, 52.6% 16QAM packets achieve the BER $< 10^{-2}$, and 31.6% packets reach the BER level of 10^{-2}.

The results of the 4×12 MIMO transmission are next demonstrated in Fig. 4.7, where the training overheads have been increased to 27.78%, 41.76% and 47.6% for QPSK, 8PSK, and 16QAM, respectively. Compared with the cases with 2 and 3 transducers, the performance improvement of the sparsity enhanced INPNLMS algorithm is greatly amplified in the 4×12 MIMO transmission. For example, the IPNLMS algorithm still works decently with the QPSK packets. Specifically, 57.9% QPSK packets achieve satisfactory performance with BER $< 10^{-3}$, and only one packet fails with BER $> 10^{-1}$. The detection results for 8PSK and 16QAM modulations, are not as satisfactory as those for the QPSK modulation, even a higher training overhead was used. A closer look at the detection results reveals the performance bottleneck lies in the third transmit stream, whose signal strength is pretty weak on the receive side.

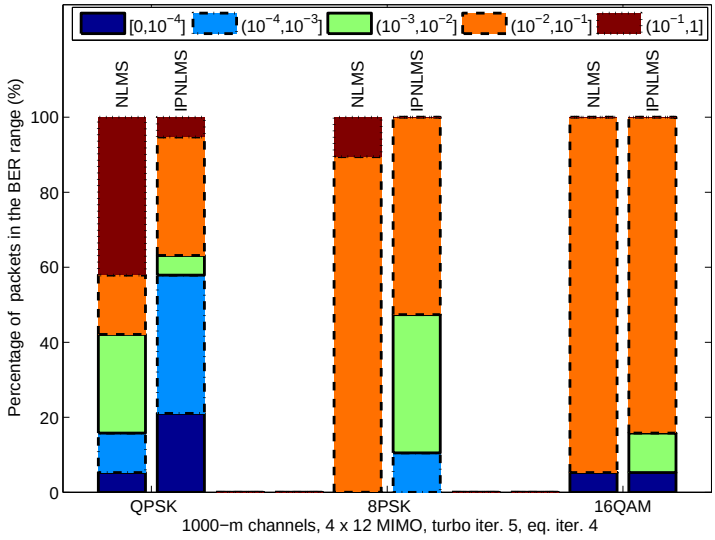

Figure 4.7. Detection results of the 4×12 MIMO transmission after 5 turbo iterations (1000-m channel).

4.2.3 Comparison Between The Proposed SD-DA-TEQ And The HD-DA-TEQ. It is found the HD-DA-TEQ experienced convergence issue in the processing of 8PSK and 16QAM packets, due to the catastrophic effect of error propagation. Even with QPSK modulation, the NLMS-based HD-DA-TEQ did not converge as also observed in [4]. Therefore, the comparison between the proposed SD-DA-TEQ and the HD-DA-TEQ is limited to the two-transducer MIMO transmission with QPSK modulation and the IPNLMS algorithm. The comparison is shown in Fig. 4.8 for the 200-m transmission. Obviously, the SD-DA-TEQ outperforms the HD-DA-TEQ dramatically. After three turbo iterations, 43 packets achieve zero BER by using the SD-DA-TEQ. On the contrary, the detection still fails for 15 packets with BER larger than 10^{-1} when the HD-DA-TEQ is adopted.

In Fig. 4.9, the detection results of the 200-m and the 1000-m transmissions are compared in terms of the percentages of different BER ranges. After one turbo iteration, 71.1% and 73.3% of packets achieve BER $< 10^{-4}$ for the 200-m channel and the 1000-m channel, respectively, with the proposed SD-DA-TEQ. With three turbo iterations, the SD-DA-TEQ successfully detected 97.8% 200-m packets and 94.8% 1000-m packets

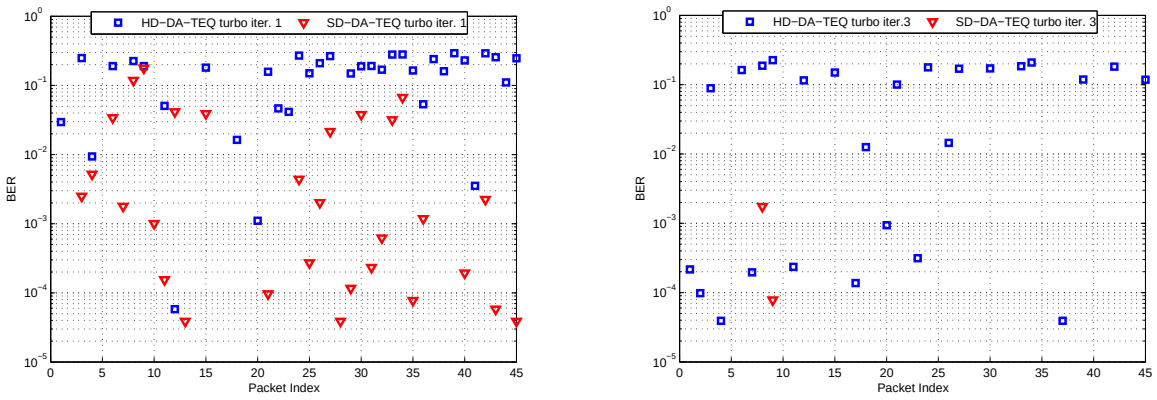

(a) (b)

Figure 4.8. BER comparison between the SD-DA-TEQ and the HD-DA-TEQ for 2×6 MIMO transmission (200-m channels). (a) Comparison after 1 turbo iteration. (b) Comparison after 3 turbo iterations.

with BER $< 10^{-4}$ (most of these packets achieved zero BER). With the HD-DA-TEQ, however, there are still 31.1% 200-m packets and 84.2% 1000-m packets failed with BER $> 10^{-1}$. This comparison again demonstrates the superiority of the proposed SD-DA-TEQ over the HD-DA-TEQ.

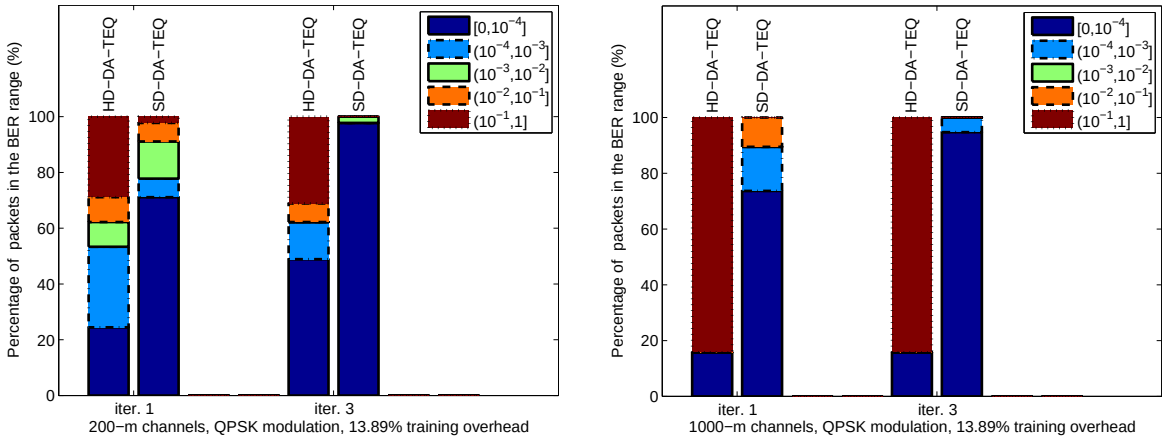

(a) (b)

Figure 4.9. BER range comparison between the SD-DA-TEQ and the HD-DA-TEQ after 1 and 3 turbo iterations for 2×6 MIMO transmission. (a) Comparison in the 200-m channels. (b) Comparison in the 1000-m channels.

Finally, the comparison in terms of MSE is presented in Fig. 4.10. From the figure, the difference in MSE between the proposed SD-DA-TEQ and the HD-DA-TEQ can be more than 5 dB. Further, the SD-DA-TEQ converges faster than the HD-DA-TEQ, as shown by the gap between the first and the third turbo iteration.

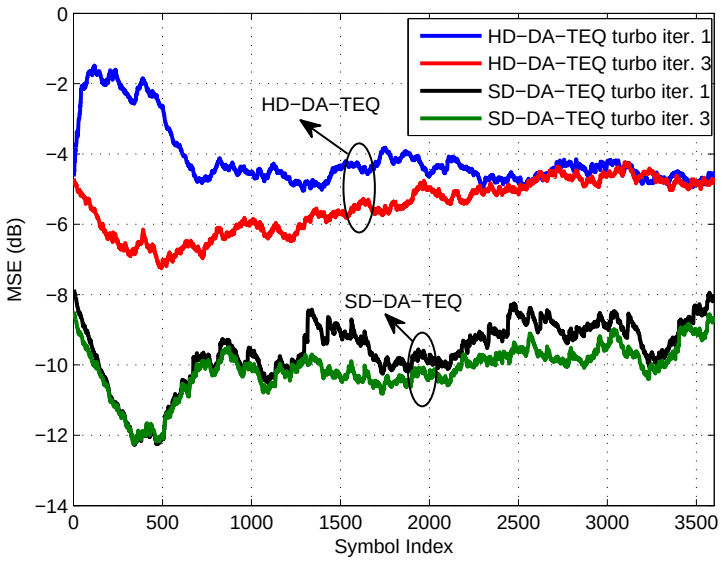

Figure 4.10. MSE comparison between the SD-DA-TEQ and the HD-DA-TEQ for 2×6 MIMO transmission (200-m channels).

4.2.4 Evolutional Behavior Of The Proposed SD-DA-TEQ. The performance gain brought by the turbo iteration of the SD-DA-TEQ, has been demonstrated in Table 4.3. In this subsection, the evolutional behavior of the SD-DA-TEQ is elaborated in more details.

In Fig. 4.11, the quality evolution of the soft decisions is presented by using 8PSK packet as an example. Each row shows the quality evolution at different equalizer iterations for a given turbo iteration, and each column demonstrates the quality evolution at different turbo iterations for a given equalizer iteration. Obviously, the quality of the soft decisions increases with the number of equalizer iterations and the

number of turbo iterations, as expected. It is also clearly shown the *a posteriori* soft decisions provide better fidelity than the *a priori* soft decisions due to the extra information gleaned over the equalization iterations.

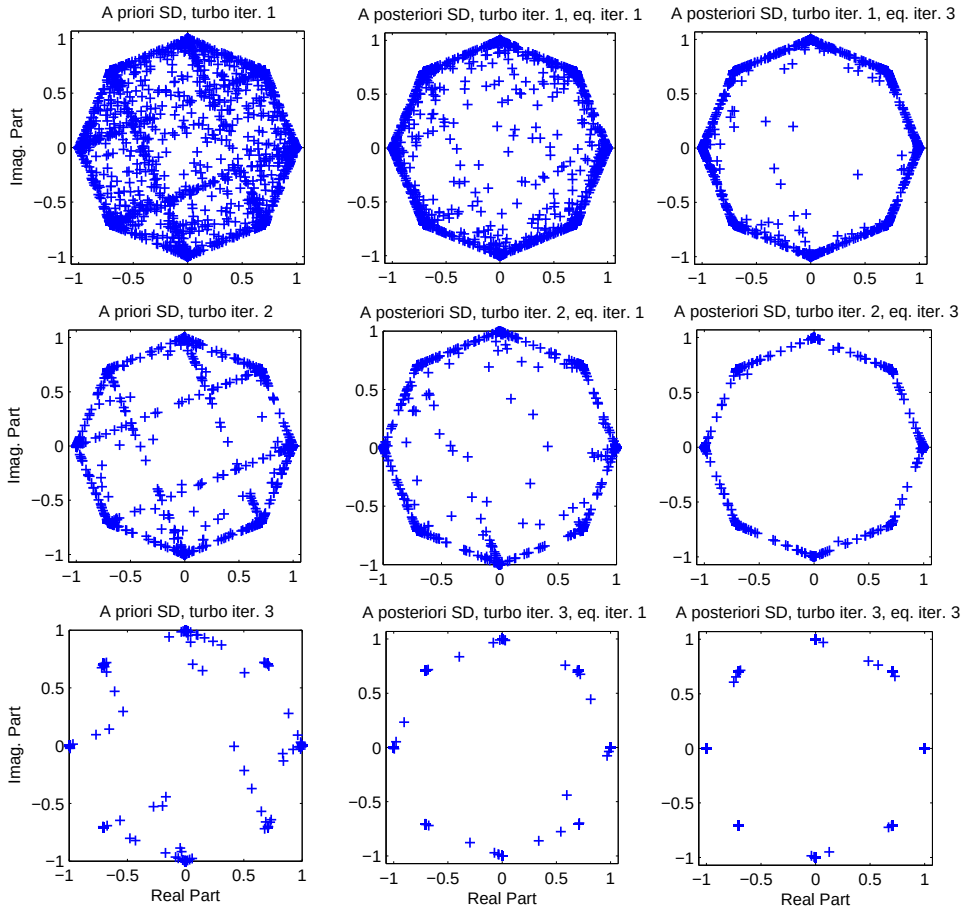

Figure 4.11. The evolution of soft decisions.

In Fig.4.12, the evolutional behavior of the IPNLMS-based SD-DA-TEQ is demonstrated by using MSE as the figure of merit. For each subfigure, the number of turbo iterations is fixed as 3, and the number of equalization iterations varies from 0 to 4. Obviously, the MSE decreases consistently with the increase in the equalization iterations, regardless of the modulation. With 4 equalization iterations, the performance gain achieved can be up to 14 dB and 6 dB during the training phase and the DD

phase, respectively. The results with the NLMS-based SD-DA-TEQ are very similar thus omitted for brevity.

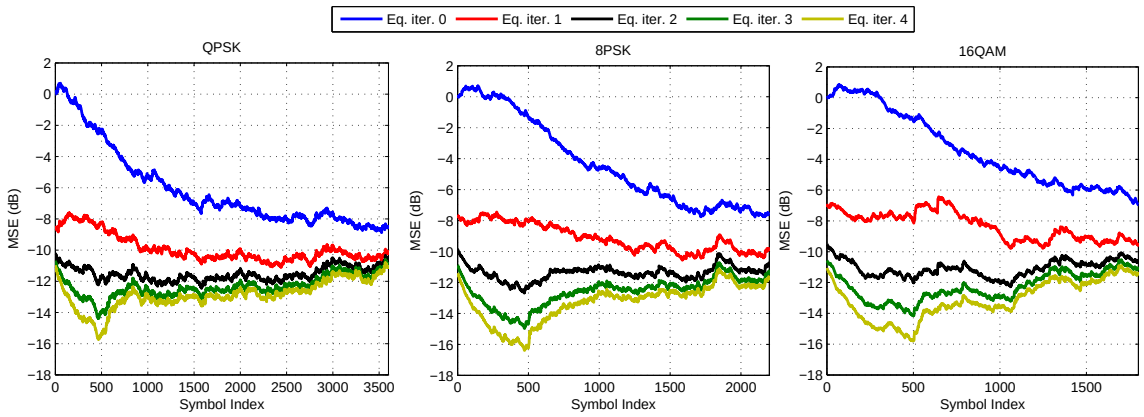

Figure 4.12. The MSE evolution of the IPNLMS-based SD-DA-TEQ.

In Fig. 4.13, the performance evolution of the NLMS-based SD-DA-TEQ with different numbers of equalization iterations is shown for the 8PSK packets, where the number of turbo iteration has been fixed as 3. Obviously, the detection fails (the BERs of all the packets are above 10^{-1}) without using any equalizer iteration. The performance keeps increasing with the increase in the number of equalizer iterations.

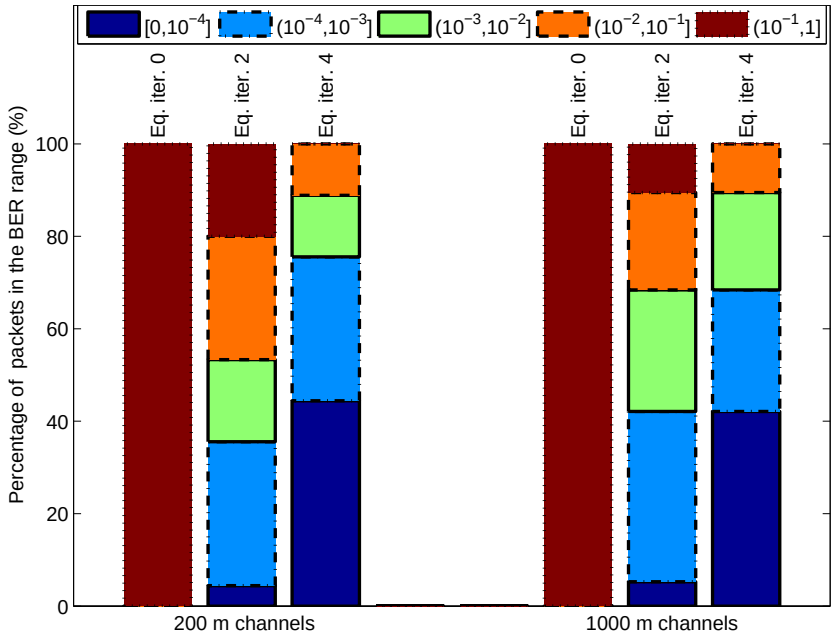

Figure 4.13. Performance evolution of the NLMS-based SD-DA-TEQ (2×6 MIMO, 8PSK, 22.73% training overhead).

5 CONCLUSION

A soft-decision driven adaptive turbo equalization scheme was proposed for MIMO underwater acoustic communications. The data reuse technique was adopted such that the adaptive equalizer itself performs iterative symbol detection, enabling the usage of *a posteriori* soft decisions for the equalizer adaptation and the soft interference cancelation. Attributed to the better fidelity of the *a posteriori* soft decisions as compared with the *a priori* soft decisions employed in the existing adaptive turbo equalization, the proposed scheme not only provided robust detection performance but was very efficient in terms of spectral utilization and processing delay. Therefore, it is a good candidate for practical use. The proposed scheme was tested by the experimental data collected in the SPACE08 undersea experiment and showed powerful detection capability. It worked successfully in MIMO transmission with multilevel modulations and more than two concurrent transmit streams, which is not found in existing literature.

6 ACKNOWLEDGEMENT

This work is supported in part by the National Science Foundation under Grant ECCS-1408316.

7 REFERENCES

[1] M. Stojanovic and J. Preisig, "Underwater acoustic communication channels: Propagation models and statistical characterization," *IEEE Commun. Mag.*, vol. 47, no. 1, pp. 84–89, Jan. 2009.

[2] T. C. Yang, "A study of spatial processing gain in underwater acoustic communications," *IEEE J. Ocean. Eng.*, vol. 32, no. 3, pp. 689–709, Jul 2007.

[3] R. Otnes and M. Tuchler, "Iterative channel estimation for turbo equalization of time-varying frequency-selective channels," *IEEE Trans. Wireless Commun.*, vol. 3, no. 6, pp. 1918–1923, Nov. 2004.

[4] Z. Yang and Y. R. Zheng, "Iterative channel estimation and turbo equalization for multiple-input multiple-output underwater acoustic communications," *IEEE J. Ocean. Eng.*, vol. 41, no. 41, pp. 232–242, Jan. 2016.

[5] A. Rafati, H. Lou, and C. Xiao, "Soft-decision feedback turbo equalization for LDPC-coded MIMO underwater acoustic communications," *IEEE J. Ocean. Eng.*, vol. 39, no. 1, pp. 90–99, Mar. 2014.

[6] J. Tao, Y. R. Zheng, C. Xiao, and T. Yang, "Robust MIMO underwater acoustic communications using turbo block decision-feedback equalization," *IEEE J. Ocean. Eng.*, vol. 35, no. 4, pp. 948–960, Oct. 2010.

[7] W. Duan and Y. R. Zheng, "Bidirectional soft-decision feedback turbo equalization for MIMO systems," *IEEE Trans. Veh. Technology*, vol. PP, no. 99, Aug. 2015.

[8] B. Peng and H. Dong, "Application of turbo equalization in ppc underwater acoustic communication," in *Proc. MTS/IEEE OCEANS Conf., San Diego, CA*, Sep. 2013, pp. 1–4.

[9] P. A. Van Walree and G. Leus, "Robust underwater telemetry with adaptive turbo multiband equalization," *IEEE J. Ocean. Eng.*, vol. 34, no. 4, pp. 645–655, 2009.

[10] L. Cannelli, G. Leus, H. Dol, and P. van Walree, "Adaptive turbo equalization for underwater acoustic communication," in *Proc. MTS/IEEE OCEANS Conf., Bergen, Norway*, pp. 1–9.

[11] J. W. Choi, T. J. Riedl, K. Kim, A. C. Singer, and J. C. Preisig, "Adaptive linear turbo equalization over doubly selective channels," *IEEE J. Ocean. Eng.*, vol. 36, no. 4, pp. 473–489, Oct. 2011.

[12] C. Laot, N. Beuzeulin, and A. Bourre, "Experimental results on mmse turbo equalization in underwater acoustic communication using high order modulation," in *Proc. MTS/IEEE OCEANS Conf., Seattle, WA*, Sep. 2010, pp. 1–6.

[13] C. Laot and R. L. Bidan, "Adaptive mmse turbo equalization with high-order modulations and spatial diversity applied to underwater acoustic communications," in *Wireless Conference 2011-Sustainable Wireless Technologies (European Wireless), 11th European*, Apr. 2011, pp. 1–6.

[14] M. Qingwei, H. Jianguo, H. Jing, H. Chengbing, and M. Chuang, "An improved direct adaptive multichannel turbo equalization scheme for underwater communications," in *Proc. MTS/IEEE OCEANS Conf., Yeosu, Korea*, May 2012, pp. 1–5.

[15] A. Yellepeddi and J. C. Preisig, "Adaptive equalization in a turbo loop," *IEEE Trans. Wireless Commun.*, vol. 14, no. 9, pp. 5111–5122, Sep. 2015.

[16] S. Roy and J. J. Shynk, "Analysis of the data-reusing LMS algorithm," in *Proc. 32nd Midwest Symp. Circuits Sys.*, vol. 2, Aug. 1989, pp. 1127–1130.

[17] J. Tao, "Single-carrier frequency-domain turbo equalization with various soft interference cancellation schemes for MIMO systems," *IEEE Trans. Commun.*, vol. 63, no. 9, pp. 3206–3217, Sep. 2015.

[18] M. Tuchler, R. Koetter, and A. C. Singer, "Turbo equalization: principles and new results," *IEEE Trans. Commun.*, vol. 50, no. 5, pp. 754–767, May 2002.

[19] M. Tuchler, A. C. Singer, and R. Koetter, "Minimum mean squared error equalization using *a priori* information," *IEEE Trans. Signal Process.*, vol. 50, no. 3, pp. 673–683, Mar. 2002.

[20] H. Lou and C. Xiao, "Soft-decision feedback turbo equalization for multilevel modulations," *IEEE Trans. Signal Process.*, vol. 59, no. 1, pp. 186–195, Jan. 2011.

[21] S. Haykin, *Adaptive Filter Theory*, 4th ed. Upper Saddle River, New Jersey, 07458.: Prentice Hall, 2002.

[22] D. L. Duttweiler, "Proportionate normalized least-mean-squares adaptation in echo cancelers," *IEEE Trans. Speech, Audio Process.*, vol. 8, no. 5, pp. 508 –518, Sep. 2000.

[23] A. J. Paulraj, D. A. Gore, R. U. Nabar, and H. Bölcskei, "An overview of MIMO communications-a key to gigabit wireless," *Proceedings of the IEEE*, vol. 92, no. 2, pp. 198–218, Feb. 2004.

III. BLOCK ITERATIVE FDE FOR MIMO UNDERWATER ACOUSTIC COMMUNICATIONS

Weimin Duan, Yahong Rosa Zheng *Fellow, IEEE*, Dajun Sun, and Youwen Zhang

ABSTRACT—In this paper, we propose a low complexity iterative detection scheme for the uncoded zero padding (ZP) single carrier (SC) transmission in Multiple-input Multiple-output (MIMO) underwater acoustic (UWA) channels. Due to the long multipath in UWA channels, ZP SC-FDE has to use large block size to achieve low computational complexity and high data efficiency. But, the higher bandwidth efficiency results in more sever channel estimation error and performance degradation. To enhance the performance of the ZP SC systems with high data efficiency, we design a soft-decision block iterative frequency-domain equalization (BI-FDE) combined with iterative channel estimation. With increasing reliability as the the iteration proceeds, the soft decision symbols obtained at the previous iteration are used to re-estimate the channel, thus improving the overall system performance. Since both the feedfoward and feedback filters are designed in frequency domain without the aid of channel coding, the proposed SD BI-FDE scheme is affordable for real-time implementation. The performance enhancement of the proposed iterative receiver has been verified through a pool test.

1 INTRODUCTION

High data-rate multiple-input multiple-output (MIMO) underwater acoustic (UWA) communications is very challenging due to severe inter-symbol interference, strong spatial correlation and fast channel variation. Currently, two classes of low-complexity transmission schemes are commonly used in high data-rate coherent UWA communications: orthogonal frequency division multiplexing (OFDM) and singer carrier frequency domain equalization (SC-FDE) [1, 2]. The OFDM system divides the data stream into multiple parallel data streams, which are transmitted with orthogonal subcarriers. Since the sub-channels can be treated as frequency flat fading channels, the (Fast Fourier Transform) FFT based receiver can be implemented with low complexity. SC-FDE transmits in wideband but converts the received signal into frequency domain via FFT, performs frequency domain equalization, and converts the equalized signal back to time domain via IFFT before detection. The SC-FDE has the same overall transceiver complexity as that of the OFDM.

Due to the long multipath in UWA channels, both OFDM and SC-FDE has to use large block size to achieve high data efficiency. But, the higher bandwidth efficiency results in more sever channel estimation error and performance degradation. Combined with channel coding, Turbo SC-FDEs have been proposed to approach the near optimal performance in MIMO (UWA) communications [2]. However, the iterative processing in Turbo SC-FDE considerably complicates the hardware design of the receiver, since the unavoidable soft-output decoding contributes a lot to the overall computational complexity. It is then of great practical interest to design an iterative frequency domain equalizer without the soft-output decoder for UWA communications.

A block iterative FDE (BI-FDE) with frequency domain decision feedback filtering was proposed for uncoded SC-FDE systems [3]. The BI-FDE operates iteratively on the same set of received signal without the help of channel coding. At each iteration,

the decisions of the estimated symbols in the previous iteration are used as the input of the frequency domain decision feedback filter. Meanwhile, the filter coefficients are computed in each iteration with the estimated correlation factor (hard decision directed design) or data signal power and disturbance variance (soft decision directed design). The BI-FDE was extended to uncoded and coded SC-MIMO systems in [4]. However, it does not apply the independence constraint when soft decision feedback is used, and the performance in MIMO systems is not shown. The application of BI-FDE in UWA communications is very limited. Most of existing work test the block iterative FDE in single-input single-output or single-input multiple output systems [5, 6].

In this paper, we investigate the BI-FDE for zero padding (ZP) SC MIMO UWA communications. In the proposed FD receive scheme, an iterative channel estimator is embedded into the BI-FDE, where the soft decisions of the estimated symbols in the previous iteration are also used to re-estimate the channel. A 2x4 MIMO UWA communication test was conducted in the pool of Harbin Engineering University to verify the proposed algorithm. Without the help of channel coding, the experimental results show that the proposed iterative receiver achieves satisfactory performance at the symbol error rate (SER) level of 10^{-3} to 10^{-4}.

2 SYSTEM MODEL

Consider an uncoded MIMO UWA communication systems with N transducers at the transmitter and M hydrophones at the receiver. At the transmitter, each independent binary information bit stream is mapped into symbols, which are chosen from a specific alphabet set $\mathcal{S} = \{\alpha_1, \alpha_2, \cdots, \alpha_{2^Q}\}$ with normalized unit average power. The mapped symbols are then grouped into blocks with length K, and K_{zp} zeros are inserted between two consecutive blocks to avoid the inter-block interference (IBI). The N parallel zero-padded (ZP) blocks are modulated with the same single carrier, then simultaneous transmitted to the MIMO UWA channel.

After front end processing at the receiver, such as synchronization, demodulation and down sampling, the received baseband signal of the m-th hydrophone at time instant k can be expressed as

$$r_{m,k} = \sum_{n=1}^{N} \sum_{l=0}^{L-1} h_l(m,n) x_{n,k-l} + w_{m,k}, \tag{1}$$

where $\{h_l(m,n)\}_{l=0}^{L-1}$ is the channel impulse response (CIR) between the $m-th$ hydrophone and $n-th$ transducer, and L is the length of the channel. Besides, $w_{m,k}$ is the sampled additive white Gaussian noise (AWGN) at the $m-th$ hydrophone with zero mean and variance σ_w^2. After stacking up the received symbols from all the M receive elements, the received signals can be written as a vector $\mathbf{r}_k = [r_k^{(1)}, r_k^{(2)}, \ldots, r_k^{(M)}]^T$

$$\mathbf{r}_k = \sum_{l=0}^{L-1} \mathbf{h}_l \mathbf{x}_{k-l} + \mathbf{w}_k \tag{2}$$

where

$$\mathbf{x}_k = [x_{1,k}, x_{2,k}, \ldots, x_{N,k}]^T \tag{3}$$

$$\mathbf{w}_k = [w_{1,k}, w_{2,k}, \ldots, w_{M,k}]^T \tag{4}$$

and

$$\mathbf{h}_l = \begin{bmatrix} h_l(1,1) & h_l(1,2) & \cdots & h_l(1,N) \\ h_l(2,1) & h_l(2,2) & \cdots & h_l(2,N) \\ \vdots & \vdots & \ddots & \vdots \\ h_l(M,1) & h_l(M,2) & \cdots & h_l(M,N) \end{bmatrix}. \tag{5}$$

To enable the low-complexity frequency domain bin-wise processing, we use an overlap-add (OLA) method to reformulate the received signal as

$$\mathbf{y} = [\mathbf{r}_1^{\mathrm{T}}, \cdots, \mathbf{r}_K^{\mathrm{T}}]^{\mathrm{T}} + [\mathbf{r}_{K+1}^{\mathrm{T}}, \cdots, \mathbf{r}_{K+K_{zp}}^{\mathrm{T}}, \mathbf{0}_{1\times(K-K_{zp})}]^{\mathrm{T}}. \tag{6}$$

Note that the OLA method is also used in ZP-OFDM [7]. Then the linear convolution in (2) is converted to a circular convolution as

$$\mathbf{y} = \mathbf{h}\mathbf{x} + \mathbf{w}, \tag{7}$$

where $\mathbf{x} = [\mathbf{x}_1, \mathbf{x}_2, \cdots, \mathbf{x}_K]^{\mathrm{T}}$ is the concatenated transmitted symbols, $\mathbf{w} = [\mathbf{w}_1, \mathbf{w}_2, \cdots, \mathbf{w}_K]^{\mathrm{T}}$ is the vector of sampled noise, and $\mathbf{h}$ is a block circulant channel matrix with $[\mathbf{h}_0^{\mathrm{T}}, \cdots, \mathbf{h}_{L-1}^{\mathrm{T}}, \mathbf{0}_{M\times\{N(K-L)\}}]^{\mathrm{T}}$ being its first column.

To convert the block-wise time domain signal into frequency domain, we define a K-point unitary discrete Fourier transform (DFT) matrix as $\mathbf{F}$. Thus $\mathbf{F}^H$ is the K-point unitary IDFT matrix. For MIMO systems, the block DFT matrix for transmitted symbol vectors and received signal vectors are further defined as $\mathbf{F}_{\mathrm{t}} = \mathbf{F} \otimes \mathbf{I}_N$ and $\mathbf{F}_{\mathrm{r}} = \mathbf{F} \otimes \mathbf{I}_M$, respectively, where $\otimes$ denotes the Kronecker product operation. Multiply $\mathbf{F}_{\mathrm{r}}$ on both sides of (7) yields

$$\mathbf{Y} = \mathbf{F}_{\mathrm{r}}\mathbf{h}\mathbf{x} + \mathbf{F}_{\mathrm{r}}\mathbf{w} = \mathbf{H}\mathbf{X} + \mathbf{F}_{\mathrm{r}}\mathbf{w}, \tag{8}$$

where $\mathbf{Y} = [\mathbf{Y}_1, \mathbf{Y}_2, \cdots, \mathbf{Y}_K]^{\mathrm{T}}$ is the frequency domain block-wise received signal, $\mathbf{X} = \mathbf{F}_{\mathrm{t}}\mathbf{x} = [\mathbf{X}_1, \mathbf{X}_2, \cdots, \mathbf{X}_K]^{\mathrm{T}}$ is the frequency domain block-wise transmitted symbols, and

$\mathbf{H} = \mathbf{F}_{\mathrm{r}}\mathbf{h}\mathbf{F}_{\mathrm{t}}^{\mathrm{H}}$ is the frequency domain channel matrix. Since the time domain channel matrix $\mathbf{h}$ is block circular, $\mathbf{H} = \mathrm{Bdiag}\{\mathbf{H}_k\}_{k=1}^{K}$ is a block diagonal matrix, with each diagonal element $\mathbf{H}_k$ being the frequency response of the MIMO channel at the k^{th} frequency bin.

3 BLOCK ITERATIVE RECEIVE SCHEME FOR MIMO SYSTEMS

We propose a block iterative receive scheme which combines the BI-FDE with iterative channel estimation for uncoded MIMO systems. As depicted in Fig. 3.1, an iterative channel estimator is embedded in a BI-FDE to perform the joint channel estimation and equalization. In each iteration, the soft decisions from the FDE are used both in channel estimation and decision feedback equalization at the next iteration.

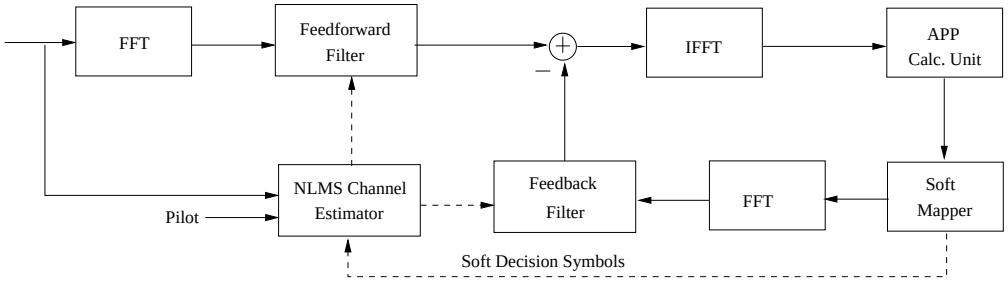

Figure 3.1. Structure of the proposed iterative receiver.

The BI-FDE consists of a FD feedforward filter $\mathbf{W}$ and a FD feedback filter $\mathbf{D}$. In the ith iteration, the estimated transmit symbols are given as [8]

$$\hat{\mathbf{x}}^{(i)} = \mathbf{F}_{\mathrm{t}}^{\mathrm{H}}\mathbf{W}\mathbf{Y} - \mathbf{F}_{\mathrm{t}}^{\mathrm{H}}\mathbf{D}\mathbf{F}_{\mathrm{t}}\tilde{\mathbf{x}}^{(i-1)}, \tag{9}$$

where $\tilde{\mathbf{x}}^{(i-1)}$ is the *a posteriori* soft decisions of the transmit symbols at the $(i-1)$-th iteration. The feedforward filter $\mathbf{W} = \mathrm{Bdiag}\{\mathbf{W}_k\}_{k=1}^{K}$ and the feedback filter $\mathbf{D} = \mathrm{Bdiag}\{\mathbf{D}_k\}_{k=1}^{K}$ are calculated by minimizing the $\mathrm{MSE}^{(i)} = \mathrm{E}\{(\hat{\mathbf{x}}^{(i)} - \mathbf{x})^{\mathrm{H}}(\hat{\mathbf{x}}^{(i)} - \mathbf{x})\}$ with the constraint $\sum_{k=1}^{K}\mathbf{D}_k[n,n] = 0$, for $n = 1, 2, \cdots, N$. Here, the constraint avoids the self-subtraction of the desired symbol in the feedback signals [8]. Using the Lagrange

multipliers method as in [8], the $\mathbf{W}$ and $\mathbf{D}$ can be solved as

$$\mathbf{W}_k = (\mathbf{I}_N + \mathbf{D}_k\mathbf{\Theta}_0^{\mathrm{H}})\mathbf{H}_k^{\mathrm{H}}(\mathbf{H}_k\mathbf{H}_k^{\mathrm{H}} + \sigma^2\mathbf{I}_M)^{-1}, \tag{10a}$$

$$\mathbf{D}_k = \mathbf{D}_k^1 - \mathbf{\Lambda}\mathbf{D}_k^2, \tag{10b}$$

where $\mathbf{D}_k^1 = \mathbf{\Gamma}_k\mathbf{B}_0\mathbf{D}_k^2$, $\mathbf{D}_k^2 = (\mathbf{B}_0 - \mathbf{\Theta}_0^{\mathrm{H}}\mathbf{\Gamma}_k\mathbf{\Theta}_0)^{-1}$, $\mathbf{\Gamma}_k = \mathbf{H}_k^{\mathrm{H}}(\mathbf{H}_k\mathbf{H}_k^{\mathrm{H}} + \sigma^2\mathbf{I}_M)^{-1}\mathbf{H}_k$. $\mathbf{B}_0$ and $\mathbf{\Theta}_0$ are correlation matrices defined as

$$\begin{aligned} \mathbf{B}_0 &= \mathrm{diag}\{\beta_1, \beta_2, \cdots, \beta_N\}, \\ \mathbf{\Theta}_0 &= \mathrm{diag}\{\theta_1, \theta_2, \cdots, \theta_N\}, \end{aligned} \tag{11}$$

where the elements of $\mathbf{B}_0$ and $\mathbf{\Theta}_0$ are obtained by

$$\begin{aligned} \mathrm{E}\{\tilde{x}_{n,k}^{(i-1)}(\tilde{x}_{n',k'}^{(i-1)})^*\} &= \beta_n\delta_{n,n'}\delta_{k,k'}, \\ \mathrm{E}\{x_{n,k}(\tilde{x}_{n',k'}^{(i-1)})^*\} &= \theta_n\delta_{n,n'}\delta_{k,k'}, \end{aligned} \tag{12}$$

and $\delta_{n,n'} = 1$, $\delta_{k,k'} = 1$ if and only if $n = n'$, $k = k'$. Besides, $\mathbf{\Lambda} = \mathrm{diag}\{\lambda_1, \lambda_2, \cdots, \lambda_N\}$ is a diagonal matrix, and each element is a Lagrange multiplier

$$\lambda_n = \frac{\sum_{k=1}^{K}\mathbf{D}_k^1[n,n]}{\sum_{k=1}^{K}\mathbf{D}_k^2[n,n]}. \tag{13}$$

The equalized symbol $\hat{x}_{n,k}^{(i)}$ is assumed to be Gaussian distributed $\mathcal{N}(\check{\mu}_n x_{n,k}^{(i)}, \check{\sigma}_n^2)$, which is similar to the broadly used gaussian approximation in turbo equalization. The parameters $\check{\mu}_n$ and $\check{\sigma}_n^2$ are given as

$$\begin{aligned} \check{\mu}_n &= \frac{1}{K}\sum_{k=1}^{K}\Big\{\mathbf{W}_k\mathbf{H}_k\Big\}[n,n], \\ \check{\sigma}_n^2 &= \frac{1}{K}\sum_{k=1}^{K}\Big\{\mathbf{\Gamma}_k + \mathbf{D}_k(\mathbf{B}_0 - \mathbf{\Theta}_0^{\mathrm{H}}\mathbf{\Gamma}_k\mathbf{\Theta}_0)\mathbf{D}_k^{\mathrm{H}}\Big\}[n,n] - \check{\mu}_n^2. \end{aligned} \tag{14}$$

Then based on the equalized symbol $\hat{x}_{n,k}^{(i)}$, the *a posteriori* probability $p(x_{n,k}^{(i)} = \alpha_j|\hat{x}_{n,k}^{(i)})$ can be computed as

$$p(x_{n,k}^{(i)} = \alpha_j|\hat{x}_{n,k}^{(i)}) = C \exp \frac{-|\hat{x}_{n,k}^{(i)} - \check{\mu}_n \alpha_j|^2}{\check{\sigma}_n^2} \tag{15}$$

where the α_j belongs to the alphabet set S and C is a constant. We use the *a posteriori* probability $p(x_{n,k}^{(i)} = \alpha_j|\hat{x}_{n,k})$ to calculate the *a posteriori* mean of the equalized symbol $\hat{x}_{n,k}^{(i)}$ as follows

$$\tilde{x}_{n,k}^{(i)} = \sum_{\alpha_j \in S} \alpha_j p(x_{n,k}^{(i)} = \alpha_j|\hat{x}_{n,k}^{(i)}), \tag{16}$$

which are treated as the *a posteriori* soft decisions of $\hat{x}_{n,k}^{(i)}$ and fed into the feedback filter at the $(i+1) - th$ iteration.

Moreover, we also use the *a posteriori* soft decisions of $\hat{x}_{n,k}^{(i)}$ as the virtual pilot to re-estimate the channel, which iteratively lower the channel estimation error. In this paper, we use a low-complexity normalized least mean squares (NLMS) algorithm to perform the iterative channel estimation. Note that in the first iteration, the soft decisions of the transmit symbols are unavailable, hence the pilot symbols are used to provide the initial estimation of the channel.

4 POOL EXPERIMENTAL RESULTS

4.1 EXPERIMENTAL SETUP AND DATA FORMAT

A pool experiment was conducted to test the proposed algorithm at Harbin Engineering University in July, 2015. In this experiment, a MIMO single carrier acoustic communication system with QPSK modulation was tested. The center carrier frequency was $f_c = 12$ kHz. The symbol rate was 4 kbps, and the roll-off factor for the square-root raised cosine pulse shaping filter was chosen as $\beta = 0.2$. Two transducers and 4 hydrophones were used to set up a 2×4 MIMO transmission.The depth of the pool was 5 m. The two transducers were positioned at 1.25 m and 2.05 m below the water surface, respectively. The four hydrophones were evenly placed with depth from 1.4 m to 3.2 m. The communication distance was approximately 15 m. Both the transducer and hydrophone were fixed, and the water surface kept calm during the experiment. Silver sand are put at the bottom of the pool to simulate the environment of an underwater channel. Besides, anechoic tile is attached on both sides of the pool to formulate far field acoustic propagation.

The data structure of the transmit blocks are presented in Fig. 4.1. The block size of data payloads are set as 2048 and 4096. In each block, 400 pilot symbols are inserted before the data payload for initial channel estimation. Besides, linear frequency modulation (LFM) signals are attached at the front and end of each packet for synchronization.

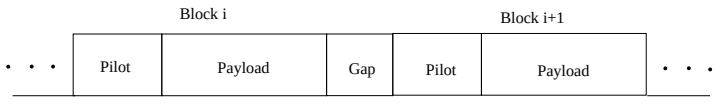

Figure 4.1. The data structure in the pool experiment.

4.2 PERFORMANCE EVALUATION

A typical channel in the experiment is shown in Fig. 4.2, which has long and severe multipath delay. Hence single carrier communications in this environment would be challenging.

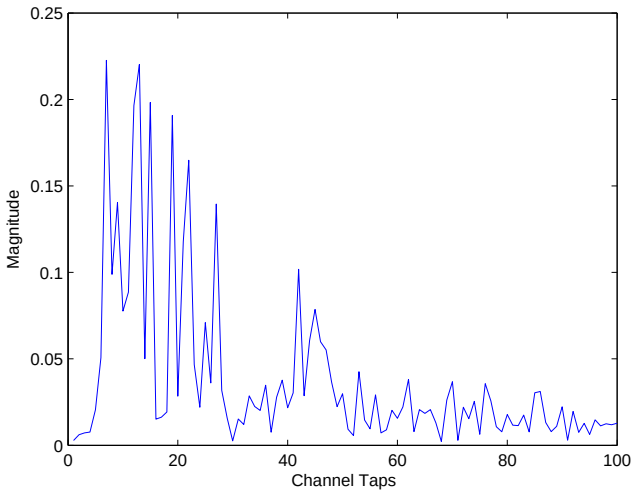

Figure 4.2. An example channel in the pool experiment.

We processed 32 blocks of size 2048 and 24 blocks of size 4096, and the pilot overheads for the two groups of data are 19.5% and 9.77%, respectively. Figure 4.3 provides a typical example of the IB-FDE process with a block of size 4096, which increases the output SNR by 4.5dB. In this example, the SER with one-time FDE is 0.047. After 6 iteration, the SER is decreased to 2.44×10^{-4}, which achieves two orders of performance improvement.

The SER performance is further summarized in Fig. 4.4 and Fig. 4.5, in terms of the percentage of the blocks that fall in the specified BER ranges. Generally, the performance of blocks with higher bandwidth efficiency are worse than blocks with lower bandwidth efficiency. In both cases of block transmission, the iterative processing progressively reduces the error of symbol detection. For blocks with size of 2048, after

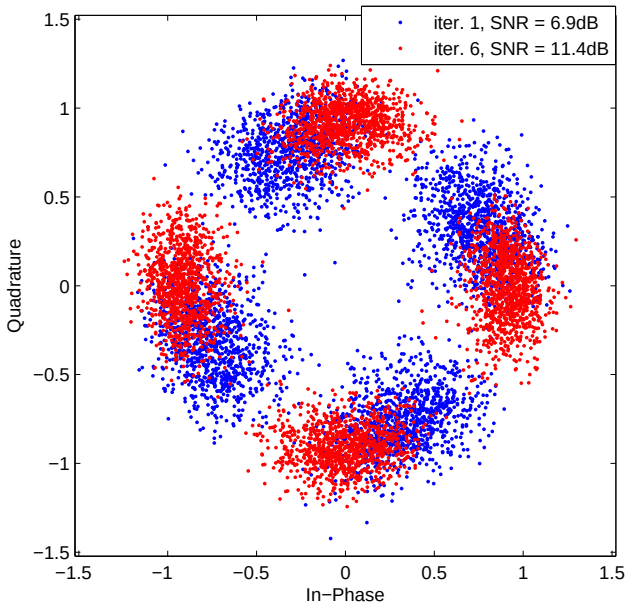

Figure 4.3. An example of performance improvement in the IB-FDE process.

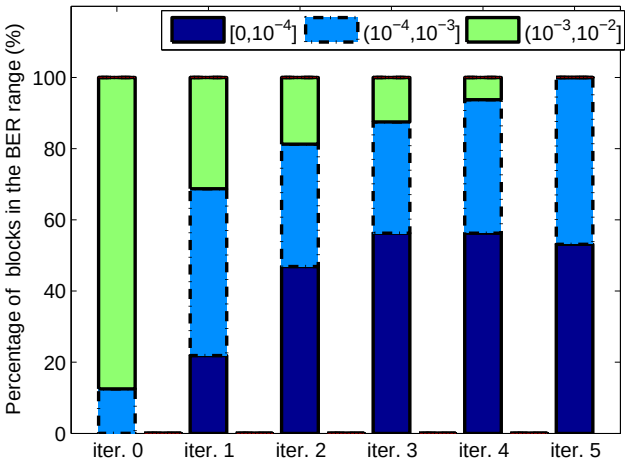

Figure 4.4. BER ranges comparison with different number of iterations (block size 2048, 2×4 MIMO UWA channels).

5 iterations, 53.1% blocks achieves SER $< 10^{-4}$ and other 46.9% blocks still have SER $< 10^{-3}$. The blocks with 4096 symbols follows a similar performance trend, which have 62.5% of blocks with SER $< 10^{-3}$ after 6 iterations.

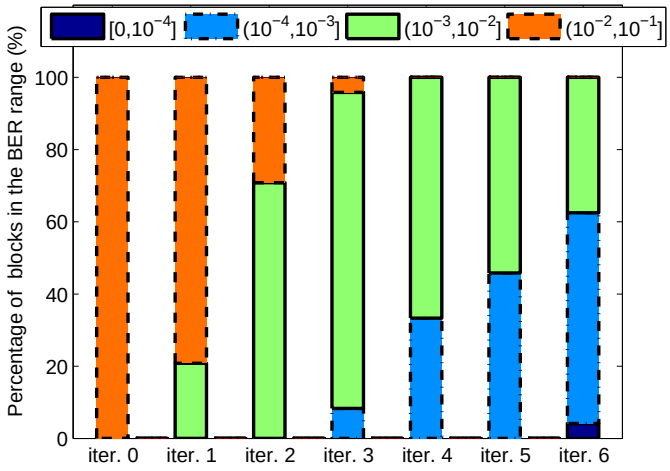

Figure 4.5. BER ranges comparison with different number of iterations (block size 4096, 2×4 MIMO UWA channels).

5 CONCLUSION

In this paper, a low-complexity block iterative frequency domain symbol detection scheme is proposed for ZP SC-MIMO UWA communications. The iterative receiver combines the BI-FDE with iterative channel estimation. The algorithm has been verified through an UWA single carrier communication test with high data-efficiency. The reliability of symbol detection and channel estimation increased iteratively, which gains obvious performance improvement over non-iterative FDE. Compared with traditional FD Turbo equalization, the complexity of the proposed receiver is further reduced, which is promising for real-time implementation.

6 ACKNOWLEDGMENTS

The work of Weimin Duan and Yahong Rosa Zheng is supported by U.S. National Science Foundation under Grant No. ECCS-1408316.

7 REFERENCES

[1] B. Li, S. Zhou, M. Stojanovic, L. Freitag, and P. Willett, "Multicarrier communication over underwater acoustic channels with nonuniform Doppler shifts," *IEEE J. Ocean. Eng.*, vol. 33, no. 2, pp. 198–209, 2008.

[2] J. Zhang and Y. R. Zheng, "Frequency-domain turbo equalization with soft successive interference cancellation for single carrier MIMO underwater acoustic communications," *IEEE Trans. Wireless Commun.*, vol. 10, no. 9, pp. 2872–2882, 2011.

[3] N. Benvenuto and S. Tomasin, "Iterative design and detection of a DFE in the frequency domain," *IEEE Trans. Commun.*, vol. 53, no. 11, pp. 1867–1875, 2005.

[4] N. Benvenuto, R. Dinis, D. Falconer, and S. Tomasin, "Single carrier modulation with nonlinear frequency domain equalization: an idea whose time has come—again," *Proc. IEEE*, vol. 98, no. 1, pp. 69–96, 2010.

[5] C. He, S. Huo, Q. Zhang, H. Wang, and J. Huang, "Multi-channel iterative fde for single carrier block transmission over underwater acoustic channels," *Communications, China*, vol. 12, no. 8, pp. 55–61, 2015.

[6] C. He, S. Huo, H. Wang, Q. Zhang, and J. Huang, "Single carrier with multi-channel time-frequency domain equalization for underwater acoustic communications," in *Acoustics, Speech and Signal Processing (ICASSP), 2015 IEEE International Conference on*. IEEE, 2015, pp. 3009–3013.

[7] B. Muquet, Z. Wang, G. B. Giannakis, M. de Courville, and P. Duhamel, "Cyclic prefixing or zero padding for wireless multicarrier transmissions?" *IEEE Trans. Commun.*, vol. 50, no. 12, pp. 2136–2148, 2002.

[8] G. M. Güvensen and A. Özgür Ylmaz, "A general framework for optimum iterative blockwise equalization of single carrier MIMO systems and asymptotic performance analysis," *IEEE Trans. Commun.*, vol. 61, no. 2, pp. 609–619, 2013.

IV. EXPERIMENTAL EVALUATION OF TURBO RECEIVERS IN SINGLE-INPUT SINGLE-OUTPUT UNDERWATER ACOUSTIC CHANNELS

Weimin Duan and Yahong Rosa Zheng, *Fellow, IEEE*

ABSTRACT—This paper presents some experimental results on both the channel estimation based minimum mean square error Turbo equalizer (CE MMSE-TEQ) and the direct-adaptation turbo equalizer (DA-TEQ) in single-input single-output (SISO) underwater acoustic (UWA) channels. For CE MMSE-TEQ, we compare the soft-decision feedback Turbo equalizer (SDFE), the bidirectional soft-decision feedback Turbo equalizer (Bi-SDFE) and the classic linear Minimum Mean Square Error (MMSE) Turbo equalizer in terms of bit error rate (BER) performance. For DA-TEQ, the recently proposed soft-decision direct-adaptation TEQ (Soft DA-TEQ) is evaluated with the same set of experimental data. Both QPSK and multilevel modulations (8PSK and 16QAM) have been tested with the symbol rate of 9.77 ksymbols/s. Experimental results show that the CE-TEQs are more robust in SISO underwater acoustic transmission under harsh channel conditions. Especially, with low pilot overheads, the recently proposed Bi-SDFE achieved low BER performance in all cases.

1 INTRODUCTION

The multi-channel receive techniques, such as time-reversal combining [1], adaptive single-input multiple-output (SIMO) decision feedback equalization (DFE) [2], are used to increase the reliability of underwater data transmission. All the multi-channel receive techniques are built on the physical hydrophone arrays. However, a practical issue for an undersea network or point to point underwater acoustic (UWA) communications is the physical size of the modems. Especially for commercial UWA modems, the multi-channel receive schemes amplify the cost in hydrophones and hardware implementation. Therefore, the design of robust receive techniques with single receive element is highly desirable.

Turbo equalization is considered as an effective iterative receive scheme to combat UWA channel dispersions [3]. In turbo detection, channel equalization and decoding are performed jointly, which is different from classic receive scheme that separates the channel equalization and decoding. Hence, the power of modern channel codings are much more efficiently used during the signal detection, which greatly enhance the robustness of the communication systems. Currently, two classes of turbo equalizers are commonly used in UWA communications: channel estimation based minimum mean squared error turbo equalizer (CE MMSE-TEQ) [4, 5, 6] and direct-adaptation turbo equalizer (DA-TEQ) [7].

In CE MMSE-TEQ, the UWA channel is explicitly estimated and incorporated into the calculation of MMSE equalizer coefficients. The existing CE MMSE-TEQs can be further classified into two categories: Turbo MMSE Linear Equalizers (Turbo LEs) [8] and Turbo MMSE Decision Feedback Equalizers (Turbo DFEs) [3]. First, the approximate implementation of MMSE-LE (approximate Turbo LE) has been considered for UWA communications, which only updates the equalizer coefficients once at each Turbo iteration [4, 7]. Second, a family of Turbo DFEs have been proposed for

tough inter symbol interference (ISI) channels, which exhibit less noise enhancement and better Bit-Error-Rate (BER) performance than the Turbo LEs. For example, the soft-decision feedback Turbo equalizer (SDFE) [9] achieves good performance in severe ISI channels while maintaining linear computational complexity. Moreover, a bidirectional SDFE (Bi-SDFE) was recently proposed to further enhance the robustness of SDFE in tough UWA channels [10].

DA-TEQ is another class of TEQ considered for UWA communications, which uses adaptive algorithms to directly estimate the coefficients of the equalizer [11, 7]. Since the large size matrix inversion operation in the CE MMSE-TEQs is avoided, the DA-TEQ exhibits lower complexity and is more attractive for hardware implementation. After initial training, most existing DA-TEQs use hard-decisions of the equalizer output to track the time-variations of the UWA channel. The main drawback of this hard decision directed adaptation is the error propagation, which may result into a catastrophic failure of the convergence. To lower the error propagation effect in coefficients adaptation, a soft-decision DA-TEQ was recently proposed for multiple-input multiple-output (MIMO) UWA communications, where the *a priori* soft decision from the decoder is used to direct the filter adaptation [12].

The performance of the turbo equalization in UWA communication systems has been verified by many oceans experiments [4,5,7,11,13,6]. But, in most of the reported experiments, turbo equalization has been tested in either SIMO or MIMO systems, which all required a hydrophone array at the receiver. It is therefore interesting to evaluate the Turbo receiver algorithms, especially the recently proposed Turbo DFEs [13,10] and Soft DA-TEQ, for how robust they can perform with the single-input single-output (SISO) setting under harsh channel conditions. In this paper, we use data collected in the SPACE08 experiment to evaluate the performance of several Turbo receiver algorithms in time-varying SISO UWA channels.

2 SYSTEM MODEL

Consider a single carrier system with bit-interleaved coded modulation (BICM) as shown in Fig. 2.1. At the transmitter side, a sequence of information bits $\{b_i\}_{i=1}^{K_b}$ are encoded and interleaved. The interleaved coded bits are grouped as $\mathbf{c} = [\mathbf{c}_1 \;\; \mathbf{c}_2 \cdots \mathbf{c}_{K_c}]$, where $\mathbf{c}_k$ denotes the kth coded bit vector $[c_{k,1} \;\; c_{k,2} \cdots c_{k,q}]$ with the jth bit $c_{k,j} \in \{0, 1\}$. The symbol mapper then maps each coded bit vector $\mathbf{c}_k$ to a symbol x_k from the 2^q-ary alphabet set $S = \{\alpha_1, \alpha_2, \cdots, \alpha_{2^q}\}$. Here α_i corresponds to a deterministic bit pattern $\mathbf{s}_i = [s_{i,1}\, s_{i,2} \cdots s_{i,q}]$ with $s_{i,j} \in 0, 1$, which maps a group of interleaved encoded bits with a specific symbol. After symbol mapping, the baseband signal is upsampled and pulse shaped. The pulse shaped signal is modulated with a single carrier, then transmitted to the SISO UWA channel.

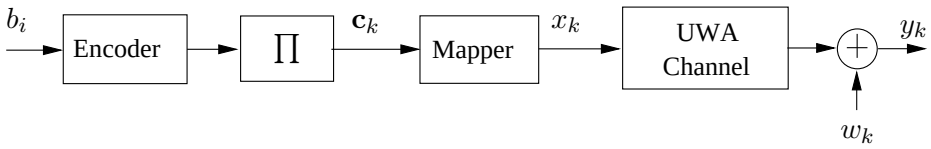

Figure 2.1. Block diagram of the single transmitter UWA communication system.

At the receiver side, the received signal is synchronized and demodulated to baseband. After downsampling, the symbol rate received baseband signal at time instant k is written as

$$y_k = \sum_{l=0}^{L-1} h_l x_{k-l} + n_k \tag{1}$$

where h_l is the lth tap of the length-L baseband equivalent UWA channel, x_{k-l} is the symbol transmitted at time instant $k - l$. In addition, n_k represents the sampled noise, which is modeled as additive white Gaussian noise (AWGN) with zero mean and variance σ_n^2. We can also stack $K = K_1 + K_2 + 1$ received symbols as a vector $\mathbf{r}_k$, and

rewrite equation (1) in matrix form

$$\mathbf{r}_k = \mathbf{H}\mathbf{x}_k + \mathbf{n}_k \tag{2}$$

where

$$\mathbf{r}_k = [y_{k-K_2}\ y_{k-K_2+1} \cdots y_{k+K_1}]^T \tag{3a}$$

$$\mathbf{x}_k = [x_{k-K_2-L+1}\ x_{k-K_2-L+2} \cdots x_{k+K_1}]^T \tag{3b}$$

$$\mathbf{n}_k = [n_{k-K_2}\ n_{k-K_2+1} \cdots n_{k+K_1}]^T \tag{3c}$$

$$\mathbf{H} = \begin{bmatrix} h_{L-1} & \cdots & h_0 & \cdots & 0 \\ \vdots & \ddots & \ddots & \ddots & \vdots \\ 0 & \cdots & h_{L-1} & \cdots & h_0 \end{bmatrix}. \tag{3d}$$

3 TURBO RECEIVER STRUCTURES

The structure of the MMSE Turbo receiver is depicted in Fig. 3.1, which is composed of two units: a MMSE Turbo equalizer and a maximum *a posterior* probability (MAP) decoder. Different from the classic separate processing scheme, the turbo receiver jointly performs the channel equalization and decoding in an iterative fashion. The MMSE equalizer estimates the transmitted symbol $\hat{x}_k$ with the received signal and the *a priori* log likelihood ratios (LLRs) $L_a(c_{k,j})$ provided by the decoder. Then, the estimated symbol $\hat{x}_k$ is mapped to the bit extrinsic LLRs $L_e(c_{k,j})$. After de-interleaving operation, the bit extrinsic LLRs are treated as the *a priori* information $L_a^d(c_{k',j'})$ for MAP decoding. The MAP decoder also outputs the corresponding bit extrinsic LLRs $L_e^d(c_{k',j'})$, which is further interleaved and fed back to the MMSE equalizer as the new bit *a priori* information $L_a(c_{k,j})$. Based on the turbo principle, the extrinsic LLRs are iteratively exchanged between the MMSE equalizer and MAP decoder, and the reliability of the soft information progressively increases with the number of iterations. After multiple iterations, the iterative processing stops, and the final hard decision $\hat{b}_i$ is made at the decoder output.

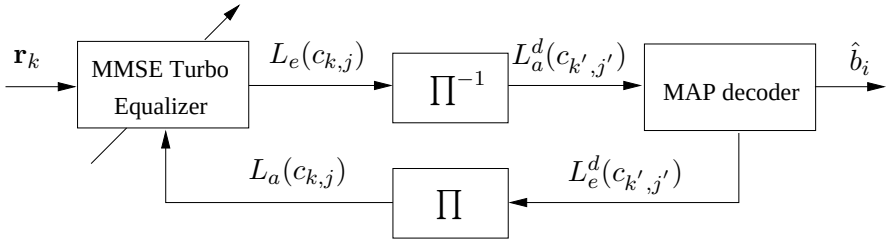

Figure 3.1. Block diagram of the Turbo receiver for SISO UWA communication system.

In the practical application of turbo receiver, the equalizer coefficients are either computed based on the estimated channel impulse response (CIR) or directly estimated

through adaptive methods. In this paper, we consider both the CE based TEQ and DA-TEQ. In the CE based Turbo receivers, we adopt an iterative channel estimation scheme, which is implemented with the Normalized Least Mean Square (NLMS) algorithm. The estimated UWA channel is then incorporated into the computation of the MMSE equalizer coefficients. In the DA-TEQ, we utilize the NLMS algorithm to directly estimate the equalizer coefficient without channel knowledge. In the following, we briefly review four TEQs evaluated in this paper.

3.1 CE-BASED LMMSE TURBO EQUALIZER

In the CE-BASED LMMSE Turbo Equalizer, the *a priori* LLRs $L_a\left(c_{k,j}\right)$ provided by the decoder are used to compute the *a priori* soft decision

$$\bar{x}_k = E\left[x_k \middle| \left\{L_a\left(c_{k,j}\right)\right\}_{j=1}^{Q}\right] = \sum_{\alpha_i \in S} \alpha_i P\left(x_k = \alpha_i\right) \tag{4}$$

where

$$P\left(x_k = \alpha_i\right) = \prod_{j=1}^{q} \frac{1}{2}\left(1 + \tilde{s}_{i,j} \tanh\left(L_a\left(c_{k,j}\right)/2\right)\right) \tag{5}$$

and

$$\tilde{s}_{i,j} = \begin{cases} +1 & \text{if } s_{i,j} = 0 \\ -1 & \text{if } s_{i,j} = 1. \end{cases}$$

The transmitted symbol x_k is estimated by a linear combining of the received signals and the *a prior* soft decisions [8]

$$\hat{x}_k = \mathbf{f}^H(\mathbf{r}_k - \hat{\mathbf{H}}\tilde{\mathbf{x}}_k) \tag{6}$$

where $\mathbf{r}_k$ is defined in (3a), $\mathbf{f}$ is the feedforward filter with length being $K = k_1 + k_2 + 1$, $\hat{\mathbf{H}}$ is the estimated channel matrix, and $\tilde{\mathbf{x}}_k = [\bar{x}_{k-K_2-L+1} \cdots \bar{x}_{k-1}\ 0\ \bar{x}_{k+1} \cdots \bar{x}_{k+K_1}]^T$.

Considering the computational complexity, we evaluate an approximate implementation of Turbo LE [8], which only computes the feedforward filter once at each

turbo iteration

$$\mathbf{f} = (\sigma_w^2 \mathbf{I}_K + \bar{v}\hat{\mathbf{H}}\hat{\mathbf{H}}^H)^{-1}\tilde{\mathbf{h}}_k \tag{7}$$

Here, $\bar{v}$ is the time averaged variances of the transmitted symbols, which is computed based on the *a priori* information [8]. Besides, $\tilde{\mathbf{h}}_k$ is the $(K_2 + L)th$ column of $\hat{\mathbf{H}}$.

3.2 CE-BASED SOFT-DECISION FEEDBACK TURBO EQUALIZER

A low-complexity CE-BASED SDFE was proposed in [9] to lower the error propagation in traditional Turbo DFEs. At the SDFE, the estimated symbol $\hat{x}_n$ is given by

$$\hat{x}_k = \mathbf{g}\mathbf{r}_k + \mathbf{b}\mathbf{x}_k^d + d_k \tag{8}$$

where $\mathbf{g}$ is the feedforward filter, $\mathbf{b}$ is the feedback filter of length $K_3 = K_2 + L - 1$, and d_k is the time-varying offset. Besides, the input vector of the feedback filter is defined as $\mathbf{x}_k^d = [x_{k-K_3}^d \; x_{k-K_3+1}^d \cdots x_{k-1}^d]^T$, and x_k^d is the *a posterior* soft decision estimated by the bit *a priori* information $L_a(c_{k,j})$ and bit extrinsic information $L_e(c_{k,j})$. Note that the low-complexity SDFE only updates the feedforward filter and feedback filter once at each turbo iteration.

The filters in the SDFE at each turbo iteration are given by

$$\mathbf{g}^H = [\sigma_w^2 \mathbf{I}_K + \hat{\mathbf{H}}(\mathbf{C}^{ff} - \mathbf{C}^{fb}(\mathbf{C}^{bb})^{-1}\mathbf{C}^{fbH})\hat{\mathbf{H}}^H]^{-1}\mathbf{s} \tag{9a}$$

$$\mathbf{b}^H = -(\mathbf{C}^{bb})^{-1}\hat{\mathbf{H}}\mathbf{C}^{fbH}\mathbf{g}^H \tag{9b}$$

$$d_k = E\{x_k\} - \mathbf{g}\hat{\mathbf{H}}E\{\mathbf{x}_k\} - \mathbf{b}E\{\mathbf{x}_k^d\} \tag{9c}$$

where $\mathbf{C}^{ff}$, $\mathbf{C}^{fb}$ and $\mathbf{C}^{bb}$ are the covariance matrices defined as

$$\mathbf{C}^{ff} = E\left\{\mathbf{x}_k\mathbf{x}_k^H\right\} - E\left\{\mathbf{x}_k\right\}E\left\{\mathbf{x}_k^H\right\} \tag{10a}$$

$$\mathbf{C}^{fb} = E\left\{\mathbf{x}_k\mathbf{x}_k^{dH}\right\} - E\left\{\mathbf{x}_k\right\}E\left\{\mathbf{x}_k^{dH}\right\} \tag{10b}$$

$$\mathbf{C}^{bb} = E\left\{\mathbf{x}_k^d\mathbf{x}_k^{dH}\right\} - E\left\{\mathbf{x}_k^d\right\}E\left\{\mathbf{x}_k^{dH}\right\} \tag{10c}$$

which are computed by the *a priori* information and the *a posteriori* information, as detailed in [9], and $\mathbf{s} = \hat{\mathbf{H}}[\mathbf{0}_{1\times(K_2+L-1)}\ 1\ \mathbf{0}_{1\times(K_1)}]^T$ is the selection vector.

3.3 CE-BASED BIDIRECTIONAL SOFT-DECISION FEEDBACK TURBO EQUALIZER

The Bi-SDFE was proposed for UWA communication in [10], which has used a time-reversed SDFE in conjunction with a normal SDFE to harvest the time-reverse diversity in decision feedback equalization. Both the normal SDFE and time reversal SDFE are the low-complexity implemented SDFE proposed in [9,14]. Besides, a simple and effective linear combing scheme was adopted to combine the extrinsic LLRs at the outputs of the SDFEs:

$$L_e(c_{k,j}) = \frac{1}{1+\varrho_j}(L_{e,f}(c_{k,j}) + L_{e,b}(c_{k,j})) \tag{11}$$

where $L_{e,f}(c_{k,j})\,, L_{e,b}(c_{k,j})$ are the extrinsic LLRs from the normal SDFE and the time-reversed SDFE with respect to the same bit position j, ϱ_j is the correlation coefficient estimated by time averaging

$$\hat{\varrho}_j = \frac{\sum_{k=1}^{K_c}\left[L_{e,f}(c_{k,j}) - \hat{\mu}_{j,f}\right]\left[L_{e,b}(c_{k,j}) - \hat{\mu}_{j,b}\right]}{(K_c-1)\hat{\sigma}_{j,f}\hat{\sigma}_{j,b}}. \tag{12}$$

Similarly, here the mean $\hat{\mu}_{j,f}$ and $\hat{\mu}_{j,b}$, standard deviations $\hat{\sigma}_{j,f}$ and $\hat{\sigma}_{j,b}$ are also estimated by time-averaging.

3.4 SOFT-DECISION DIRECT-ADAPTATION TURBO EQUALIZER

At the DA-TEQ, the estimated symbol $\hat{x}_k^{(n)}$ is a linear combining of the received signals and the *a prior* soft decisions

$$\hat{x}_k = \mathbf{w}_k^H \mathbf{r}_k + \mathbf{q}_k^H \tilde{\mathbf{x}}_k \tag{13}$$

where $\mathbf{w}_k$ is the feedforward filter and $\mathbf{q}_k$ is the soft interference cancelation (SIC) filter. We can reformulate equation (13) as $\hat{x}_k = \mathbf{G}_k^H \mathbf{U}_k$. Here $\mathbf{G}_k = [\mathbf{w}_k^T \, \mathbf{q}_k^T]^T$ is the concatenation of the feedforward and SIC filters, and $\mathbf{U}_k = [\mathbf{r}_k^T \, \tilde{\mathbf{x}}_k^T]^T$ is the overall input of the filters. The DA-TEQs utilize the adaptive algorithms, such as NLMS, to directly estimate the eqaulizer coefficients

$$\mathbf{G}_{k+1} = \mathbf{G}_k + 2\frac{\mu}{\epsilon + \mathbf{r}_k \mathbf{r}_k^H}(x_k - (\mathbf{G}_k)^H \mathbf{U}_k)\mathbf{U}_k \tag{14}$$

where the μ is the step size, ϵ is a small number for regularization.

To track the time variations of the UWA channles, the filter adaptation continues in decision-directed (DD) mode after training phase, where the x_k in (14) is replaced with the tentative hard decision of $\hat{x}_k$. Such an empirical processing method is widely used in existing DA-TEQs for underwater acoustic communication systems. The main drawback of the hard decision directed adaptation is the error propagation, which may results into a catastrophic failure of the convergence. Recently, a soft-decision DA-TEQ (Soft DA-TEQ) was proposed for MIMO UWA communication systems [12], which utilized the *a priori* soft decision $\bar{x}_k$ from the decoder to direct the equalizer coefficients adaptation. In this paper, we evaluate the performance of the Soft DA-TEQ in SISO UWA channels.

4 EXPERIMENT DESCRIPTION

The SPACE08 experiment was conducted at the coast of Martha's Vineyard, Edgartown, MA, in October 2008. The single carrier modulation frame structure, shown in Fig. 4.1, was adopted for transmission, where the data frame consisted of a header, three data packets, and a tail. The header and tail of the transmitted signal were LFMB and LFME, respectively, each having a 1000-symbol length of linear frequency modulation (LFM) signal surrounded by some gaps. The header and tail were for Doppler estimation, frame synchronization, and carrier synchronization purposes. The three data packets were QPSK, 8PSK and 16QAM modulated symbols, respectively. The transmission signal strength was the same for all three modulation schemes, making the received SNR the same for all modulation schemes. Each packet started with an m-sequence (maximal-length sequence) of length 511, followed by a small gap and a data packet of 30,000 symbols. Note that N is the number of transducers, and n is the transducer index. For SISO transmission, n and N are both set as 1.

A rate 1/2 convolutional code with a generator polynomial $G = [17, 13]_{oct}$ was chosen as the forward error correction code. The center carrier frequency was $f_c = 13$ kHz. The symbol interval was 0.1024 ms, and the roll-off factor for the square-root raised cosine pulse shaping filter was chosen as $\beta = 0.2$. Thus the occupied bandwidth of the transmitted signal was 11.71875 kHz. The receiver sampling rate was 39.0625 kilo-samples/s. The communication distance was 200 meters.

The depth of the experimental water was about 15 m. A transducer located on a fixed tripod at about 4 m above the ocean bottom was used in the SISO communication test. At the receiver, 24 hydrophones were also fixed with tripods to form a vertical array, where the top hydrophone of the array was about 3.3 m above the ocean bottom. The sixth hydrophone from the top was used to form the SISO communication system. Seven received data frames at different transmission times were processed to test the

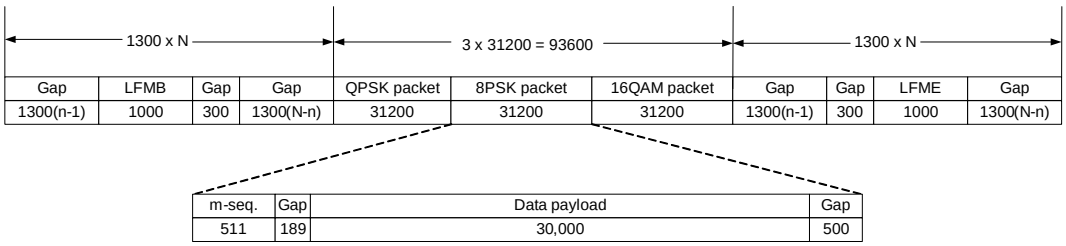

Figure 4.1. The burst structure of the nth transmit branch in the SPACE08 experiment.

performance of the Turbo receivers in SISO UWA channels.

Figure 4.2 shows the time evolution of four typical channel impulse responses (CIRs) in the experiment. The CIRs were fast time-varying, although both the transducer and hydrophone were fixed during the experiment. In some packet transmissions,

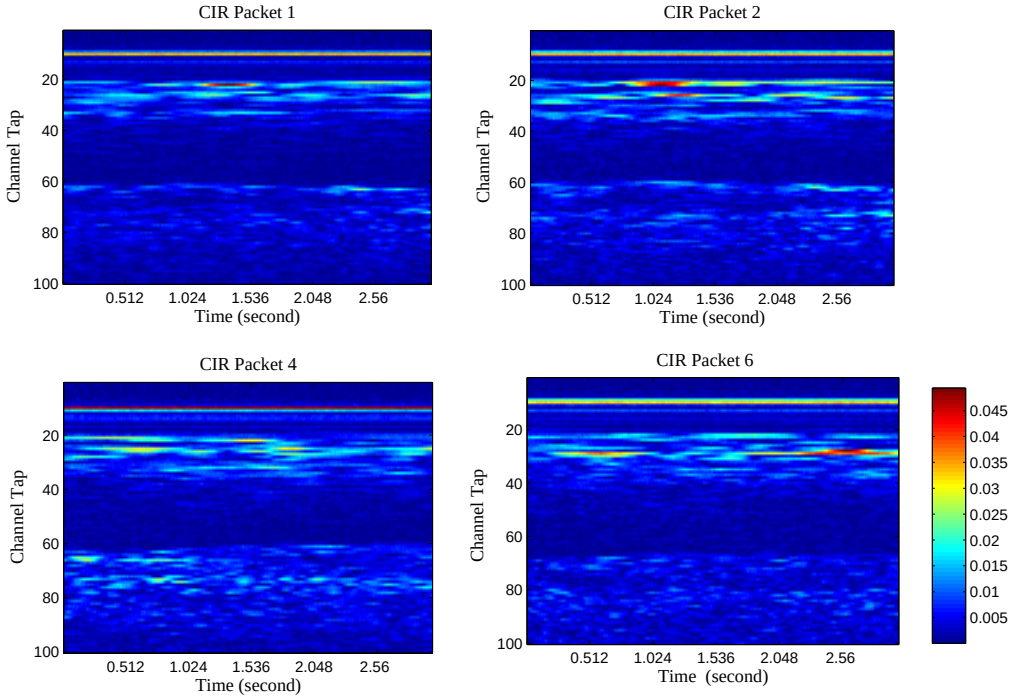

Figure 4.2. CIRs over one packet transmission.

the channels were also non-minimum phase systems since the strongest multipath components were not located at the very beginning of the CIR.

5 PERFORMANCE EVALUATION

In the following subsections, we first present the performance of 3 CE MMSE-TEQs: Linear MMSE (LMMSE) Turbo eqaulizer [6], Soft Decision Feedback Turbo equalizer (SDFE) [13] and the recently proposed Bidirectional Soft Decision Feedback Turbo equalizer (Bi-SDFE) [10]. Then, we present some results of a recently proposed Soft-decision DA-TEQ [12].

5.1 CE-BASED TURBO EQUALIZATIONS

The BER performance of the CE-based Turbo receivers is shown in Fig. 5.1. Note that "iter. 0" denotes the non-iterative processing, i.e., one-time equalization and one-time decoding. Besides, the packets with 0 BER are not shown in the BER figures due to log scale.

For QPSK modulation, the pilot overhead was set as 12%, and the BER of different Turbo detectors are compared in Fig. 5.1(a), where only one iteration of Turbo equalization achieved significant performance gain over the non-iterative equalizers. Especially, using the Bi-SDFE, 6 packets achieved 0 BER with only one iteration. In the second iteration, 6 and 7 packets reached 0 BER with the SDFE and Bi-SDFE, respectively. The LMMSE Turbo equalizer converged slowest, and only 1 packet achieved 0 BER after 2 iterations. Hence with QPSK modulations, both the SDFE and Bi-SDFE enable robust SISO underwater acoustic single carrier transmission.

For 8PSK modulation, the performance comparison of different CE-TEQs are given in Fig. 5.1(b). The pilot overhead was 14.81%. The iterative processing provides tremendous performance improvement over the one-time equalization and decoding. The Bi-SDFE has obvious performance gain over the SDFE and LMMSE equalizer. After 4 iterations with the Bi-SDFE, one packet achieved 0 BER, 5 packets were with the BER level of 10^{-4}, and 1 packet was with BER level of 10^{-3}.

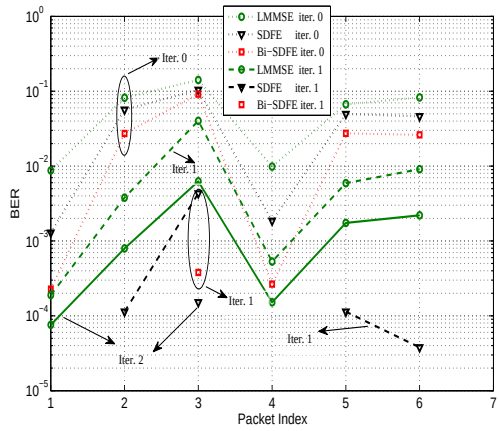

(a) QPSK, 12% pilot overhead

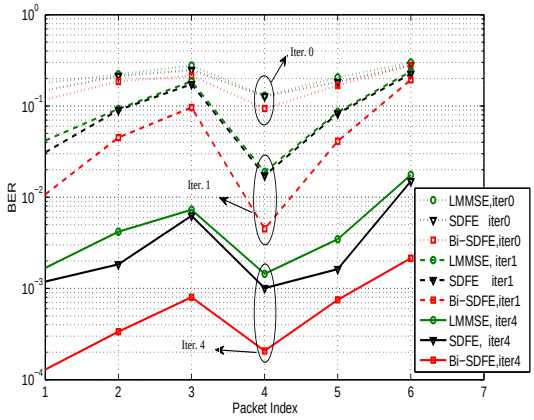

(b) 8PSK, 14.81% pilot overhead

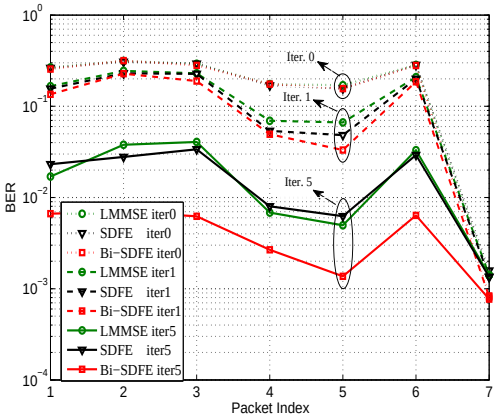

(c) 16QAM, 22.22% pilot overhead

Figure 5.1. BER performance of CE-based TEQs. Packet 7 reached 0 BER for all algorithms with Iter 0 in QPSK and 8PSK transmissions.

We also tested the CE-TEQs using the 16QAM data with pilot overhead 22.22%, and the data processing result is presented in Fig. 5.1(c). The performance trends among the 3 CE-TEQs are very similar to 8PSK transmission. After 5 iterations, most packets with Bi-SDFE achieved the BERs at the level of 10^{-3}. Another interesting observation in Fig. 5.1(c) is that the performance gap between the SDFE and LMMSE equalizer are very minor, even after multiple iterations. With packet 7 (good channel condition), the iterative algorithms exhibited no improvement in BER with multiple iterations.

Overall, the QPSK and 8PSK transmissions with CE-TEQs were robust in SISO UWA channels. The turbo receivers achieved low level of BERs, even with low pilot overhead. The single carrier transmission with 16QAM modulation in SISO transmission is challenging due to their low E_b/N_0. However, the recently proposed Bi-SDFE greatly enhanced the system performance.

5.2 SOFT-DECISION DIRECT-ADAPTATION TURBO EQUALIZATION

Figure 5.2 shows the performance of the recently proposed soft-decision DA-TEQ in SISO UWA channels [12]. Since the hard-decision DA-TEQ was shown to perform worse than the soft-decision DA-TEQ [12], we only present the results of the soft-decision DA-TEQ.

For QPSK, 20% pilot overhead was required to achieve low BER performance. As shown in Fig. 5.2(a), packet 1 and 7 achieved 0 BER, and 4 packets were with the BER level of 10^{-4}. Only the third packet stayed at the BER level of 10^{-3} after multiple iterations. For higher level modulations, the DA-TEQ required much higher pilot overhead to achieve satisfactory performance. For example, when 8PSK modulations was used, 30% pilot overhead was used to achieve the results in Fig. 5.2(b) and 16QAM required 42% pilot overhead to barely converge. Hence, the direct-adaptation equalizer with high level modulations is spectral inefficiency in time-varying SISO UWA chan-

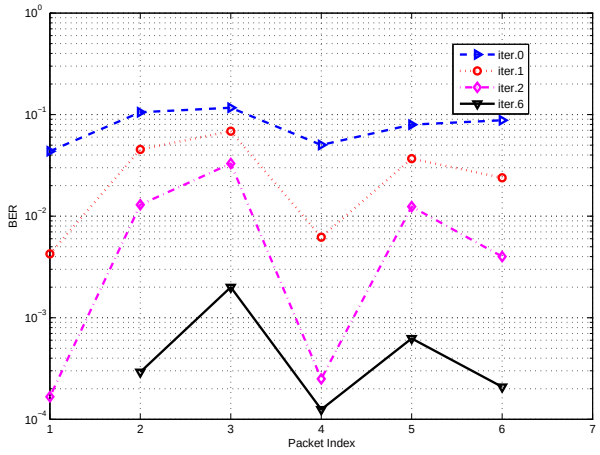

(a) QPSK, 20% pilot overhead

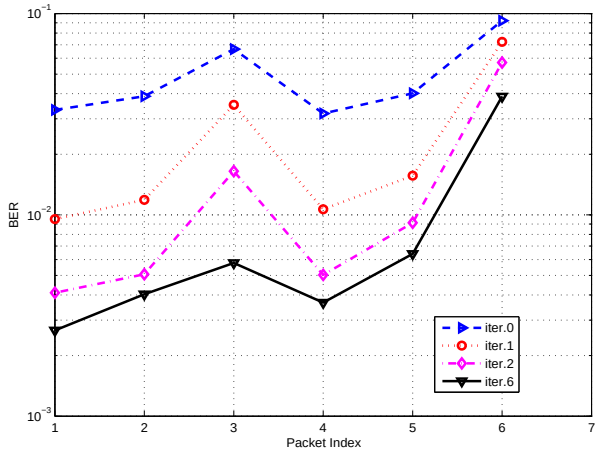

(b) 8PSK, 30% pilot overhead

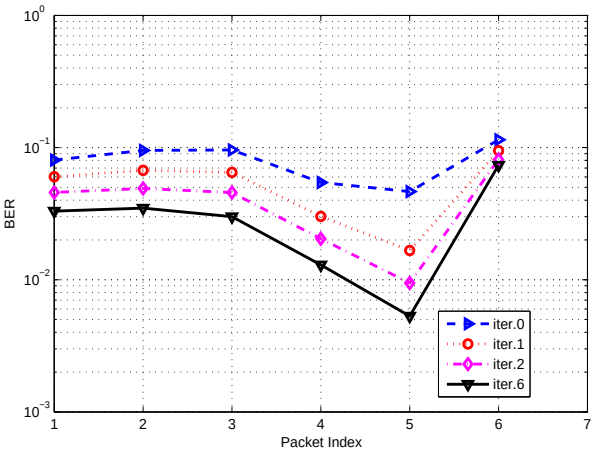

(c) 16QAM, 42% pilot overhead

Figure 5.2. BER performance of Soft-Decision DA-TEQ. Packet 7 achieved 0 BER at Iter 0 for all modulation schemes.

nels. However, with QPSK modulation, the recently proposed Soft-decision DA-TEQ may achieve a good trade-off between complexity and performance with reasonable percentage of pilot overhead.

Note that Packet 7 achieved 0 BER at Iter 0 for all modulation schemes, but the overhead was a lot higher than the CE-based algorithms. When the overhead was reduced to the same levels as in Fig. 5.1, then the DA-TEQ of packet 7 performed similarly to the CE-based algorithms.

6 CONCLUSION

We tested four MMSE-TEQs in time-varying SISO UWA channels. Experimental results show that the CE-TEQ algorithms are robust in SISO underwater acoustic transmission under harsh channel conditions. With reasonable pilot overhead, the recently proposed Bi-SDFE achieved the lowest BER performance in all channels with slightly higher computational complexity. In contrast, the DA-TEQ exhibited low-complexity but requires high pilot overhead to achieve satisfactory BER performance. The pilot overhead of the DA-TEQ is especially high in high-level modulation schemes, making the high-level modulation unattractive in low SNR conditions. Overall, the QPSK modulation can achieve extraordinary low BER performance for all CE-TEQs and DA-TEQ algorithms in all packets because of the reasonable SNR levels.

7 ACKNOWLEDGEMENT

This work is supported in part by the National Science Foundation grant ECCS1408316 of the United States.

8 REFERENCES

[1] G. F. Edelmann, H. Song, S. Kim, W. Hodgkiss, W. Kuperman, and T. Akal, "Underwater acoustic communications using time reversal," *Oceanic Engineering, IEEE Journal of*, vol. 30, no. 4, pp. 852–864, 2005.

[2] M. Stojanovic, J. Catipovic, and J. G. Proakis, "Adaptive multichannel combining and equalization for underwater acoustic communications," *J. Acoust. Soc. Amer.*, vol. 94, no. 3, pp. 1621–1631, 1993.

[3] Y. Zheng, J. Wu, and C. Xiao, "Turbo equalization for single-carrier underwater acoustic communications," *IEEE Communications Magazine*, vol. 53, no. 11, pp. 79–87, November 2015.

[4] R. Otnes and T. H. Eggen, "Underwater acoustic communications: long-term test of turbo equalization in shallow water," *IEEE J. Oceanic Eng.*, vol. 33, no. 3, pp. 321–334, Mar. 2008.

[5] J. Tao, Y. R. Zheng, C. Xiao, and T. Yang, "Robust MIMO underwater acoustic communications using turbo block decision-feedback equalization," *IEEE J. Ocean. Eng.*, vol. 35, no. 4, pp. 948–960, Oct. 2010.

[6] Z. Yang and Y. R. Zheng, "Iterative channel estimation and turbo equalization for multiple-input multiple-output underwater acoustic communications," *IEEE J. Ocean. Eng.*, vol. 99, Feb. 2015.

[7] J. W. Choi, T. J. Riedl, K. Kim, A. C. Singer, and J. C. Preisig, "Adaptive linear turbo equalization over doubly selective channels," *IEEE J. Ocean. Eng.*, vol. 36, no. 4, pp. 473–489, Oct. 2011.

[8] M. Tuchler, A. C. Singer, and R. Koetter, "Minimum mean squared error equalization using *a priori* information," *IEEE Trans. Signal Process.*, vol. 50, no. 3, pp. 673–683, Mar. 2002.

[9] H. Lou and C. Xiao, "Soft-decision feedback turbo equalization for multilevel modulations," *IEEE Trans. Signal Process.*, vol. 59, no. 1, pp. 186–195, Jan. 2011.

[10] W. Duan and Y. R. Zheng, "Bidirectional soft-decision feedback turbo equalization for mimo systems," *IEEE Trans. Veh. Technology*, vol. PP, no. 99, Aug. 2015.

[11] C. Laot, N. Beuzeulin, and A. Bourre, "Experimental results on mmse turbo equalization in underwater acoustic communication using high order modulation," in *OCEANS 2010-Seattle*, 2010, pp. 1–6.

[12] W. Duan and Y. R. Zheng, "Soft direct-adaptive turbo equalization for MIMO underwater acoustic communications," in *MTS/IEEE Oceans - Washington, DC, 2015*, 2015, pp. 1–6.

[13] A. Rafati, H. Lou, and C. Xiao, "Soft-decision feedback turbo equalization for ldpc-coded mimo underwater acoustic communications," *IEEE J. Oceanic Engineering*, vol. 39, no. 1, pp. 90–99, 2014.

[14] ——, "Low-complexity soft-decision feedback turbo equalization for MIMO systems with multilevel modulations," *IEEE Trans. Veh. Technology*, vol. 60, no. 7, pp. 3218–3227, Jul. 2011.

SECTION

2 CONCLUSIONS

This dissertation investigates the low-complexity Turbo receiver algorithms for multiple-input multiple-output (MIMO) underwater acoustic (UWA) communications. First, an iterative bidirectional soft-decision feedback equalizer (Bi-SDFE) is proposed for robust communication in severe triply selective fading channels. A simple and effective linear combining scheme is derived to harvest the time-reverse diversity of the extrinsic information at the output of the two soft-decision feedback equalizers (SDFEs) for MIMO systems with multilevel modulation. Both bit error rate (BER) simulation and extrinsic information transfer (EXIT) chart analysis show that the proposed Bi-SDFE obviously outperforms the original SDFE. The Bi-SDFE even outperforms the near optimal but high-complexity exactly implemented minimum mean square error (MMSE) Turbo linear equalizer at the medium-to-high SNR region. The complexity of Bi-SDFE is roughly twice that of SDFE, but still remains a linear function of the channel length, MIMO size and modulation constellation size. The performance gain of the proposed MIMO SDFE has been verified by undersea communication experimental data.

Second, this dissertation proposes a *a posteriori* soft-decision driven direct adaptation turbo equalization (DA-TEQ) scheme for MIMO UWA communications. The data reuse technique is adopted such that iterative symbol detection is performed inside the adaptive equalizer itself. Attributed to the better fidelity of the *a posteriori* soft decisions as compared with the *a priori* soft decisions used in the existing DA-TEQ, the proposed scheme not only achieves robust detection performance but also is very efficient in spectral efficiency. Therefore, it is a good candidate for practical application. The powerful detection capability of the proposed iterative receive scheme was demonstrated by the experimental data collected in an undersea experiment. Especially, the

proposed DA-TEQ works successfully in MIMO transmission with multilevel modulations and more than two concurrent transmitted data streams, which is not found in existing literature.

Third, a frequency domain (FD) low-complexity block iterative detection scheme is proposed for uncoded zero-padding single carrier MIMO UWA communications. The proposed iterative receiver combines the block iterative frequency domain equalization with the iterative channel estimation. The reliability of symbol detection and channel estimation increased iteratively, which achieves obvious performance gain over the non-iterative FDE. Compared with FD Turbo equalizer, the complexity of the proposed receiver is further reduced, which is promising for real-time application. The performance of the proposed iterative receive scheme has been test through a pool experiment.

Finally, this dissertation also evaluates four MMSE Turbo equalizers in time-varying single-input single-output (SISO) UWA channels. Experimental results show that the channel estimation based Turbo equalizers are robust in SISO systems under tough channel conditions. With reasonable pilot overhead, the recently proposed Bi-SDFE achieves the lowest BER performance in all cases with slightly higher computational complexity. In contrast, the DA-TEQ exhibits low-complexity but requires high pilot overhead to achieve satisfactory BER performance.

3 PUBLICATIONS

[1] W. Duan, J. Tao, and Y. R. Zheng, "Efficient Adaptive Turbo Equalization for MIMO Underwater Acoustic Communications", *IEEE J. Ocean. Eng.*, Apr. 2016. [Submitted]

[2] W. Duan, and Y. R. Zheng, "Experimental Evaluation of Turbo Receivers in Single-Input Single Output Underwater Acoustic Channels", in *Proc. MTS/IEEE OCEANS*, Shanghai, China, Apr. 11-14, 2016. [Accepted]

[3] H. Huang, Y. R. Zheng, and W. Duan, "Pseudo-Noise Based Time of Arrival Estimation for Underwater Acoustic Sensor Localization", in *Proc. MTS/IEEE OCEANS*, Shanghai, China, Apr. 11-14, 2016. [Accepted]

[4] W. Duan, Y. R. Zheng, D. Sun, and Y. Zhang, "Block Iterative FDE for MIMO Underwater Acoustic Communications", in *Proc. MTS/IEEE COA*, Harbin, China, Jan. 9-11, 2016. [Accepted]

[5] W. Duan, and Y. R. Zheng, "Soft Direct-Adaptive Turbo Equalization for MIMO Underwater Acoustic Communications", in *Proc. MTS/IEEE OCEANS*, Washington, DC, USA, Oct. 19-22, 2015. pp. 1–6.

[6] W. Duan, Y. R. Zheng,"Bidirectional Soft-Decision Feedback Turbo Equalization for MIMO Systems", accepted by *IEEE Trans. Veh. Technol.*, Aug. 2015. [In press]

[7] W. Duan, and Y. R. Zheng, "Bidirectional Soft-Decision Feedback Equalization for Robust MIMO Underwater Acoustic Communications", in *Proc. MTS/IEEE OCEANS*, St. Johns, NL, Canada, Sep. 14-18, 2014. pp. 1–6.

VITA

Weimin Duan was born in China in 1987. He received the B.S. degree in electrical engineering and M.S. degree in underwater acoustic engineering from Harbin Engineering University, Harbin, China, in 2010 and 2013, respectively. He began his Ph.D study in August 2013 at the Department of Electrical and Computer Engineering at Missouri University of Science and Technology (formerly: University of Missouri-Rolla), USA. His research interests include MIMO signal processing, iterative detection, wireless and underwater acoustic communications. He received his Ph.D. degree in Electrical Engineering from Missouri University of Science and Technology in July 2016.